ISTANBUL TECHNICAL UNIVERSITY ★ GRADUATE SCHOOL

CONTRIBUTIONS TO SHORT-CIRCUIT PROTECTION OF ELECTRIC VEHICLE BATTERY SYSTEMS BY IMPLEMENTING SiC SWITCHES

M.Sc. THESIS

Murat Kubilay ÖZGÜÇ

Department of Electrical Engineering

Electrical Engineering Programme

FEBRUARY 2021

ISTANBUL TECHNICAL UNIVERSITY ★ GRADUATE SCHOOL

CONTRIBUTIONS TO SHORT-CIRCUIT PROTECTION OF ELECTRIC VEHICLE BATTERY SYSTEMS BY IMPLEMENTING SiC SWITCHES

M.Sc. THESIS

Murat Kubilay ÖZGÜÇ
(504181060)

Department of Electrical Engineering

Electrical Engineering Programme

Thesis Advisor: Asst. Prof. Dr. Derya Ahmet KOCABAŞ

FEBRUARY 2021

İSTANBUL TEKNİK ÜNİVERSİTESİ ★ LİSANSÜSTÜ EĞİTİM ENSTİTÜSÜ

SiC ANAHTAR UYGULAMASI İLE ELEKTRİKLİ ARAÇ BATARYA SISTEMLERİNİN KISA DEVRE KORUMASINA KATKILAR

YÜKSEK LİSANS TEZİ

Murat Kubilay ÖZGÜÇ
(504181060)

Elektrik Mühendisliği Anabilim Dalı

Elektrik Mühendisliği Programı

Tez Danışmanı: Dr. Öğr. Üyesi Derya Ahmet Kocabaş

ŞUBAT 2021

Murat Kubilay ÖZGÜÇ, a M.Sc. student of ITU Graduate School student ID 504181060 successfully defended the thesis entitled "CONTRIBUTIONS TO SHORT-CIRCUIT PROTECTION OF ELECTRIC VEHICLE BATTERY SYSTEMS BY IMPLEMENTING SiC SWITCHES", which he prepared after fulfilling the requirements specified in the associated legislations, before the jury whose signatures are below.

Thesis Advisor :	**Asst. Prof. Dr. Derya Ahmet KOCABAŞ** Istanbul Technical University	.....
Jury Members :	**Assoc. Prof. Dr. Salih Barış ÖZTÜRK** Istanbul Technical University	.....
	Prof. Dr. Kamuran Nur BEKİROĞLU Yıldız Technical University	.....

Date of Submission : **19 January 2021**
Date of Defense : **21 February 2021**

This is the way.

FOREWORD

First of all, I would like to thank my advisor Asst. Prof. Dr. Derya Ahmet KOCABAŞ at Istanbul Technical University for his encouragement and guidance. I am grateful for his patience and enlightening attitude throughout this thesis. Secondly, I would like to thank Eymen İPEK, MSc. for his valuable ideas and supports. Also, I want to present my greatest gratefulness to Obi-Wan Kenobi from the Jedi High Council. I express my eternal gratitude for helping me to find "the force" to overcome all difficulties. Last but not least, I express my lifelong gratitude to my parents for supporting me throughout my education.

February 2021

Murat Kubilay ÖZGÜÇ
(Electrical Engineer)

TABLE OF CONTENTS

Page

ABBREVIATIONS

ADC : Analog to Digital Converter
AC : Alternating Current
AEC : Automotive Electronics Council
BCU : Battery Control Unit
BEV : Battery Electric Vehicle
BJT : Bipolar Junction Transistor
BMS : Battery Management System
DC : Direct Current
EMC : Electromagnetic Compatibility
EV : Electric Vehicles
FUL : Fault Under Load
GaN : Gallium Nitride
HV : High Voltage
HSF : Hard Switch Fault
IC : Integrated Circuit
ICE : Internal Combustion Engine
IEC : International Electrotechnical Commission
ISO : International Organization for Standardization
JFET : Junction Field-Effect Transistor
LA : Lead-Acid
LCO : Lithium Cobalt Oxide
LFP : Lithium Iron Phosphate
LMO : Lithium Manganese Oxide
LV : Low Voltage
MCU : Module Control Unit
MOSFET : Metal Oxide Semiconductor Field Effect Transistor
NCA : Lithium Nickel Cobalt Aluminium Oxide
NiCd : Nickel Cadmium
NiFe : Nickel Iron
NiH : Nickel Hydrogen
NiMH : Nickel Metal Hydride
NiZn : Nickel Zinc
NMC : Lithium Nickel Manganese Cobalt Oxide
Si : Silicon
SiC : Silicon Carbide
SoC : State Of Charge
SSR : Solid-State Relays
WBG : Wide-Bandgap

SYMBOLS

°C	**:** Degree Celcius
A	**:** Ampere
Ah	**:** Ampere-hour
eV	**:** Band Gap Energy
F	**:** Farad
H	**:** Henry
I	**:** Current
$\mathbf{I_{DS}}$	**:** Drain Source Current
L	**:** Inductance
MV/cm	**:** Breakdown Field
$\mathbf{Q_G}$	**:** Gate Charge
R	**:** Resistance
V	**:** Voltage
$\mathbf{V_{DS}}$	**:** Drain Source Voltage
$\mathbf{V_{GS}}$	**:** Gate Source Voltage
$\mathbf{V_{TH}}$	**:** Treshold Voltage
W/cmK	**:** Thermal Conductivity
W	**:** Power
Wh	**:** Energy
Wh/kg	**:** Specific Energy
τ	**:** Time Constant
Ω	**:** Ohm

LIST OF TABLES

Page

LIST OF FIGURES

Page

CONTRIBUTIONS TO SHORT-CIRCUIT PROTECTION OF ELECTRIC VEHICLE BATTERY SYSTEMS BY IMPLEMENTING SiC SWITCHES

SUMMARY

Due to the increasing population, the number of vehicles is increasing everyday, and emissions are becoming an important environmental issue. In this context, in line with the laws enacted by governments, reducing CO_2 emission and increasing energy efficiency have become very important fields of study. The ultimate goal of these studies is to significantly reduce emissions. The automotive industry is one of the key players in this global change. Electric vehicles (EV) are becoming a solution to minimize environmental pollution. However, although they have been used in consumer electronics for a long time, EV's have come back to the agenda since the introduction of high energy and high power batteries. Development in battery systems for EV's, becoming a most important study area to compete with internal combustion engine vehicles. These developments have opened up many new fields of study from the cell level to the pack level.

One of the most important development areas is the safety of battery systems. Battery systems may become a hazardous element in case of a possible electrical, mechanical, environmental, and chemical failure. Therefore, battery management systems (BMS) is ensuring electrical safety with continuous measurement, protection, and control operation. In order to protect from over-current and short circuit failures, the protection strategy is achieved by the BMS. Each component is taken into account when implementing this shut-off strategy. Current zones are determined for the shut-off strategy to be realized through the protection components such as contactors and fuses. In line with these boundaries, a shut-off algorithm is implemented by considering the protection capacities of protection components and pack requirements.

The trend towards 800V+ voltage levels in EV battery packs brings insufficient overcurrent protection performance because of the switching performance of conventional components. To overcome this problem, new switching components which produced for higher voltage levels are causing some design problems in battery packs due to bulky size. In order to bring a reasonable solution to the table, it is questioned whether semiconductor-based switching components, which are currently used in low voltage (LV) batteries, can be developed for high voltage (HV) batteries.

Especially, wide-bandgap (WBG) semiconductors paving the way for the development of semiconductor-based HV switches. Silicon carbide (SiC) semiconductors are superior to other WBG semiconductors in terms of high temperature, high voltage, and short circuit capabilities, which are quite important for HV battery switches. However, the conventional shut-off algorithm is quite slow compared to the short circuit withstand durations of semiconductors. For this reason, special methods are required for short circuit protection with semiconductor switches. Based on this, special semiconductor protection methods, which constitute the main motivation of

this thesis, have been examined. Among these methods, de-saturation, and gate-charge are determined as the most suitable for HV battery switches.

In this study, short circuit protection was proposed with a SiC MOSFET based semiconductor switch. For this purpose, the requirements were determined and the protection system was created by combining the two protection methods. It has been seen from the simulation results that such a system provides much faster protection than a conventional solution, and thus, not only the semiconductor switch but also all the components of the battery system are protected. Due to the different voltages of lithium-ion batteries at different state of charge levels, the simulation was repeated with different voltage values and the results were presented in comparison. However, since the effect of inductance is also important, especially when switching under load, the simulation was repeated with various inductance values and these results were also presented. Finally, according to the simulation, switching performance under load was examined and the switching losses were revealed. In addition, the snubber circuit was designed and the switching performance was improved. All in all, within the scope of this thesis, a new perspective has been brought and contributions have been made to short circuit protection of electric vehicle battery systems in line with the advantages of SiC semiconductor switches.

Although semiconductor-based HV battery switches are not yet mature enough to be used in automotive applications, they can be utilized with electromechanical contactors as hybrid switches. However, the rising performances of semiconductor switches and the inadequacy of conventional protection components are the inevitable motivation for alternation to HV semiconductor switches. Considering the protection method used in this thesis, automotive rated hardware development shall be realized and real-world test results need to be presented.

SiC ANAHTAR UYGULAMASI İLE ELEKTRİKLİ ARAÇ BATARYA SISTEMLERİNİN KISA DEVRE KORUMASINA KATKILAR

ÖZET

Şehirlerde hızla artan nüfus nedeniyle araç sayısı her geçen gün artmakta ve buna bağlı olarak gaz emisyonları önemli bir çevre sorunu haline gelmektedir. Bu bağlamda hükümetler tarafından çıkarılan yasalar doğrultusunda, CO_2 salımını azaltma ve enerji verimliliğini artırma konuları oldukça önemli çalışma alanları haline gelmiştir. Bu çalışmaların en büyük amacı emisyonları önemli ölçüde azaltmaktır. Otomotiv endüstrisi bu küresel değişimin en önemli oyuncularından biridir. Dolayısıyla bu endüstrideki gelişim trendleri, emisyonları azaltmaya yöneliktir. Çevre kirliliğini en aza indirmeyi hedefleyen elektrikli araç (EA) teknolojisi, hem ekonomik hem de çevre dostu olması nedeniyle hızla gelişerek tercih edilen bir seçenek haline gelmektedir.

Bununla beraber, tüketici elektroniğinde çok uzun zamandır kullanılsa da, yüksek enerji kapasiteli pillerin piyasaya sürülmesinden bu yana elektrikli araçlar (EA) tekrardan gündeme gelmiştir. Bu sebeple EA ile otomotiv endüstrisi çevreci çözümlere yönelmiş ve bu konudaki çalışmalarına hız kazandırmıştır. EA'ların içten yanmalı motorlu araçlar ile rekabet edebilmesi için en önemli gelişim batarya sistemlerinde olmaktadır. Batarya sistemleri, elektrikli araçların gelişmesinde en önemli yapı taşı olsa da, güç aktarım sistemindeki diğer bileşenlerde bu amaçta önemli rol oynamaktadır.

Tüketici elektroniğinde çok önemli bir yeri olan lityum iyon bataryalar, yüksek kapasite yoğunluğuna ve yüksek güç yoğunluğuna sahip bataryaların tanıtılmasıyla markette çok önemli bir yer elde etmişlerdir. Özellikle araç içi elektronik sistemlerin gelişmesi ve sayılarının artmasıyla oluşan güç talebine karşı çözüm oluşturmuştur. Daha sonra, 90'ların başından beri gelişmekte olan modern elektrikli araçların, batarya teknolojilerinin de gelişmesiyle, günümüzdeki ivmeyi yakalaması sağlanmıştır. Bu gelişmeler, hücre seviyesinden paket seviyesine birçok yeni çalışma alanı ortaya çıkarmıştır.

Bu alanlardan en önemlisi, batarya sistemlerinin güvenliği olmuştur. Olası bir elektriksel, mekanik, çevresel ve kimyasal hatada, batarya sistemleri tehlike yaratmaktadır. Bu nedenle, batarya sistemlerinde güvenlik konusu günümüzde en önemli gelişim alanlarındandır. Batarya sistemlerinde ölçme, koruma ve kumanda işlemleri elektriksel güvenliği sağlamak için Batarya Yönetim Sistemleri (BYS) üzerinden yapılmaktadır. BYS içindeki çeşitli algoritmalar ile anlık olarak bütün sistemin güvenliği sağlamaktadır.

Batarya sistemlerindeki elektriksel hataların başında gelen, aşırı akım ve kısa devre akımını korumak amacıyla, BYS tarafından gerçekleştirilen koruma stratejisi kullanılır. Bu koruma stratejisi gerçekleştirilirken her bir bileşen dikkate alınır. Koruma komponentlerinden, kontaktör ve sigorta üzerinden gerçekleştirilecek koruma stratejisi için akım limitleri belirlenir. Bu limitler doğrultusunda koruma elemanlarının

koruma kapasiteleri ve paket gereksinimleri göz önüne alınarak, devre kesme algoritması gerçekleştirilir.

EA batarya paketlerindeki 800V ve üzeri gerilim seviyesine doğru eğilim, geleneksel koruma komponentlerinin, aşırı akım koruma performansı konusunda geri kalmasına neden olmaktadır. Yüksek gerilim seviyesine uygun olarak üretilmeye başlanan yeni anahtarlama elemanları ise büyük boyutları nedeniyle, batarya paketlerinde tasarım sorunlarına yol açmaktadır. Dolayısıyla, bu komponentler EA'ların gelişiminde bir bariyer oluşturmaktadır. Bu problemi çözmek amacıyla, bu tezin de motivasyon kaynağını oluşturan, hali hazırda alçak gerilim (AG) bataryalarda kullanılan yarı iletken tabanlı anahtarlama elemanlarının, yüksek gerilim (YG) bataryaları için de geliştirilebilmesi sorgulanmıştır.

Özellikle yüksek bant genişlikli yarı iletkenlerin, silikon (Si) tabanlı yarı iletkenlere göre verimlilik, boyut ve maliyet bazında gelişmeler sağlaması, yarı iletken tabanlı YG anahtarların gelişiminin önünü açmıştır. Silisyum karbür (SiC) yarı iletkenler, YG batarya anahtarları için çok önemli olan yüksek sıcaklık, yüksek gerilim ve kısa devre dayanımları açısından diğer yüksek bant genişlikli yarı iletkenlere göre daha güçlüdür.

Ancak BYS üzerinde çalışan konvansiyonel kısa devre koruma algoritması, dijital haberleşme ve akım sensörlerinin gecikmeleri düşünüldüğünde, yarı iletkenlerin kısa devre dayanım süreleriyle karşılaştırıldığında çok yavaş kalmaktadır. Bu sebeple, yarı iletken anahtar ile kısa devre koruması için özel yöntemler gerekmektedir. Bundan yola çıkarak, bu tezin ana motivasyonunu oluşturan özel yarı iletken koruma yöntemleri incelenmiştir. Bu yöntemlerden desatürasyon ve kapı-şarj yöntemleri en başarılı yöntemler olarak belirlenmiştir.

Bu çalışmada konvansiyonel anahtarlama elemanları ile yapılacak kısa devre koruması, SiC MOSFET tabanlı bir yarı iletken anahtar tasarımı ile önerilmiştir. Bu amaçla gereksinimler belirlenip, seçilen iki koruma yöntemi kombine edilerek koruma sitemi de oluşturulmuştur ve mantık devresi ile sürme devresine bağlanmıştır. Simülasyon sonuçlarında görülmektedir ki böyle bir sistem konvansiyonel korumadan çok daha hızlı koruma sağlamaktadır ve bu sayede sadece yarı iletken anahtar değil batarya sisteminin bütün elemanları da daha az büyüklükte ve daha az sürede hata akımına maruz kalmıştır.

Farklı kapasite seviyelerinde, lityum iyon bataryaların farklı gerilimlere sahip olmalarından dolayı, simülasyon farklı gerilim değerleriyle tekrarlanmış ve sonuçlar ortaya konulmuştur. Bununla beraber, özellikle yük altında anahtarlama yapıldığında endüktansın etkisi önemli olduğundan, çeşitli endüktans değerleri ile simülasyon tekrarlanmıştır ve sonuçlar ortaya konulmuştur. Ek olarak, bu sistemin algoritmasını oluşturan mantık devresi oluşturulmuş ve hem yarı iletken yapısını hem de bütün sistemi koruyacak bir kısa devre koruma performansına erişilmiştir. Son olarak, seçilen yarı iletkenin simülasyon sonuçlarına göre, yük altında anahtarlama performansı incelenmiş ve anahtarlama kayıpları ortaya konmuştur. Bununla beraber, sönümlendirme (snubber) devresi tasarlanmış ve anahtarlama performansı geliştirilmiştir. Sonuç olarak, bu tez çalışması kapsamında, SiC yarı iletken anahtarların avantajları, elektrikli araç batarya sistemlerinin kısa devre korumasına yeni bir bakış açısı getirilmiş ve katkılar sağlanmıştır.

Yarı iletken tabanlı YG batarya anahtarları, henüz otomotiv uygulamalarında kullanılmak için yeterli olgunlukta olmasa da, elektromekanik kontaktör ile hibrit

bir şekilde kullanılabilir. Ancak yarı iletken anahtarlarının gelişen performansları ve konvansiyonel koruma elemanlarının yetersizliği değişimin motivasyon kaynağı olmaktadır. Bu çalışmada kullanılan yöntemler göz önüne alınıp, otomotiv sistemlerine uyumlu donanım gerçeklendiğinde ve test edilip sonuçları ortaya konulduğunda, gerçek uygulamalarda kullanılabilirliği ortaya çıkacaktır. Ek olarak sadece kısa devre korumada değil, ön şarj anında da yarı iletken anahtarın getirdiği avantajlar değerlendirilmelidir.

1. INTRODUCTION

The automotive industry, which has been active for more than 200 years, has been greatly affected by the measures taken against climate change, which has catastrophic effects worldwide. Electrification of the vehicle powertrain has become indispensable for almost all vehicle manufacturers to reduce CO_2 emissions and curtail reliance on fossil fuels. However, apart from the environmental laws and emission targets set by the politicians, the motivation of customers against the environment tenderness is increasing day by day. For these reasons, the internal combustion engine (ICE) vehicles have begun to leave their places to electric vehicles (EV). EVs have a long way to go to achieve the performance level of ICE, especially on range capability. However, today's studies on electrical powertrain structure and sub-components reveal great hope for the future. Developments in battery systems, power electronics, electric motors, and charging infrastructures, create powerful EV rivals against ICE vehicles.

The use of battery technology in highway-capable modern EVs started with GM EV1, which was introduced in 1996 and was the first mass-produced EV. While lead-acid (LA) was the first battery chemistry used in EVs, they were replaced by Nickel-based batteries after a short time due to cost and weight reduction [1]. Nowadays, since lithium-ion (Li-ion) batteries are more advanced in every aspect, they have taken their place in electric vehicles. For this reason, scientists and engineers have focused on studying Li-ion batteries. As range anxiety is a prominent topic, studies generally focus on the capacity increase [2]. However, the safety of the battery is also vital. Especially a fault that may occur in battery packs can have fatal consequences. Therefore, battery management systems (BMS) and electrical safety are becoming a very essential study field [3, 4].

The trend on EV battery pack tends to over 800V batteries [5]. Therefore, EVs with 400V batteries on the road will be replaced soon. As the voltage level increases, automotive compliance high-voltage (HV) components in the market such as electromechanical contactors and fuses becomes unavailable. Product development

for those components lagging against battery development. Therefore, the lack of sufficient maturity becomes a show stopper. Not only battery technology but also semiconductor technology is very important for the development of electric vehicles. Especially the efficiency and high power handling capability of the inverter and charger has a significant impact on EV development. As a result of those advancements, semiconductor-based HV battery protection and control components are an important development area.

In this chapter, the past, present, and future of automotive battery systems are analyzed, with an emphasis on HV protection. Moreover, different types of semiconductors and their short circuit protection methods are exhibited.

1.1 Purpose of Thesis

The purpose of this thesis is to propose a semiconductor-based HV battery switch and short circuit protection scheme. Furthermore, the state-of-the-art battery switching elements used in automotive battery systems and their short circuit protection scheme were examined and compared. Within the scope of this study, firstly the semiconductors investigated from the material level to structure level, predominantly short circuit robustness. After the semiconductors were investigated, short circuit protection methods in the literature were compared in detail. Finally, a semiconductor switching circuit has been introduced and presented with a short circuit protection scheme. The main motivation of this study is to overcome the off-the-shelf product restraint for battery system switching components such as contactors and fuses in the market to fulfill high-performance battery requirements. A semiconductor switch system will settle this development and thus contribute to future battery designs.

1.2 Literature Review

The interest in EVs has become a necessity with the increasing sensitivity to environmental activities. For this reason, as a chain reaction, the development of EVs has created a sparking event for secondary battery usage. Considering LA batteries are not sufficient to prevent the range deficiency, nickel-based batteries and later Li-based batteries have been used [1].

Especially the introduction of Li-ion batteries in 1980 by John Goodenough [6] and their use in EVs in the late 90s [7], have initiated the spread of Li-ion batteries in the automotive sector. The widespread use of electric vehicles has revealed the safety drawbacks of Li-ion battery technologies [8]. Therefore, the safety of Li-ion batteries has become a very important field of study [3,4]. However, safety must be ensured not only at the cell level but also at the pack level.

The voltage increase trend in battery packs as a result of high-power demand [5] has also increased the hazard that may be caused by electrical faults. In the automotive industry, voltages above 60V are classified as HV [9]. For this reason, protective measures and test details should be determined against the risk of electric shock in high voltage (HV) parts. Those measures are ensuring electrical insulation, designing according to clearance-creepage distances, and defining test voltages [10]. Besides from design associated measures for electrical safety, some functional measures should be taken. These include double or reinforced insulation, equipotential bonding, insulation monitoring, touch protection, and HV interlock [11]. To achieve and monitor passive and active protections due to prevent electrical faults, measurements with temperature, voltage, and current sensors are utilized in battery packs. Apart from the measurement components, today HV batteries have protection components such as contactors, pyro fuses, and melting fuses to protect the battery system in case of fault [12]. Among these components, contactor and melting fuses have been used in battery packs with various voltage levels and current capacity to provide a shut-off strategy [13]. Nowadays, pyro-fuse has gained a place in high voltage battery packs as a switching component [14–16]. Later, smart fuses offer a new option with their standalone current measurement and control features [17].

As a common drawback for all of these switching components in case of fault events, they have a limited number of switching cycles that they can achieve under load. The reason behind this limitation comes from phenomena such as contact erosion, contact welding, and arc movement [18]. Since contactors have limited switch-off current, the system must be protected from currents higher than contactors are capable of safely switch-off. In situations where overcurrents higher than contactors maximum switching capability occurs protection is ensured by a fuse. However, switching limits are not only for contactors but also for fuses. If the thermal energy associated with the

current is greater than the fuse can absorb, the fuse may explode [19]. Hence, those components are required to be constantly monitored to prevent component related errors [13]. As aforementioned higher voltage and current demand with component related limitations, brings the necessity for a new switching component for HV battery packs.

Although standalone semiconductor-based switches are not currently available on the market to operate on HV automotive batteries, hybrid solutions can be used in HV battery systems [20, 21]. However, semiconductor-based solutions, which are becoming widespread in low voltage (LV) batteries, have begun to enter the automotive battery market by pioneer semiconductor manufacturers and solid-state relay suppliers [22–25]. This tendency in the market and the rapid development of semiconductor technology is an indication of utilization for HV semiconductor-based switches in the battery packs [26].

Until recently, silicon (Si) was in the lead in power electronics applications [27]. Despite the fact that its rapid development, Si semiconductors have reached their performance limit [28]. For this reason, the search for new semiconductor types has brought to wide-bandgap (WBG) semiconductors. WBG semiconductors have offered an improvement in efficiency, size, and cost against Si-based semiconductor devices [28, 29]. The best assuring WBG semiconductors in the market are silicon carbide (SiC) and gallium nitride (GaN). GaN is quite notable for high-frequency switching applications and SiC is stronger in terms of high temperature, high voltage, and short circuit capabilities, which is crucial for solid-state relays [30, 31]. SiC metal-oxide-semiconductor field-effect-transistor (MOSFET) started to be used in electric vehicles as they were introduced to the market by ROHM and CREE respectively in 2010 and 2011 [32].

The high voltage and current demands for EVs, bring tough short circuit protection. Considering the short circuit durability of SiC semiconductors in HV applications, special care is necessary regarding protection. Many experimental studies have been done on short circuit performances of SiC semiconductors and the importance of the reliability of protection circuits has been emphasized [33–37]. There are several methods have been proposed to achieve fast and accurate protection for semiconductor switches. In studies [19, 38–41] de-saturation based protection is presented for

MOSFETs. In the [42–46] it is shown the availability of de-saturation driver integrated circuits (IC) for MOSFETs. In [47–49] shunt resistor method is presented. The main drawback of the shunt method is power losses [49]. For MOSFETs with a special sense pin, a sense FET based method is provided in [50–55]. For devices which has a kelvin source pin, short circuit protection is shown in [54–59] with an inductive measurement method. However, the methods that require these special pins are generally not compatible with discrete devices. The gate-charge method that provides short circuit protection by sensing the change in the gate-source voltage without requiring a high voltage connection is shown in [60, 61]. Finally, the Rogowski coil method, which requires special design in [62, 63], the method made by measuring over the air-gap transformer in [64] and the relatively slow method based on the temperature sensor information over the case temperature of the device in [65] are also examined.

The literature review shows that there are numerous studies in the fields of semiconductors, especially short circuit resistance and their short circuit protection schemes. However, when it comes to automotive battery switches, there are only a few studies in the literature. Moreover, there are only LV semiconductor based switches on market for automotive applications. This study contributes to HV battery switch design and its capabilities regarding short circuit protection. Proposed HV battery switch with protection circuit simulated on SPICE environment. Moreover, in this study, the short circuit robustness of SiC devices and comprehensive analysis of short circuit protection methods are exhibited.

2. ENERGY STORAGE SYSTEMS FOR ELECTRICAL VEHICLES

2.1 Types of Batteries

Although batteries have many features that distinguish them from each other, they are divided into primary and secondary batteries according to their rechargeable properties. Primary batteries are batteries that are not rechargeable. On the other hand, the term secondary battery is used for batteries that can be charged more than once. Today, rechargeable batteries play a very important role in the automotive industry. High power or high energy secondary battery packs are the most important building block of the powertrain in HEV and EVs. The most known rechargeable battery chemistries are LA, nickel-based, and Li-ion in the automotive industry.

2.1.1 Lead-Acid batteries

Used since the 1800s, LA batteries today have a large market share in terms of both sales volume and production volume of MWh [66]. These batteries are economical (150–200 $/kWh) and long-lasting (Cycle Life 1500–5000 and Duty Life 15 years) [67]. On the other hand, they have low energy density (35–50 Wh/kg) [67]. It is commonly used for wheelchairs, golf cars, lighting, uninterruptible power supply (UPS), and automotive with its largest market share as 12V power supply. Lead is toxic and cannot be disposed of in landfills [66]. The principal structure of a LA battery is given in Figure 2.1.

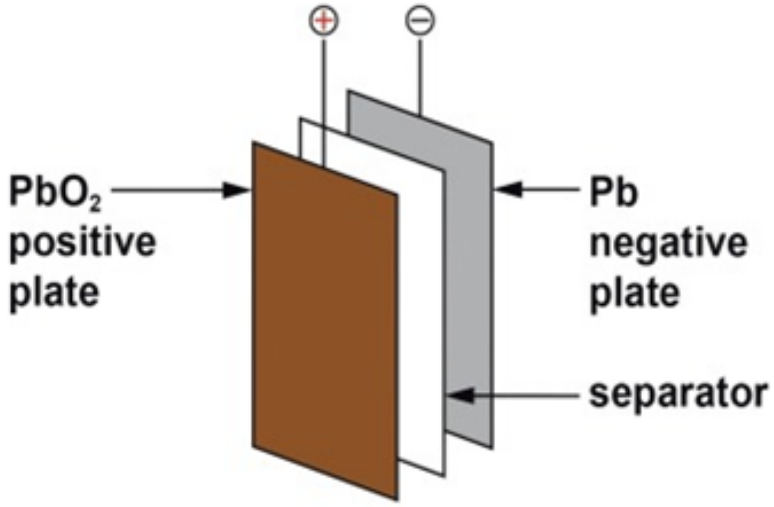

Figure 2.1 : Structure of LA battery [67].

2.1.2 Nickel-based batteries

After its invention in 1899, Nickel-based batteries have been actively used. It was first produced as Nickel Cadmium (NiCd) batteries. They have an energy density of 40-60 Wh/kg which is higher than Lead Acid. Besides being a safe and cheap technology, nickel-cadmium batteries have a life cycle of up to 1000 cycles with proper maintenance [68]. Although they were used in electric vehicles in the past, other battery technologies have now replaced the Ni-Cd battery. Due to the toxic substance called Cadmium, the industry has turned to other Ni-based batteries such as Nickel-metal hydride battery (NiMH), Nickel-Iron (NiFe) Nickel-zinc (NiZn), and Nike hydrogen (NiH). The most prominent one, nickel-metal hydride battery technology which has a life cycle up to 2000 cycles and 60-120 Wh/kg of energy density was developed as an alternative to nickel-cadmium batteries [69]. Moreover, NiFe has 50 Wh/kg, NiZn has 100 Wh/kg and NiH has 75Wh/kg of energy density [68]. The principal structures of nickel-based batteries are given in Figure 2.2.

2.1.3 Li-ion batteries

Li-ion batteries were invented by John Goodenough in 1980 [6]. 5 years later, the development of the Li-ion battery prototype was achieved by Akira Yoshino [70]. Since then, the Li-ion battery is widely used in portable electronics, electric vehicles, and many other industries. Standing out with its powerful features such as cycle life,

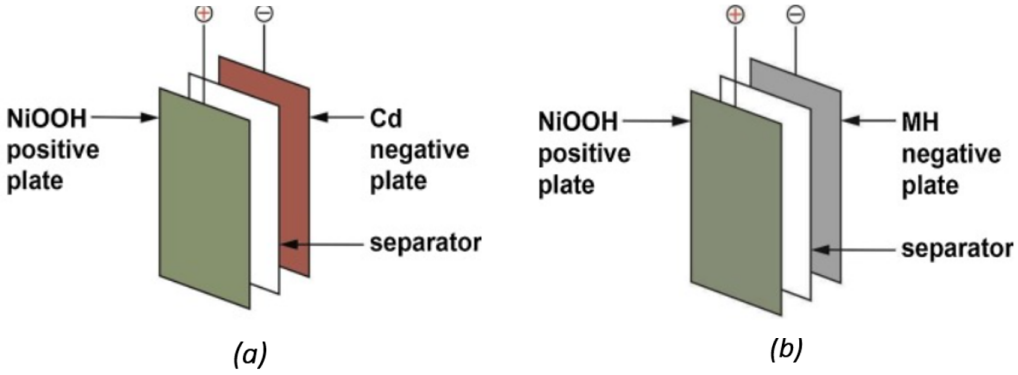

Figure 2.2 : Structure of nickel-based batteries a)NiCd, b)NiMH [67].

high power density, high energy density, and low power losses, the Li-ion battery has significant advantages over other rechargeable battery types and frequently preferred by car manufacturers for electric or hybrid electric vehicles [71].

The structure of Li-ion batteries consists of 4 main parts. These are cathode, anode, electrolyte, and separator [72]. The term anode (or negative electrode) refers to the electrode where oxidation occurs during the discharge cycle; the other electrode is the cathode (or positive electrode). During the charge cycle, the positive electrode becomes the anode, and the negative electrode becomes the cathode. The electrolyte consists of a solution of lithium salt in an organic solvent. The separator is simply the wall with a microporous structure between the anode and cathode. There are three main packaging types of Li-ion EV batteries available on the market which are prismatic, pouch, or cylindrical as can be seen in Figure 2.3 [73].

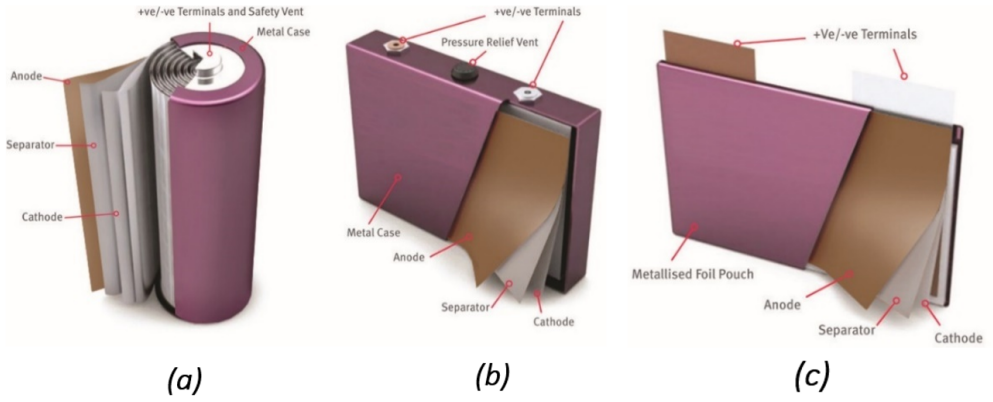

Figure 2.3 : Packaging types a)Cylindrical, b)Prismatic c)Pouch [73].

During charging, the lithium atoms in the cathode are converted to ions and carried towards the anode through the electrolyte, and are deposited as lithium atoms between the carbon layers. On the other hand, during the discharge process, li-ions flow from the anode electrode to the cathode electrode and create a current flow. Figure 2.4 shows the electron and ion flow of Li-ion battery cell [74]. Electron flow in Li-ion batteries is in the same direction as the flow of ions, while the direction of the current is opposite.

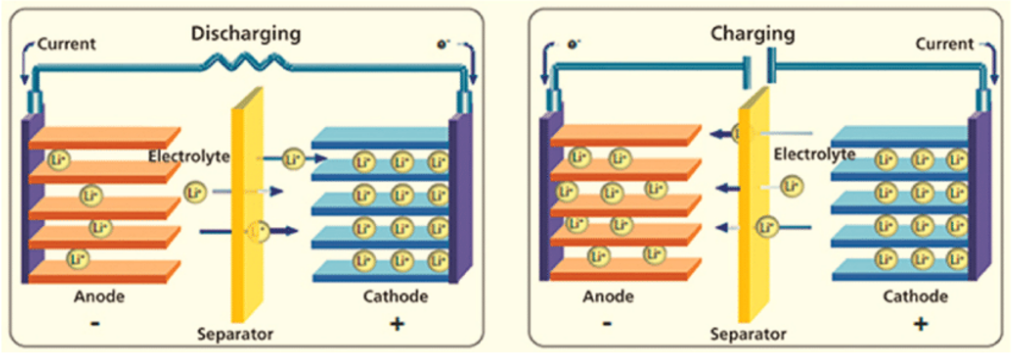

Figure 2.4 : Li-Ion battery electron flow during discharge and charge [74].

Today, there are many types of li-ion battery chemistries with different types of anode and cathode combinations. These batteries are usually named based on the active materials in their cathodes. There are a number of fundamental factors that determine the overall performance in a battery, such as high energy, power density, low internal resistance, and high voltage, which varies with cell chemistry. These factors determine the specific capacity of the battery cell and therefore the battery performance. Today, commercial Li-ion batteries cover a range of specific energy, roughly from 90 to 250 Wh/kg [75]. Several lithium metal oxides are frequently used in many industries, especially in energy storage applications. Those are lithium cobalt oxide - $LiCoO_2$ (LCO), lithium manganese oxide - $LiMn_2O_4$ (LMO), lithium iron phosphate - $LiFePO_4$ (LFP), lithium nickel cobalt aluminum oxide - $LiNiCoAlO_2$ (NCA), and lithium nickel manganese cobalt oxide - $LiNiMnCoO_2$ (NMC). Different lithium-ion chemistries have been studied in detail [73–76]. Table 2.1 shows the comparison of li-ion cells according to their preferences such as release date, specific capacity, nominal voltage, specific energy, cycle life, and market status.

Table 2.1 : Comparison of lithium ion batteries [73-76].

Cathode Material	Become Commercial [Year]	Specific Energy [Wh/kg]	Nominal Voltage [V]	Cycle Life [Cycles]	Market Status
LCO	1991	150-190	3.6	500-1000	The EV sector is not interested due to safety issues.
LMO	1996	100-140	3.7-3.8	1000-1500	Generally preferred for e-bikes, power tools,and medical devices.
LFP	1999	90-140	3.3	2000	Marginal role in EVs, while achieving better success in e-bikes.
NCA	1999	200-250	3.6	1000-1500	Used in EVs, and grid storage. Used by Tesla in its EVs.
NMC	2004	140-200	3.6-3.7	1000-2000	The major role in BEV and PHEV, while also being used in commercial electronic.

2.1.4 Future battery technologies

Studies to develop lithium-based battery technologies are continuing rapidly and new electrochemical battery chemistries are being developed. With the studies, it is aimed to reduce the price of lithium-based batteries and increase the gravimetric and volumetric energy density. In line with these goals, some of the most promising technologies are solid-state batteries (SSB), lithium-air (Li-air), and lithium-sulfur (Li-S) battery chemistries. SSB, one of the most promising Li-ion technologies, has a solid interface to realize ionic conductivity rather than an electrolyte solution. However, there is a problem of long-term stability and manufacturability, particularly low ionic conductivity at room temperatures. Solid-state batteries have higher internal resistance at room temperatures and must be heated to achieve sufficient ionic

conductivity. Since it consists of Li metal as an anode which is highly sensitive and reactive to many elements, utilizing SSB is challenging [77].

Another advanced technology, Li-S, is a prominent candidate for meeting high energy density requirements (up to 400 Wh/kg). Li-S battery uses lithium metal as the negative electrode. Li-S battery cells have a better cycle life and higher efficiency than Li-air battery cells. Due to the low cost of sulfur, Li-S batteries have a high potential to compete with other Li-based batteries. However, the Li-S battery has poor ionic conductivity inside the cell, low power density, and high self-discharge rates. Also, in Li-S batteries, the Li element accumulates as dendrites, creating the possibility of an internal short circuit inside the battery that could cause fire [78].

Another promising Li-air battery is a technology that is still in a fairly nascent stage and is currently only obtained under a laboratory environment. This technology stands out with its promised high energy density of up to 800 Wh/kg. A Li-air battery cell consists of a positive porous carbon electrode and a negative lithium metal electrode. By reacting lithium with oxygen from the air, much higher energy density can be achieved than other Li-Ion battery technologies can provide. This value comes from the lighter materials. However, as oxygen enters the cell during the discharge process, the weight of the cell increases [79].

2.2 Battery Systems for EVs

2.2.1 Voltage levels

Classification of voltage levels is specified according to EN 50110 standard for the generation, transmission, and distribution of electrical energy. Correspondingly, voltages up to 1000V AC and 1500V DC are stated as low voltage [80].

In contrast, the ISO 6469 standard, which is an international standard for electrically propelled road vehicles, covers with protective measures against electrical shock and classification of voltage levels of electric vehicles. As can be seen in Table 2.2, electrically propelled vehicles are divided into voltage classes A and B. Low voltage class is defined as letter A, which is rated as lower and equal to 60V DC and 30V AC. While voltage class B, which stands for high voltage, refers to voltages above 60 V DC and 30 V AC. These voltage levels are limited to 1000 V AC and 1500 V DC.

The components used for energy distribution (e.g., HV cables, busbars) of class B are generally color-coded orange. Moreover, B1 and B2 are subclasses of voltage class B. They split according to the special requirements specified in the same standard [9, 10]

Table 2.2 : Voltage classes [9].

Voltage Class	Maximum Working Voltage	
	DC in V	AC in V (RMS value)
A	$0 < U \leqslant 60$	$0 < U \leqslant 30$
B	$60 < U \leqslant 1500$	$30 < U \leqslant 1000$
B1	$60 < U \leqslant 75$	$30 < U \leqslant 50$
B2	$75 < U \leqslant 1500$	$50 < U \leqslant 1000$

2.2.2 Battery pack architecture

The vehicle battery system consists of separate, rechargeable cells connected in series and in parallel to achieve the desired system voltage and energy capacity. As aforementioned, the open-circuit voltage is between 3 V and 4 V depending on the active materials of the cell. For li-ion batteries containing Nickel-Manganese Cobalt (NMC) as a cathode material, the nominal cell voltage is around 3.7 V. The cut-off voltages and safety limits during cell discharge and charge are 2.6 V and 4.2 V, respectively. Cell cutoff voltages were taken into account to calculate the minimum and maximum pack voltage. Currently, available small and medium-sized electric vehicles on the road have a rated system voltage of around 400 V. This results in a series connection of about 100 cells (depending on the cell chemistry) which results in the 250–420 V DC-link voltage range. In contrast, sports cars and commercial vehicles have higher voltages up to 800V DC which results in the maximum DC-link voltage around 850 V. In this case, such system voltages can be achieved with about 200 cells in series. Higher voltage enables lower current demand at the same power level which in turn allows usage of smaller wires diameter [5]. Beyond that, the Lucid present a 924V battery pack with the new Air model [81]. The nominal voltage versus release year of the vehicles in the market are given in Figure 2.5 [81–91]. Since based on voltage class B states maximum voltage for EVs today as 1500 V DC. Vehicles with such high voltages are currently not commercially available on the market.

Battery packs are configured from cells to the module by connecting cells in series and parallel then modules are connected in series and parallel to form a battery pack.

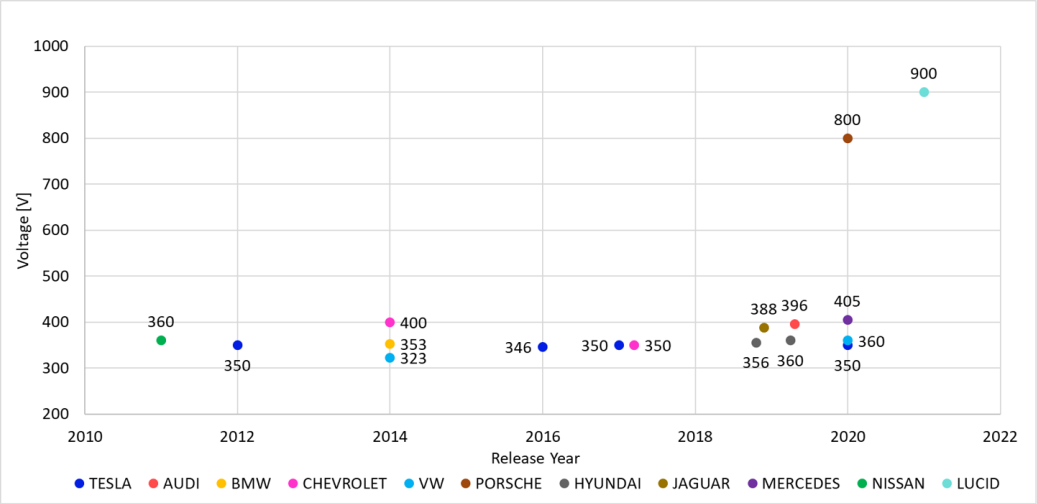

Figure 2.5 : Nominal battery pack voltage based on release year [81–91].

However, there are several vehicles on the market which has a cell to pack structure. Optimization of the size of the module is investigated in [92]. While connection cells in series raise the output voltage, parallel connection of cells leads to an increase of the output current and energy capacity. An EV HV battery architecture is given in Figure 2.6.

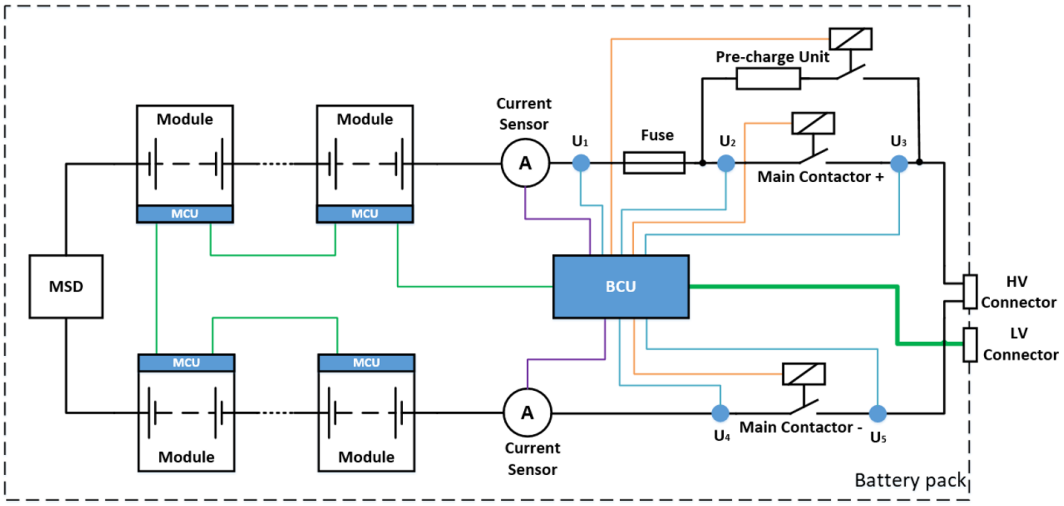

Figure 2.6 : The architecture of EV HV battery pack.

The battery is actively controlled by the BMS. General BMS functions are given in Figure 2.7. BMS consists of two main components which are BCU (battery control unit) and MCU (module control unit). Generally, MCU responsible for communication to BCU, measurement of individual cell voltages, measurement module temperatures, and cell balancing. On the other hand, BCU provides functions such as communication and supervisory control of the modules, high voltage measurement, pre-charging

control, isolation detection, current measurement, control over main contactors, control over cooling components, forced shutdown, abuse protection, diagnostics, etc. Moreover, the main contactors connect and disconnect the battery to the rest of the vehicle. On start-up, the pre-charge unit limits the inrush current due to the DC-Link capacity. The main fuse protects against fault currents such as a short circuit. Manual service disconnect (MSD), which is a service switch and shall be accessed from outside of the battery. There are current sensors for current measurement. Lastly, HV and LV connectors connect to the rest of the vehicle with the battery [71].

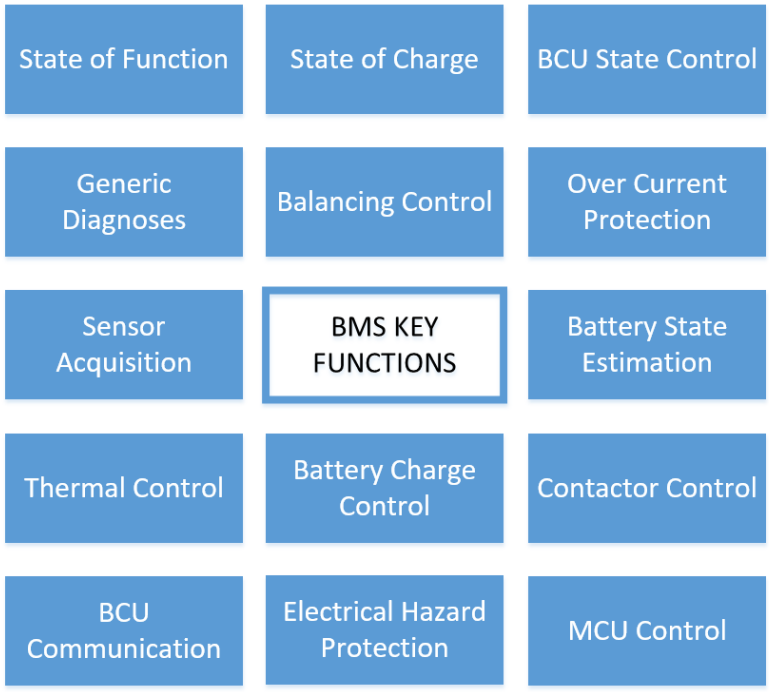

Figure 2.7 : Key functions for BMS.

2.2.3 Review of standards

With the increasing demand for electric vehicles, international standards have been developed in parallel with EV development to ensure protective measures to electrical safety, mechanical robustness, environmental withstand, and functional safety compliance. The relevant standards for this study are covered in this chapter as an overview.

– IEC 60664 -1: Insulation coordination for low-voltage supply systems: Principles, requirements, and tests: The standard deals with the insulation coordination for LV supply systems up to 1000 V AC or 1500 V DC. The definitions and the principles

can be applied for electric vehicles to avoid hazards such as electrical shock based on requirements like clearances, creepage distances, and criteria for solid insulation [93].

– ISO 6469 - 1/2/3: Electrically propelled road vehicles - Safety specifications: The standard deals with safety requirements for rechargeable energy storage systems (RESS) for the protection of persons inside and outside of EVs. Part 1 covers the safety requirements for RESS systems of EVs [10]. Part 2 specifies the requirements for operational safety measures and protection against failures for EVs [94]. Part 3 deals with the requirements of the components inside the EVs for the protection of persons against electrical shock [9].

– ISO 26262: Road vehicles - Functional safety: The standard deals with methods and requirements provided for the functional safety of electric and electronic components in vehicles. In the standard, each system function is classified into the Automotive Safety Integrity Level (ASIL) from A to D, where D is the highest classification level [95].

– ISO 16750 Road vehicles—Environmental conditions and electrical testing for electrical and electronic equipment: The standard guides environmental conditions related to electrical and electronic systems installed in vehicles. The standard has 5 chapters, which consist of general, electrical, mechanical environmental, and chemical requirements [96].

– AEC-Q101 Failure Mechanism Based Stress Test Qualification For Discrete Semiconductors: The standard defines stress requirements and conditions for discrete (active) electronic components such as transistors used in automotive applications [97].

3. SHORT CIRCUIT FAILURE IN BATTERY SYSTEM

3.1 Introduction

The short circuit is the most prevailing cause of a fault current in the automotive battery system. A short circuit can be caused by an internal or external fault. Considering at the cell level, an internal short circuit occurs when the insulating separator layer between the electrodes fails. Electrode fail can be caused by aged cells or external factors. On the other hand, an external short circuit occurs when the battery tabs are connected by a low resistance path. Both failure types will cause a high amount of current flow through the anode current collector to the cathode current collector. As shown in Figure 3.1, Both internal and external short circuits, cause an undesired connection of the current collectors. As a consequence of this failure, a short circuit current flows between the electrodes [98].

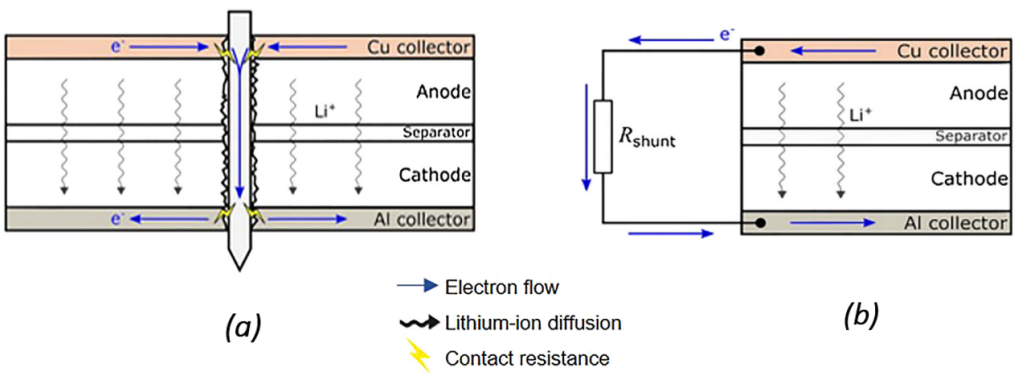

Figure 3.1 : Electron movement on short circuit (a)internal (b)external [98].

Both short circuit scenarios can result in a very high amount of energy discharge for a short amount of time. Thereupon, this will constitute high heat generation in the cells [99]. Since the heat in short circuit conditions will be rise rapidly, it is most likely leading to thermal runaway. Whether cells will come to thermal runaway or not is related to the difference between heat generation and heat dissipation. If heat generation is much higher than dissipation, the remaining heat will cause a temperature

rise on the cell [98]. If the cell reached a limited temperature, it will lead to a thermal runaway. Since heat generation increasing exponentially, whilst the rate of heat dissipation increases linearly. Therefore, after the short circuit fault occurs, it cannot be overcome without damage [100]. Thus, inevitable thermal runaway causing fire, gassing, and explosion due to exothermic reactions [101, 102]. Heat dissipation is depending on the thermal durability of the cell and the design of the cooling system [103].

3.2 Characteristics of Short Circuit in EV Battery Packs

The maximum value of short circuit current is depending on the maximum voltage and the minimum equivalent impedance of the circuit. Moreover, increasing the speed of the short circuit current is related to the inductance of the circuit. Considering the short circuit fault at the pack level rather than a single cell individually, since the HV battery packs are created by cells connected in series, short circuit currents up to kA level can be seen. It is very important to handle the currents as quickly as possible at these current levels. Since there is a limited time that each component can withstand a short circuit current, switching elements must be utilized according to the duration and magnitude of the current to protect against the fault. The location of the short circuit fault will determine the characteristics of the fault current.

Increasing power demand leads to developing HV battery packs more widespread. Producing components that can be used in an HV battery pack is becoming much more difficult from the perspective of product development. Components used in the battery pack need to be utilized to work on not only normal operating conditions but also withstand fault currents that can be occurred in the pack. Protection of the pack in case of overcurrent is called the shut-off strategy. The strategy is designed by considering the safety specifications of components and managed by BMS. To achieve the proper shut-off strategy for the battery pack, each component shall be considered. Electromechanical contactors, melting fuses, current sensors, HV connectors, conductors (busbars, cables), and even isolation tapes can affect the overall system's safety performance by creating a drawback. Therefore, the weakest component can cause failure. As can be seen in Figure 3.2, the utilization of components is based on current zones. Those zones are defined based on maximum

short circuit current, components current carry capabilities, switching capabilities of switching elements as well as defined load profile. Switching components will be detailed in the next chapter. However, as a foresight contactor can switch-off lower currents (yellow area) to ensure sustainability, while fuse cutting-off high currents (red area) where the relay only can carry but can't switch off [104]. To validate the shut-off strategy, the switching components such as contactor and fuse shall be tested for different current values for a defined amount of time.

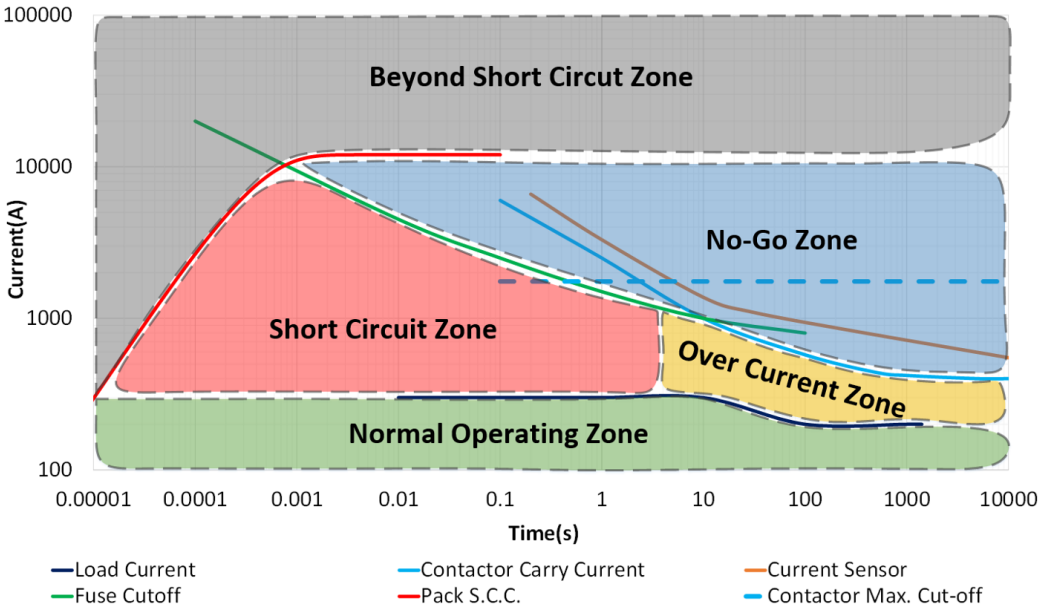

Figure 3.2 : Current zones in HV battery pack [104].

As seen in Figure 3.3, there is a high possibility of two types of short circuits can occur for battery packs in automotive battery systems. One of them is between HV Path and ground, and the other one is between HV+ and HV- paths. Fault between the HV paths typically has low fault impedance, total short circuit impedance is limited with only cell, component, busbar, and wiring resistances. While the path to ground fault can have either low impedance or high impedance, depending on the short circuit point.

Path to ground faults are less critical, but most frequent. Therefore, those faults can be detected and handled with an isolation measurement circuit. Eventually, the path-to-path faults creates the highest fault currents to the battery system, short circuit calculation, and short circuit protection are performed based on this case.

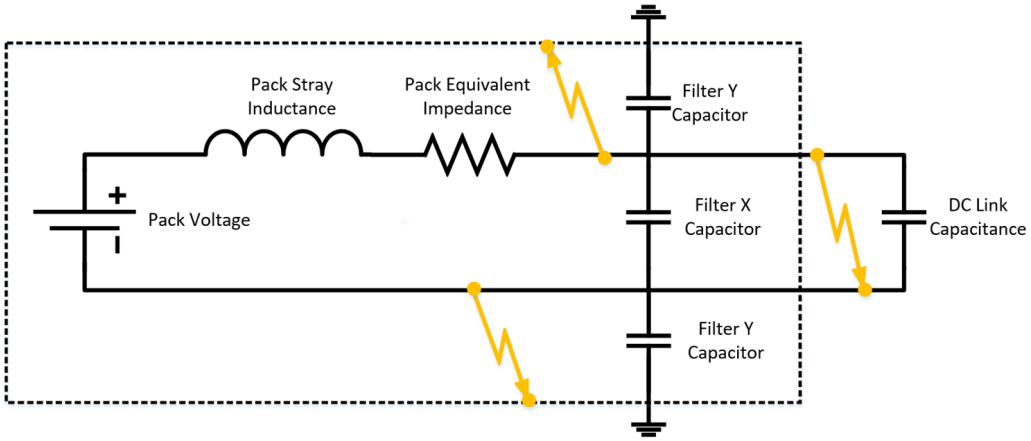

Figure 3.3 : Possible short circuit faults in battery systems.

Before deciding how to handle the short circuit current, the maximum short circuit value must be calculated. For calculation, the equivalent system circuit in Figure3.3 is used. The minimum internal resistance value (R_{DCIR}) of the cells, the resistance values of the components (R_{COMP}), the resistance values of the busbars (R_{BUSB}), and the resistances to be formed from the connections (R_{CONN}) used to calculate the total equivalent resistance (R_{PACK}) as given in Equation 3.1. This resistance will be the minimum possible equivalent resistance value.

$$R_{PACK} = ((R_{DCIR} + 2 * R_{CONN}) * ns/np) + R_{BUSB} + R_{COMP} \tag{3.1}$$

Moreover, with the maximum possible voltage (V_{MAX}) value of the pack, the maximum short circuit current value is calculated as given in Equation 3.2.

$$I_{MAX} = V_{MAX}/R_{PACK} \tag{3.2}$$

Besides the maximum value, the instantaneous current value (I_{SSC}) is important. When the instantaneous value is examined, the increase in short circuit current can be calculated like a simple R-L circuit. The instantaneous current value can be expressed for DC sources such as battery packs as given in Equation 3.3.

$$I_{SSC} = I_{MAX} * (1 - e^{-t/\tau}) \tag{3.3}$$

Maximum fault current depends on the equivalent impedance between the respective source and the fault location. Moreover, how fast will this current have reached the maximum value is also crucial regarding the safety concept. Therefore, the time constant of the equivalent system is important and can be expressed as in Equation 3.4.

$$\tau = L/R \tag{3.4}$$

R and L are equivalent resistance and inductance of the circuit, respectively, which are calculated from the source to the fault position. The inductance value is approximately 30µH for 400V HV battery packs [105]. Therefore, to ensure proper safety when interrupting fault currents, protection devices must have a short response time. The fault current at the short-circuit point is needed to deal with based on the superposition principle in case there are packs connected in parallel.

Battery packs are connected to a power electronics component for both charging and discharging operations. These power electronics components are usually equipped with a filter capacitor. When the fault occurs on the battery pack terminals, a high amount of reverse inrush current will flow with a small time constant. However, since this current will flow charge direction instead of discharge direction, the responsibility of this kind of short circuit interruption is not taking into consideration in this study.

3.3 Utilization of Protective Devices for EV Battery Packs

As mentioned in the previous chapter, the HV contactor and fuse are used as switching components in automotive battery systems. While fuses can be melting, a pyro, or even smart, the contactors can be electromechanical, solid-state, or a hybrid combination of the two. In EVs, contactors inside the battery are utilized to connect and disconnect the battery from the vehicle drivetrain. In HV battery systems, two contactors are used to switch both, the positive and the negative HV path as can be seen in Figure 3.4. This is concluded in order to achieve redundancy according to functional safety measures [95], to achieve homogeneous switching behavior, and provide a galvanic separation of the battery pack from the rest of the powertrain.

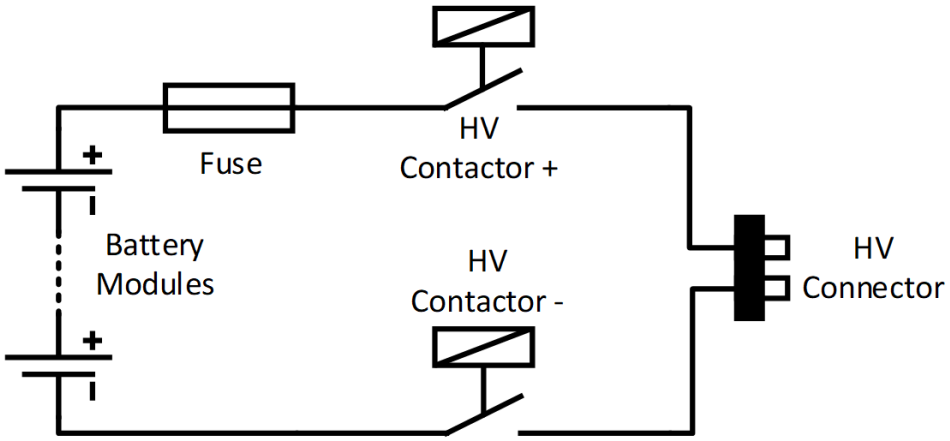

Figure 3.4 : Switching components inside HV battery pack.

When the vehicle starts, the contactors connect the battery to the rest of the powertrain with commands from the BMS. The contactors shall remain closed during both charging and discharging operations and disconnect the battery after the vehicle is turned off. Under normal operating conditions, contactors will not be switched under the electrical load. But there are events when they need to disconnect under electrical load. Contactors can make and break up to a certain fault current, this point is called the maximum switching current of contactors. The phenomena behind such limitations are contact erosion, contact welding, and arc movement of the contactor. The possible number of switching operations of the contactors is also limited depending on the electrical load [18]. However, the battery system must be protected from currents that the contactors are not capable to safely switch off. Over-current protection up to maximum short-circuit current shall be ensured by a fuse, which cuts off large fault currents before any other component is damaged. Under normal operation conditions, the fuse shall carry the operating current without aging or early trigger. Thus, the fuse dimensioning is curial with consideration of the load demand from the pack. Breaking in the event of an overcurrent or short-circuit, the fuse will break the fault current. The breaking process consists of phases of pre-arcing (melting) and arcing. If the thermal energy correlated with the current, is higher than the fuse can absorb, the fuse may explode [106].

Today, very solid studies regarding switching performances have been carried out on automotive battery systems at 400V [18]. However, the high-power requirements bring to the necessity of higher voltage battery packs around 800V [5] and switching

components. Both the high voltage and high current requirements bring bulky components. Not only weight and volume problems but also switching stresses on these components are increased, especially due to voltage level. Hybrid solutions have been developed to minimize the switching stresses on these components. In the usage of hybrid switches, the mechanical switch is solely used for switching without load and can be small in size and weight. The semiconductor, however, creates additional losses during conduction [107]. However, these solutions bring complexity to control.

3.4 Comprehensive Analysis of Protective Devices Technologies

In automotive battery systems, various switching elements are used. Those components can be controlled or uncontrolled. Among these components, the contactor and the melting fuse are utilized in the battery packs of many electric vehicles. As aforementioned, the shut-off concept created by the alignment of contactor and fuse is preferred due to their maturity. However, recent development has brought that, contactor or melting fuses can be replaced with pyro switches [14, 15] or smart fuses [17] in HV battery systems. For example, in the study [16] pyro-fuse clears 1200V short circuit in 2ms which is much faster than the conventional system.

The recent development of semiconductor technologies shows that semiconductor relays might be replacing electromechanical contactors in near future. As semiconductor circuits not only bring advantages in normal operation and fault current interruption but also with bidirectional current control features. It enables to control of the in-rush current at the pre-charge event, the recuperation current, and the equalization current between parallel packs in the case of a modular battery system.

Considering the use of semiconductor-based switches in the battery pack, one of the most important issues is the current-carrying capacity. Especially in today's sports vehicles and commercial vehicles, a high amount of power will result in high current at high voltage battery systems. Even though, current carry requirements can be fulfilled by components, switching performance at fault currents creates a bottleneck. As seen in Figure 3.5, depending on the size, design, and switching cycles, electro-mechanical contactors on the market sits on the red-dashed line as an average.

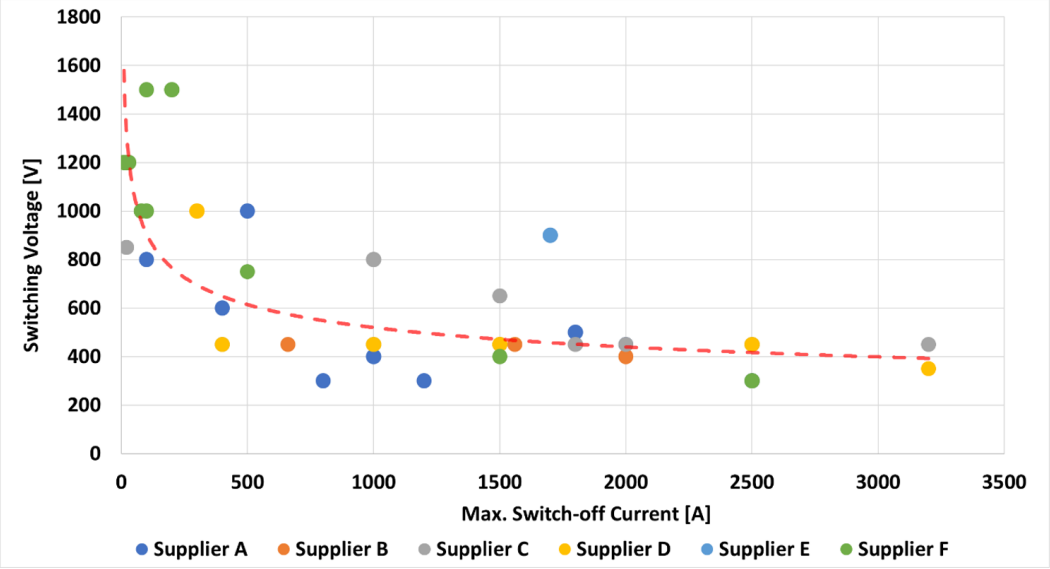

Figure 3.5 : Switching capability of electromechanical contactors.

Even if they increase their switching power with hybrid switching methods, they are still weak against the mechanical requirements such as vibration and shock. Therefore, high electrical, environmental, and mechanical performances, have greatly paved the way for the replacement of electromechanical contacts with semiconductor switches. Considering that they are widely used in low voltage battery packs [22–25], it is possible to see solid-state switches in the HV packs with rapid development in semiconductor technology.

3.5 Solid State Relays

As achieved with electromechanical contactors, all make, and break functions can be achieved with solid-state relays (SSR). The biggest advantage of SSRs are not having moving mechanical parts within them. They are electrical switching devices that rely on the electrical, magnetic, and optical properties of semiconductors and peripherals components to achieve their functions. The control methods of SSRs are similar to electromechanical contactors. Both use an internal or(and) external driving circuit for switching. When SSRs are driven with a voltage applied to its input (as can be seen in Figure 3.6 they are generally driven by optically energized light-emitting diode) the SSR turns into an ON state and allows current flow. In case of the removal of the input voltage, the control circuit is disabled and the SSR turns into an OFF state, thus load current flow stops.

Even though electromechanical contactors are widely used in all industries and have proven sufficient maturity in systems requiring high power, there are still many drawbacks such as slow response, presence of moving parts, noise, power consumption, short life cycle, electric arcs, bulky size, and weight. Those drawbacks are can be overcome by utilizing semiconductor-based devices [108].

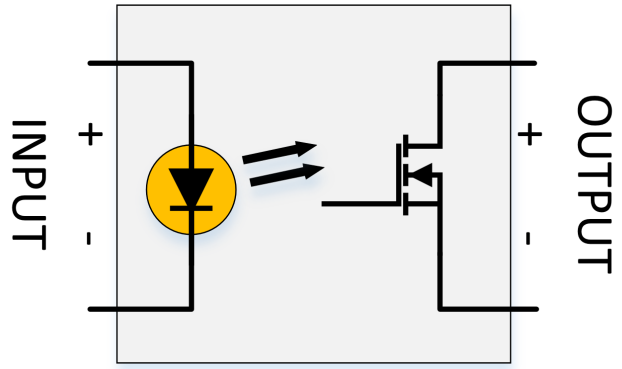

Figure 3.6 : Typical SSR circuit.

SSRs need to be bidirectional in some DC applications as well as in AC applications. Especially in battery systems, it must be bidirectional in order to operate in both charge and discharge directions. Thus, the inner structure of the SSR varies according to the semiconductor used. For example, an Insulated-gate bipolar transistor (IGBT) is a unidirectional device. Therefore, it can only flow current in the forward direction (from Collector to Emitter). An anti-parallel connection of IGBT's or anti-series connection IGBT + Reverse Diode structure enables bi-directional voltage blocking and a current flow like SiC MOSFETs [108]. Therefore, as can be seen in Figure 3.7 they can be connected reverse series or anti-parallel to achieve bi-directional current flow and switching ability. Although structural differences have advantages and disadvantages compared to each other, SiC MOSFETs are frequently used within the SSR.

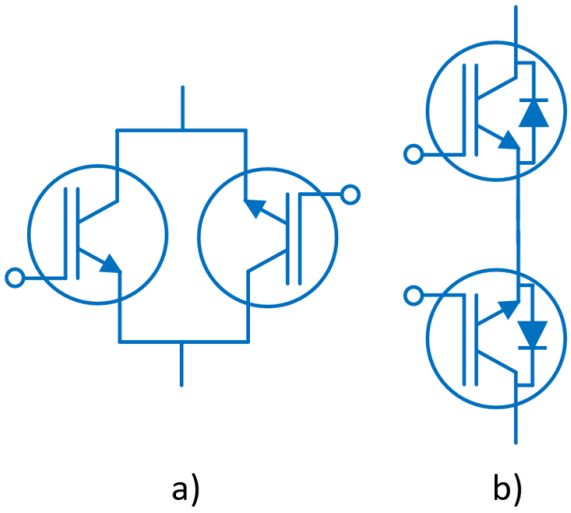

Figure 3.7 : Bi-directional connection of IGBTs a)Anti-parallel b)Reverse-series.

Due to zero voltage turn-on and zero current turn off, SSR generates low electrical noises, despite that electromechanical contactors generates switching noises as a result of a mechanical structure. Moreover, SSRs are more durable against shock and vibration and they do not cause unwanted operational errors such as electromechanical contactors due to external forces. Additionally, the response time to control signal of electromechanical contactors are between 5-15 ms [18], response time is less than 1 µs for SSRs depending on the semiconductor used [108]. Thanks to this feature, they can respond quite fast to fault currents. Despite these advantages, the relatively high semiconductor conduction loss remains a major drawback of the SSR against electromechanical contactors. Correlation with these conduction losses it is also less redundant to heat and requires a cooling system. As a result, SSRs are more dynamic based on performance and they feature more functionalities compared to electromechanical contactors. However, as aforementioned electromechanical contactors have the advantage of thermal durability. Even so, in case of usage of the colling system, which increases the overall upfront cost, SSRs can be used instead of electromechanical contactors.

4. POWER SEMICONDUCTOR DEVICES IN SOLID-STATE RELAY

4.1 Introduction

Power semiconductor switches are the fundamental components in the SSR. Characteristics of semiconductor devices affect directly the quality, efficiency, and reliability of SSR. Until quite recently, Si has been the pioneer semiconductor for power electronics applications [27]. With their fast development, the production and performance of Si semiconductors are optimized and reached their limit in power electronics [28, 109]. Moreover, using WBG semiconductors has brought improved efficiency, reduced size, and lower overall system cost against Si devices. [28, 29].

SiC and GaN are the best promising WBG semiconductors on the market as off the shelf available. Although GaN is gained importance due to its quite remarkable high frequency switching performance, SiC is much more successful in terms of high temperature, high voltage, and short circuit capabilities, which is especially important for SSRs. The reasons behind the advantages of SiC materials are high breakdown electric field strength, the high saturated drift velocity of electrons, high thermal conductivity, and lower intrinsic carrier concentration [110]. Therefore, these properties make SiC ideally suited for a vast number of high-power applications. With those material-based advantages, SiC-based semiconductor applications are decreasing the size of the passive components and bulky cooling units such as heat sinks, by that lowering the total volume, weight, and cost of the switching device [28, 29]. Additionally, those advantages of material brought the specifications of lower on-state resistance, high frequencies switching, and higher temperatures operation [111].

Nowadays, SiC is considered to have high commercial maturity. Therefore, it has the best trade-off between other materials. Not only maturity but also considerable potential for both high-temperature ability and high-power withstand makes SiC devices preferable. Moreover, the industrial interest for GaN power devices is

increasing recently for high-speed switching necessities. For this reason, SiC and GaN are the more attractive candidates to replace Si in future applications.

In addition, the theoretical advantages of C (diamond) material is not only superior to Si but also other WBGs. However, there are some drawbacks of C that make it not preferable. First of all, production technology for this material less mature and much less developed than for SiC and GaN. Secondly, the thermal expansion coefficient for C is very low [112]. So, there is a thermodynamic mismatch. Lastly, the diamond is one of the most expensive materials, which makes costly devices. As aforementioned, when GaN and SiC are compared to C, they are also well suited for most of the applications, besides they provide better thermodynamic strength. Therefore, there is no diamond-based power device in the market, and it seems it will not be in the next decade.

4.2 Comparison of Semiconductor Materials

A comparison of semiconductor materials based on their fundamental properties is given in Table 4.1. WBG semiconductors have many advantages over Si. Between SiC materials, as given on the table based on the properties, the 4H poly-type of silicon carbide has been superior to the other poly-types of silicon carbide. Comparison of semiconductor materials is also given in Figure 4.1 as a summary.

Table 4.1 : Properties of major WBG materials [28,31].

	Si	**SiC (3C)**	**SiC (6H)**	**SiC (4H)**	**GaN**	**C**
Band Gap Energy (eV)	1.14	2.36	3.02	3.26	3.39	5.62
Breakdown Field / Ec (MV/cm)	0.3	1.4	1.7	2.2	2.0	10
Thermal Conductivity (W/cm.K)	1.5	4.9	4.9	4.90	1.3	20
Coefficient of Thermal Expansion (10^{-6}/°C)	2.6	2.8	5.1	5.1	6.4	1.0
Electron Saturation Velocity (10^7cm/s)	1.0	2.0	1.9	2.2	2.0	3.0
Electron Mobility (10^3cm^2/V.s)	1.45	1.0	0.42	1.02	2.0	4.0
Melting Point (1000°C)	1.67	2.10	3.10	3.10	2.73	4.30

Electron mobility is an indicator of high frequency switching capability [113]. Therefore, GaN devices are capable of operating at high frequency due to high electron mobility. Correspondingly, there is a transistor is called a high electron mobility transistor (HEMT) which is based on GaN [114]. Saturation velocity is the maximum velocity of a charge carrier in a semiconductor. When the velocity is no longer found to increase in proportion to the electric field, the velocity approaches a constant value known as the saturated drift velocity [115].

Bandgap energy generally refers to the difference of energy between the top of the valence band and the bottom of the conduction band. Bandgap energy (eV) is a major factor determining the electrical conductivity of material [30]. Wider the bandgap, the higher the high-temperature operation ability and smaller impact ionization coefficients at any given electric field. It is defined as the number of electron-hole pairs created by a hole traversing 1 cm through the depletion layer along the direction of the electric field. Smaller impact ionization coefficients create a high localized electric field. Therefore, a much larger critical electric field occurs, and this leads to a larger breakdown voltage [31].

Breakdown field or critical electric field indicates the highest possible electric field value. Higher electric breakdown field and higher doping density lead to reduced drift region and achievable high junction temperatures. Thus, these result in much lower on-resistance and larger breakdown voltage. For example, at the same doping density, the theoretical breakdown voltage of a Diamond diode is 514 times higher than that of a Si diode and on-resistance of SiC polytypes and GaN devices is approximately 10 times less than that of Si devices [112].

An increase in temperature generally leads to a change in the physical properties of the device, which normally negatively affects the device. The coefficient of thermal expansion (CTE) indicates the change in length or volume of a material for a temperature change. Therefore, as aforementioned CTE for Diamond is 0.8 ppm/k which is very low as compared to other materials [112]. A material's thermal conductivity is the ability to transfer heat through itself. The high thermal conductivity of SiC allows for more efficient heat transfer from the heat sink and yields a lower junction temperature [113]. Thermal conductivity impacts the material's temperature withstand. In high-power applications, due to inefficient productions, the materials'

junction temperature increased thus, subsequently changing its electrical properties. For example, GaN has a thermal conductivity of 1.3 W/cmK, which is almost the same as Si. However, SiC superior to those two with thermal conductivity of 5 W/cmK, making itself, better at transferring thermal loads. This feature makes SiC highly worthwhile in high-power and high-temperature applications [116].

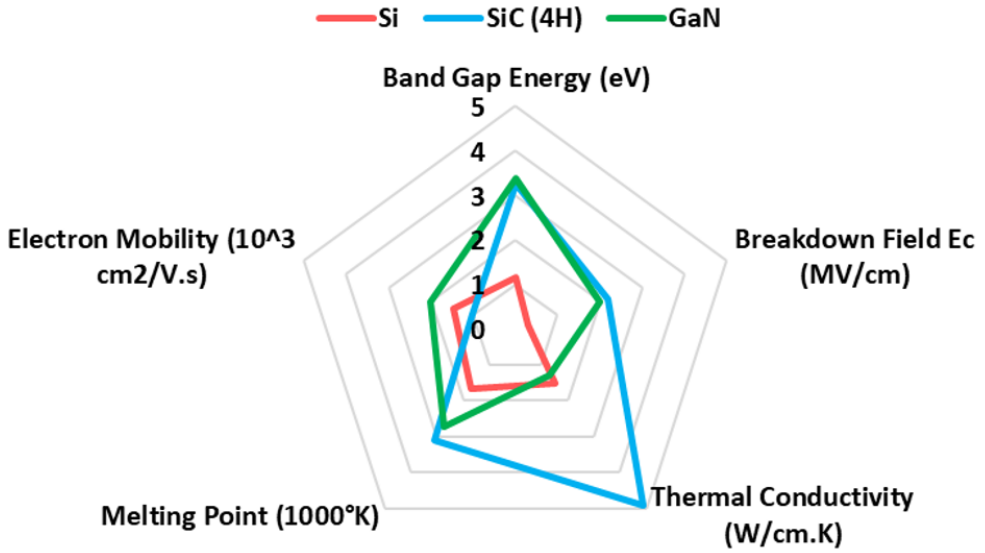

Figure 4.1 : Comparison between SiC, GaN, and Si.

4.3 Structure of SiC Devices

In high power applications, silicon carbide (SiC) semiconductor devices have proven their maturity. Therefore, they are frequently available commercially both as discrete and power modules. These commercial devices are mainly found in 3 main structures, SiC MOSFETs, SiC junction field-effect transistors (JFETs), and SiC Bipolar Junction Transistor (BJT). Figure 4.2 shows the switching ratings of SiC active switches available in the market as discrete devices [117–119].

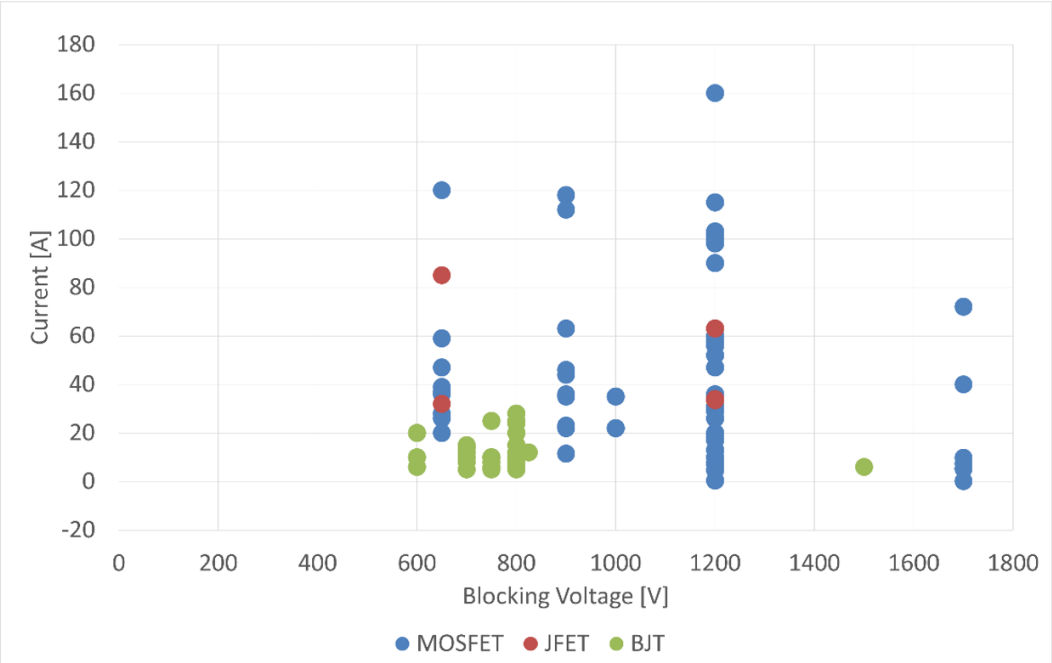

Figure 4.2 : Off-the-shelf discrete SiC switch ratings @25°C [117–119].

4.3.1 SiC MOSFETs

The most popular SiC switch is MOSFET. It is highly preferred in the industry, especially in the automotive industry. MOSFET is a gate-source voltage control transistor. It has a structure that separates the silicon dioxide insulation material and n-channel or p-channel from the metal oxide gate electrode. As can be seen in Figure 4.3, they have 2 main structures, the first one is planar (D-MOSFET) SiC MOSFET and the other is trench (U-MOSFET) SiC MOSFET [32].

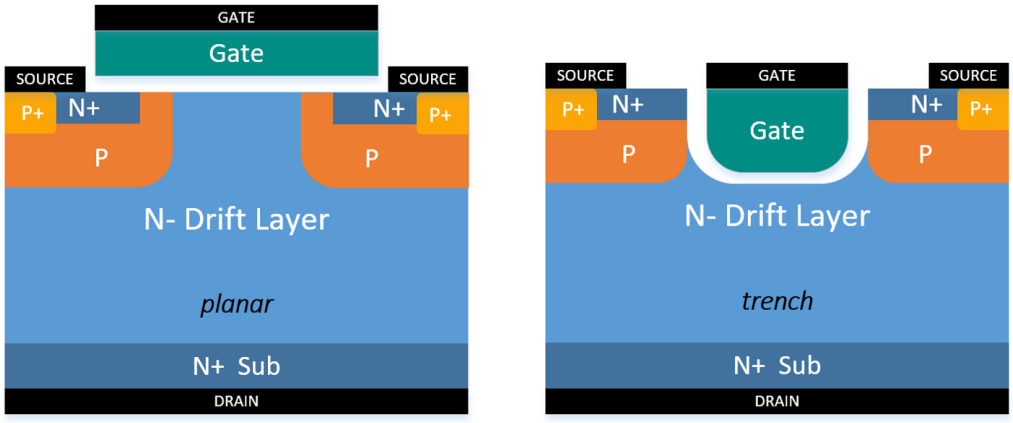

Figure 4.3 : Cross-section of SiC MOSFET structures [Based on 32].

The biggest problem in applications is the gate-oxide reliability in low specific on-resistance. Especially in the trench (U-MOSFET) oxide field rises more in the corners and causes failures. Therefore, the blocking voltage of the trench is limited. To avoid this problem, a double-implanted planar (D-MOSFET) has been introduced and the blocking voltage has been increased [120]. The on-resistance of the SiC MOSFET has three main aspects: JFET region resistance, channel resistance, and drift region resistance [121]. Another problem is the low channel mobility thus, the actual specific resistance is more than normally required [120]. This drawback can be improved by increasing the channel density. With the trench (U-MOSFET) structure seen in Figure 4.3, the JFET region is eliminated and channel density is improved. Hence the specific on-resistance decreases. For this reason, the trade-off should be considered in order to select an optimum structure.

4.3.2 SiC JFETs

Previously, SiC JFETs were preferred more because of their easy applicability and gate-oxide problem seen in SiC MOSFETs [32]. However, their normally-on nature was not found suitable by many applications, especially as an automotive battery switch. However, with the cascade structure, this problem has been eliminated. SiC JFETs are also voltage controlled devices, they are structured by a carrier consisting of P-type or N-type silicon carbide called channel that creates a connection between drain and the source electrically. A significant structure related difference between the JFET and the MOSFET is that the MOSFET is normally-off, whereas the JFET can be either normally-on or normally-off. There are two types of JFET used in the market. The first is the lateral-vertical JFET (LV-JFET), this JFET vertical channel in combination with the lateral of the drift region. The other consists of a completely vertical channel called a vertical JFET (V-JFET). It exists in the system consisting entirely of horizontal channels, but it is not available in the market. While SiC LV-JFETs are only normally-on, V-JFETs can be found both normally-off (enhancement-mode) and normally-on (depletion-mode). The cross-sections of these JFET structures are shown in Figure 4.4. Since LV-JFET is normally on, they require a negative voltage lower than the threshold voltage to turn-off. Small gate and drain areas in LV-JFETs reduce the shaft capacitance and provide an advantage in switching speed. In contrast,

V-JFETs offer advantages such as low on-state resistance and high integration density. Therefore normally-on JFET offers a higher saturation current.

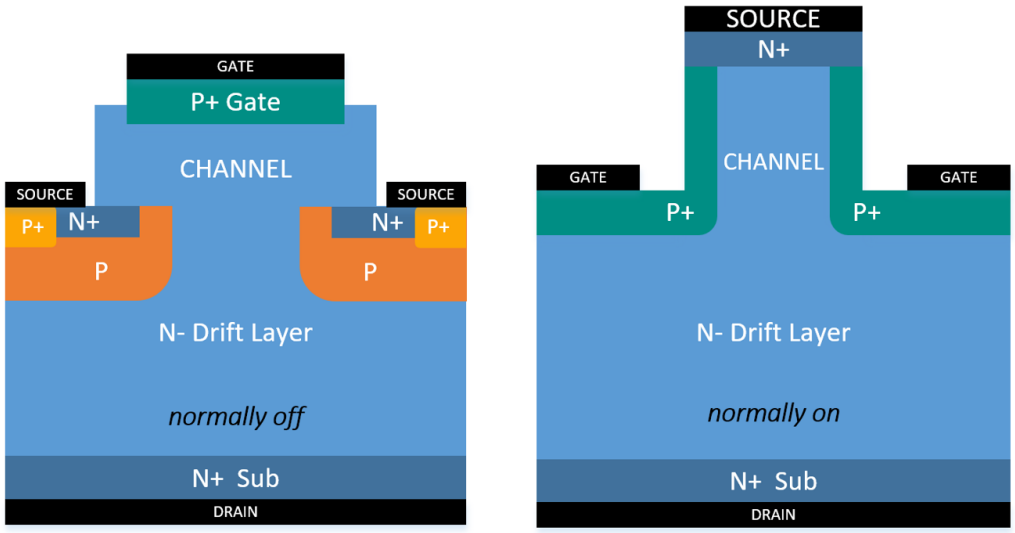

Figure 4.4 : Cross-section of SiC JFET structures [Based on 31].

4.3.3 SiC BJTs

The switching speeds of SiC BJTs are close to MOSFETs. Due to the lack of base-emitter and base-collector junction voltages, there are low transmission losses in saturation mode. Therefore, they can achieve high switching speeds. Plus, BJTs do not have channel regions. Therefore, their on-resistance is lower than SiC MOSFETs. However, their current-driven control specification makes them less preferred for some applications. The SiC BJT is a current-driven semiconductor, so a continuous base current is required for the collector current to flow. Another problem with BJTs is bipolar degradation that occurs when exposed to high-temperature stress for a long time. Bipolar degradation also causes the collector-emitter voltage to increase and the current gain(β) to decrease. SiC BJTs structures are shown in Figure 4.5.

4.4 Ruggedness and Reliability of SiC Devices

Ruggedness and reliability of SSR are still a big concern for automotive HV battery system applications. The reliability of an SSR is firmly dependent on the reliability of semiconductor switches used. When the electrical absolute maximum limits of semiconductors have exceeded that results in destruction. Such limits can be addressed

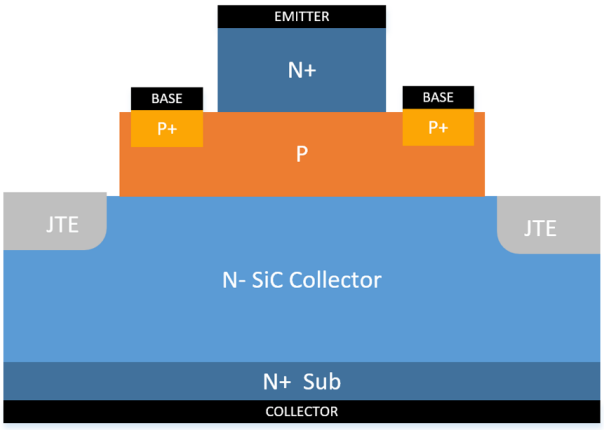

Figure 4.5 : Cross-section of SiC BJT structure [Based on 31].

from many angles. However, three main faults result in destruction or degradation. The first one is usually an overcurrent error resulting from a short circuit that causes a faster than expected current increase. Secondly, an overvoltage error that will cause avalanche puncture by producing new electron/hole pairs and multiplication mechanisms, and finally a high current error in the gate of the semiconductor.

As can be seen in previous chapters where the materials are compared, SiC material is by far the most successful for applications with high power requirements. By means of unique thermal properties depending upon thermal conductivity and thermal capacity, it is expected they also have superior short circuit withstand. However, when it comes to comparison between semiconductors not only the material but also the structure of the semiconductor device influence the device's reliability and ruggedness. The snubber circuit can be used to eliminate the overvoltage failures, and the correct driver circuit and a properly adjusted gate resistor can be used for gate mode failures. However, a special current protection method is required for overcurrent failures.

4.4.1 Short circuit robustness of SiC devices

Many studies have been carried out on the short circuit protection of SiC devices [33–37]. One of the dedicated test circuits is shown in Figure 4.6. Tests were made at 600V DC level in the study [33] with 1200 V SiC MOSFETs and normally-off SiC JFETs.

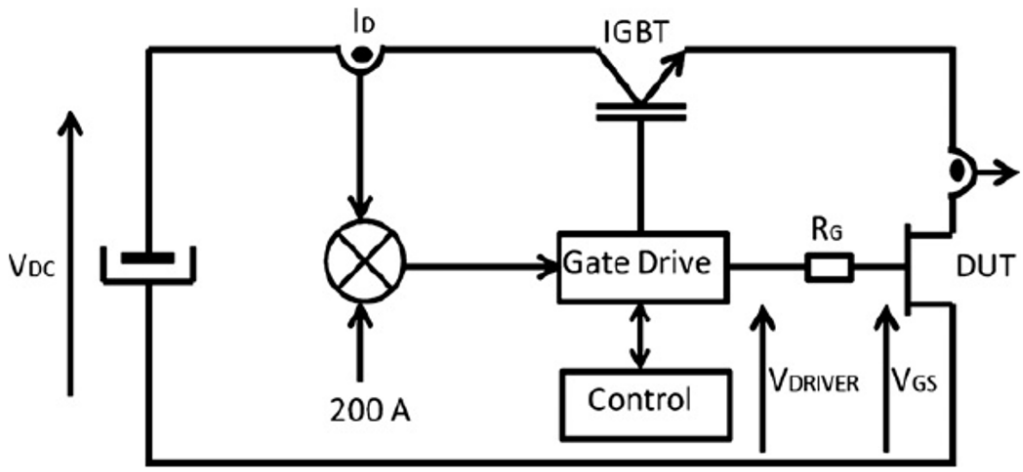

Figure 4.6 : Test setup used for short circuit analysis [33].

In the test performed on SiC MOSFETs, the first device failed within 16µs and 761 mJ energy was dissipated. However, the fault was associated with the gate-source, the short circuit between the drain-source resulted in a thermal runaway after 21µs. Another test with SiC MOSFET resulted in failure at 13µs. However, both show a significant amount of leakage current after 5µs. This situation indicates that the change in the gate-source voltage seen in Figure 4.7 causes degradation between the gate and source electrodes. As the third of the same tests with normally-off SiC JFETs, the component withstood the short circuit for 1.17 ms with an energy dissipation of 122 mJ.

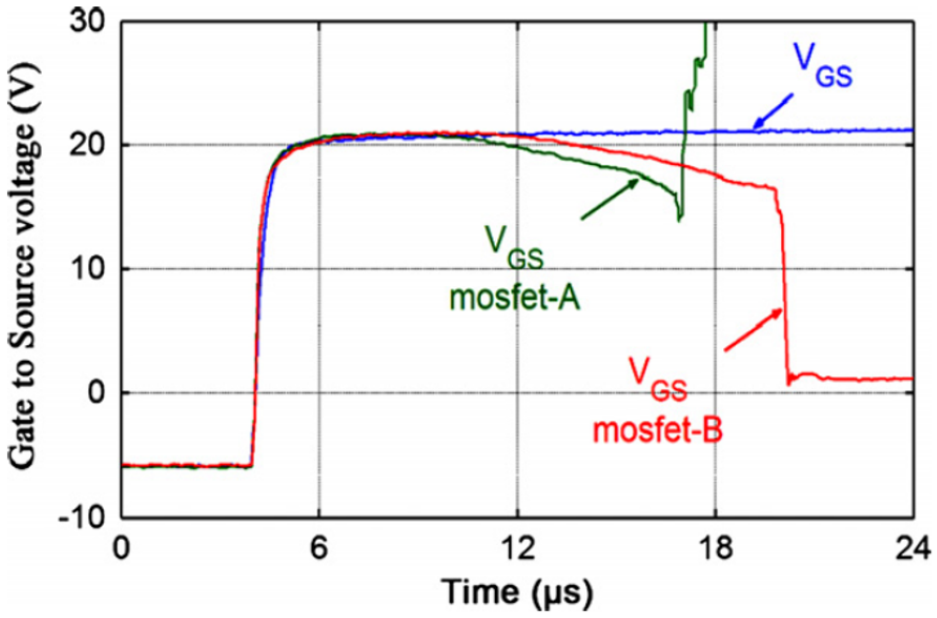

Figure 4.7 : V_{GS} for MOSFETs at destructive short-circuits [33].

In the study [34], 1200V / 0.1Ω SiC MOSFETs and normally-off SiC JFETs were characterized from room temperature to 125°C and subjected to short circuit analysis with 400VDC. As a result of these tests, SiC MOSFETs have shown 80µs short circuit resistance at 10V gate voltage and 50µs at 15V gate voltage. On the other hand, normally-off SiC JFETs showed 1.44ms short circuit resistance. The study [34] made a theoretical short-circuit strength comparison by characterizing the semiconductors, whereas the study [33] revealed a finding with higher voltage and real test results. However, both tests did not examine the temperature-dependent short circuit characteristic and the related fault mechanism behind short-circuit failure.

In [35] thermal characteristics of SiC MOSFET were investigated experimentally and both thermal generated current induced thermal runaway and high temperature linked gate oxide failure used to exhibit short-circuit failure mechanism. In the same study, 1200V SiC MOSFETs were used. Devices have the same on-resistance. However, their current ratings and die sizes are different. In this study, tests are performed at 600V DC, as seen in Figure 4.8. The first tested MOSFET with case temperature Tc = 25°C, withstands 11.5µs short circuit current under full load, this duration decreases to 10µs at Tc = 200 °C. For the same device, this period decreases to 6.6µs under Tc=200°C at 750V DC voltage. Same tests performed on a different MOSFET, this device showed withstand both Tc=25°C and Tc=200°C 8µs at 600V DC. However, when 750V DC is applied at Tc=200°C, it withstands the failure duration of 5µs.

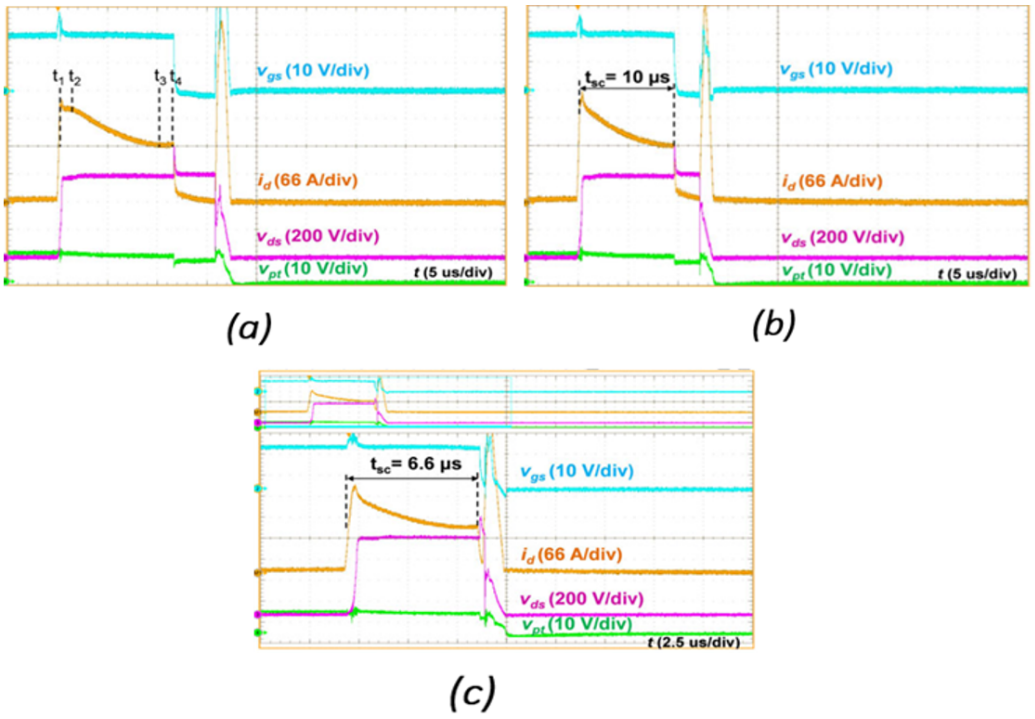

Figure 4.8 : Test results a)600V@Tc=25°C b)600V@Tc=200°C c)750V@Tc=200°C [35].

During short circuit transient, junction temperature increases and reaches the boundary of the depletion region. High current density leads to a rapid temperature rise and a wider temperature gradient. In addition to that high temperature in the depletion region becomes positive thermal feedback on the intrinsic carrier density. Due to positive feedback, this fast increase creates a thermal generation current which controls the leakage current during the short-circuit transient. Besides, there are many parameters of the limiting factor (DC bus voltage level, temperature, fault type, device type, etc.) in short circuit capability.

In an experimental study [36], SiC MOSFETs, JFETs, and BJTs were compared with 600V DC short circuit test. Although BJT showed an inhomogeneous test result, while MOSFET reached critical energy at 10µs, JFET reached 600µs. Since JFET provides the opportunity to be used in the current limiting mode, in this mode it has also shown short circuit resistance for 200ms in the 400V DC test.

In the study [37], SiC MOSFETs and SiC BJTs are tested and compared in terms of short circuit strengths. In these tests, 3 different 1200V SiC MOSFETs were used and these devices were compared with the performance of 1200V SiC BJT in the short

circuit test. Critical energy is very important for the robustness of semiconductors. The maximum energy that the device can sustain during a short circuit can be regarded as critical energy. It is seen in the tests conducted at 600V DC that MOSFETs show gate leakage a few µs after the short circuit, and this leakage causes failure. In tests at Tc=25°C, the first MOSFET showed 16 µs resistance and the critical energy was 1118mJ. The test with the second MOSFET results 12.5 µs and 714mJ, and finally the third MOSFET 18 µs and 1567mJ. In the examination with BJT based on the short circuit test, a short circuit has occurred between the base and the emitter, and an open circuit occurs between the collector and the emitter. Therefore, it is becoming some kind of safe fault clearing due to no current flowing between collector and emitter.

The performance of SiC devices under short circuit conditions is given in Table 4.2 as a summary. The results conclude that the SiC MOSFET can withstand short-circuit conditions for 8–80 µs depending on its gate-source voltage, drain-source voltage, and ambient temperature. Moreover, SiC JFET is found to be more robust than the SiC MOSFET. It can withstand a short circuit for 1.44ms at 400V DC and 1.22ms at 600V DC. Finally, SiC BJT has been investigated and the result was approximately 30 µs withstand a 600V DC short circuit.

Table 4.2 : Summary of short circuit test of SiC JFET, MOSFET, and BJT.

	V DC (V)	**t_{fail} (µs)**	**Ambient Temperature (°C)**
SiC MOSFET	400	80	125
	600	8-16	25
	600	8-10	200
	750	5-6.5	200
SiC BJT	600	30	25
SiC normally-on JFET	400	660	25
	600	1170	25
SiC normally-off JFET	400	1440	125
	600	1220	25

4.5 Aging of SiC Devices Under Short Circuit

Electromechanic contactors can be exposed to short circuit current only a limited number of times, while this number is much higher in SSRs. However, various tests were conducted to understand the repetitive short circuit performance of semiconductors. In the short circuit tests performed at 600V in [122], 3 different

MOSFETs are exposed to short circuit for the duration of 0.8 µs, 2 µs, and 3 µs, respectively. As a result, after 36000, 10240, and 4680 cycles, V_{TH} and I_D are affected as shown in Figure 4.9, but how much it will affect device performance is not emphasized.

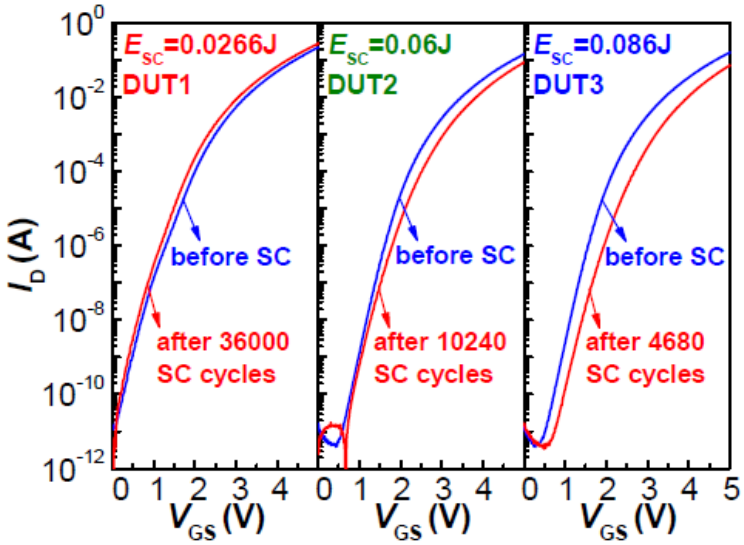

Figure 4.9 : Test result for repetitive short circuit [122].

In the study [123], both planar and trench MOSFETs are subjected to repetitive short circuit test. Two devices have been short-circuited 400 times consecutively at different gV_{GS}, 10V and 20V. As a result, the threshold voltage V_{TH} of the planar MOSFET changed by 5% at 10 V_{GS}, while at 20V it changed by 16%. These results are 2% and 38% for trench MOSFET, respectively. It shows that the planar MOSFETs have better short-circuit robustness than trench ones. Moreover, as the gate voltage increases, degradation in the two devices has increased.

Finally, the case temperature effects on short circuit behavior are examined in [124] with planar MOSFET. First, it is shown with one time tests that the short circuit withstand decreases with the increase of the case temperature. Later, 140 repetitive tests were carried with static characterization after every 10 repeats. As a result, it is seen that gate oxide failure occurs as the number of repetitions increases. However, as can be seen in Figure 4.10, as the initial temperature of the tests increases, the number of repetitions that devices can realize is also increased. The reason behind this phenomenon is, at high temperatures, the drain current decreases, resulting in less short circuit energy on the device.

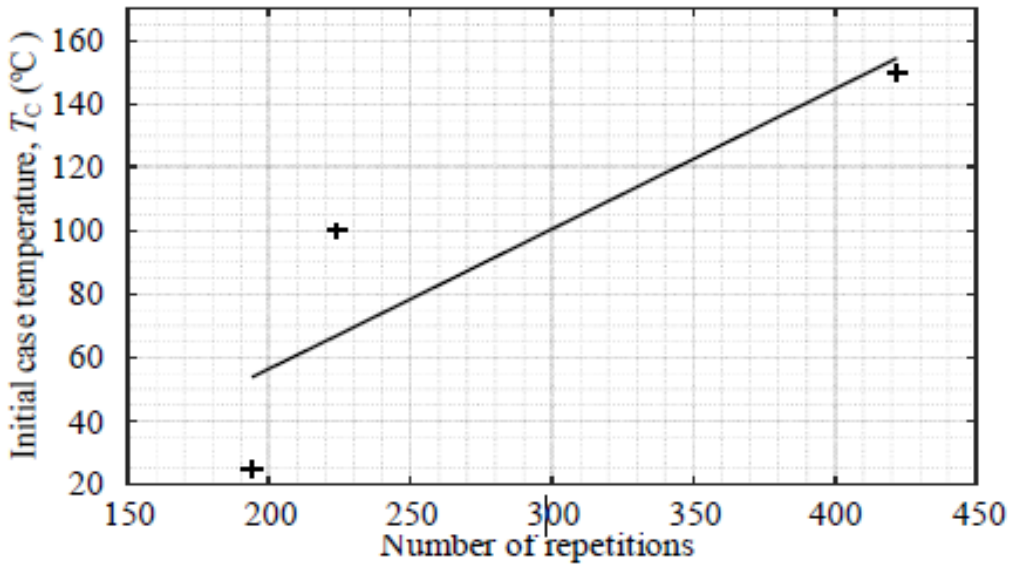

Figure 4.10 : Number of repetition based on case temperature [124].

5. SHORT CIRCUIT PROTECTION METHODS FOR SEMICONDUCTOR SWITCHES

Short circuit protection studies for semiconductors in the literature take into accounts two types of fault. The first one is called Fault Under Load (FUL), this type of fault occurs when the device is in ON state and a short circuit occurs in the system. The second one is Hard Switch Fault (HSF), which occurs when the device previously OFF state and when it's turning ON short circuit occurs due to already shorted system. In addition, in some studies, HSF is called Type I, and FUL is called Type II short circuit faults. Therefore, short-circuit protection should be applied by considering not only the type of fault but also the type of semiconductor used and the entire power system. These protection circuits should not only be designed as an instantaneous protection tool but also should be utilized to prevent slow degradation problems such as aging in the device to prevent long term faults.

5.1 De-saturation (V_{DS} Sensing) Detection Method

The de-saturation method has been used for overcurrent protection both as a discrete and a module semiconductors for a very long time, especially in IGBTs. The reason for this is both simplicity and its integration to commercially available into many driver circuits. With MOSFETs taking over the market, this method has also been applied in MOSFETs [19,38–41] and the de-saturation method in many driver ICs is available for MOSFETs in the market [42–46]. As seen in Figure 5.1, this circuit basically consists of a resistor, a blanking capacitor, and a diode.

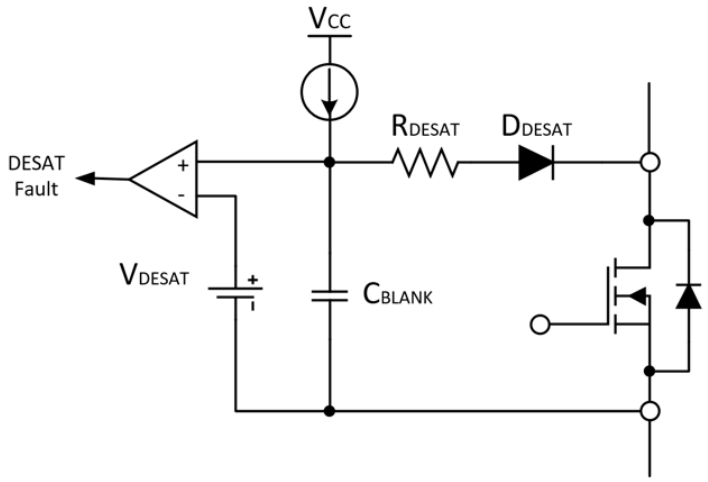

Figure 5.1 : De-saturation detection circuit.

When the device turns on, the current source charges the capacitor, and the diode is become conducting. In normal operation, the capacitor becomes a clamp in the forward voltage of the semiconductor. In the case of a short circuit, the capacitor is charged up to the threshold voltage and causes a closing signal to the device. The charging time of the capacitor is called the blanking time, this time is calculated as given in equation 5.1 and determines the reaction time of the protection circuit. Although this method is easy to implement and inexpensive, it requires a re-design each time depending on the discrete device or module to be used. However, a self-adaptive blanking circuit based on VCE measurement was proposed in [125]. With this method, not only the minimum blanking time interval adjusted to be adaptive, but also the response time of 1.8µs was improved to 0.5µs.

$$t_{\mathrm{BLANK}} = \frac{C_{\mathrm{BLANK}} * V_{\mathrm{DESAT}}}{I_{\mathrm{CHARGE}}} \tag{5.1}$$

As can be understood from those short circuit protection durations, the de-saturation threshold voltage is set close to the transition voltage in IGBTs, while the current can be limited later because of the longer durability time. Since the transition voltages are high, the current cannot be limited thus, blanking time must be shorter in MOSFETs. Therefore, the desaturation threshold voltage should be set lower to achieve the desired short circuit protection times such as 200ns.

In addition, while fast switching times seem to be an advantage, it can be trigger with turn-on noise and can cause false short-circuit triggering. Therefore, blanking time should be long enough at the same time. Since a much more sensitive circuit is required especially in MOSFETs, it is necessary to use a circuit that understands the type of short circuit and makes the protection as proposed in [40]. For example, Type 1 errors require a high desaturation threshold and short blanking time for fast response, while Type 2 and 3 errors require a low desaturation threshold and a long blanking time to avoid false triggering during normal operating moments. At the same time, a capacitive gate stabilizing circuit can be used at the turn off time instead of the Miller clamp circuit as in IGBTs [19]. The summary of highlighted specifications of the de-saturation method is given in Figure 5.2.

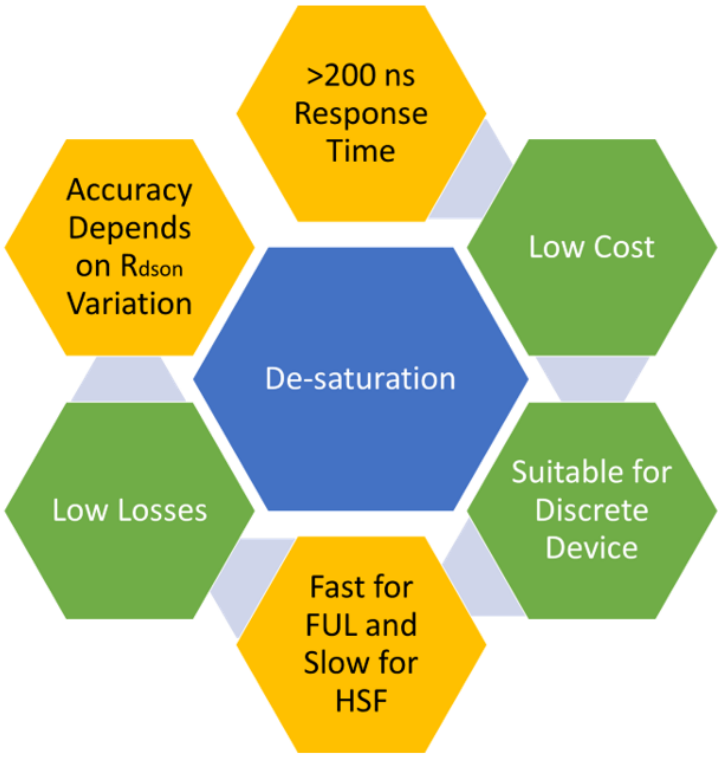

Figure 5.2 : Summary of de-saturation method.

5.2 Shunt Resistor Current Sensing Method

Shunt current based protection method is carried out by measuring the voltage over a series resistor which is proportional to the current flows on the circuit. The shunt resistor current sensing circuit is shown in Figure 5.3. This method is simple and

can be applied to almost any system. Different shunt resistor structures for current measurement are also compared in [59]. Although there are differences within resistors, it is the most accurate method in both AC and DC with a low tolerance resistor and a fast analog to digital converter (ADC) [47, 126]. Being accurate makes them very advantageous for protection, especially in FETs. However, it adds an extra power loss to the system based on I^2R losses. Thus, it is not preferred in high power systems. Although protections faster than 100ns can be provided, it still makes this method costly because fast ADCs are expensive. In some systems, with a module integrated shunt resistor, suitable for SiC and relatively cheap [47, 48].

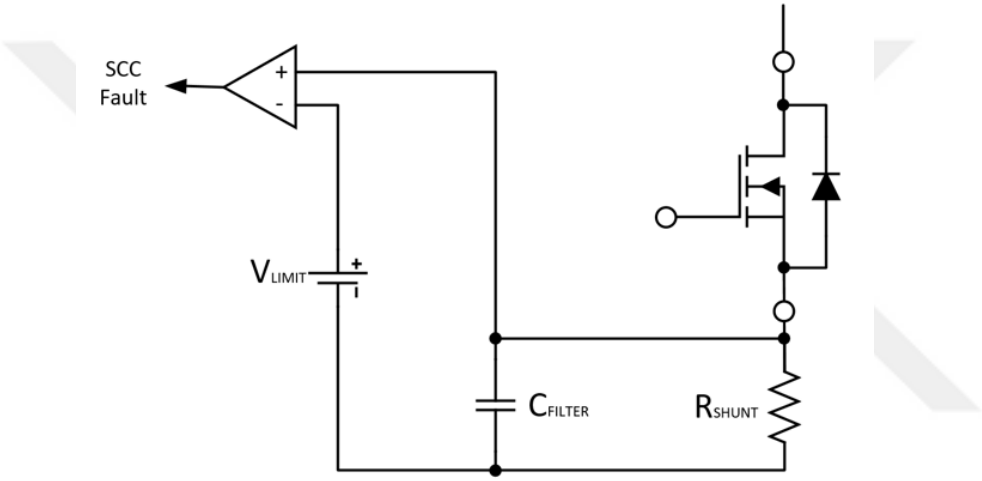

Figure 5.3 : Shunt resistor sensing circuit.

To shorten the fault response time, a coaxial shunt resistor is used in [49] to measure the short circuit current, and the achieved time was less than 10 ns. Since coaxial shunt resistors have high bandwidths, the ICs that are used to process the fault signals are going to be expensive, and the printed circuit board (PCB) layout will be very crucial since semiconductor protection is quite sensitive application. Nonetheless, the main disadvantage besides power loss of the shunt method is the additional stray inductance in the commutation loop, which disrupts the switching performance of fast switching SiC or GaN devices and creates a noise that will end up false triggering. A summary of highlighted specifications of the shunt method is given in Figure 5.4.

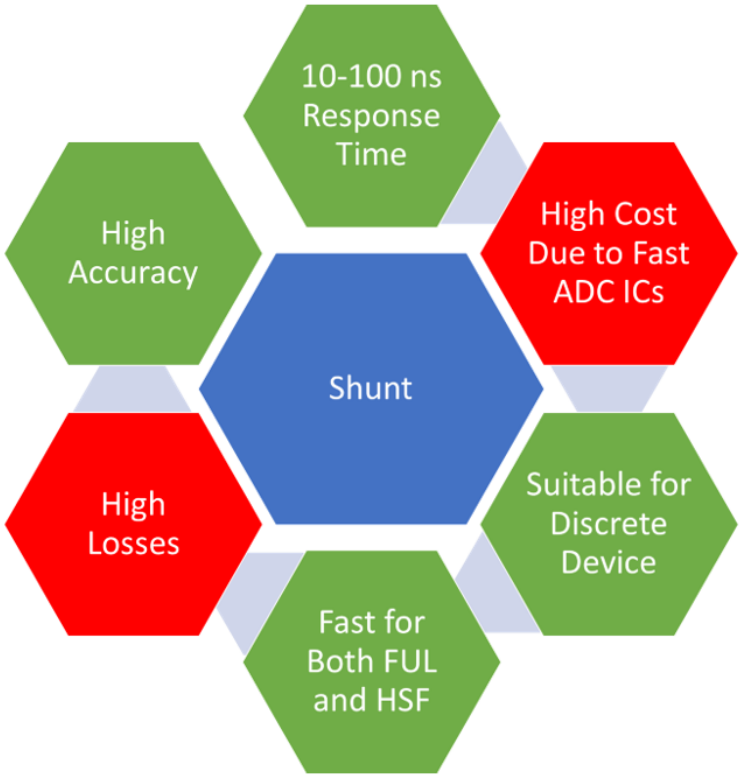

Figure 5.4 : Summary of shunt method.

5.3 Sense FET (Current Scaling) Method

In some semiconductor switch modules, a small amount of their dies is used to mirror the main drain current to achieve a scaled version to facilitate current measurement. Providing short circuit protection by using this method is rarely used [50–55]. In test [54], the module handles the short circuit current under 150ns, and in [55] short circuit current is detected in 80ns. If such a system is used in MOSFETs, it is called Sense FET. The sense current is lower than the normal current by a certain ratio [51]. As can be seen in Figure 5.5, the current is measured with a shunt resistor to be connected between the sense pin and the source pin of the module. Thus, the current is measured with consideration of the scaling ratio. Since the current to be measured in such structures is lower than the main current, the losses on the sense shunt resistor are also lower. Despite these advantages, the number of SiC FET modules with sense feature is almost non-exist in the market. A summary of highlighted specifications of the Sense FET method is given in Figure 5.6

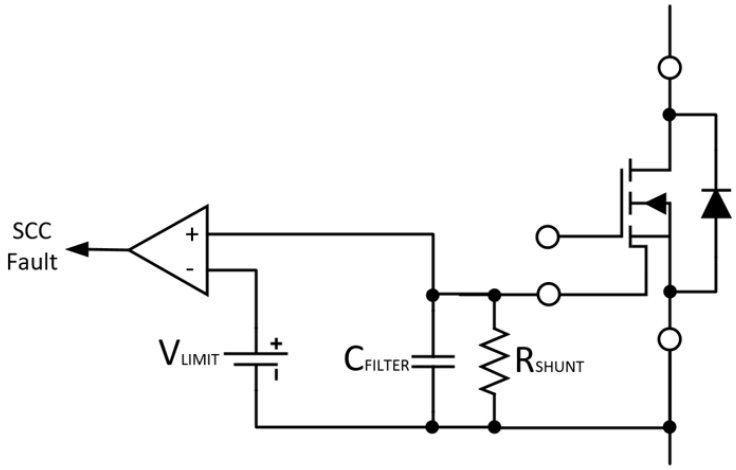

Figure 5.5 : SenseFET sensing circuit.

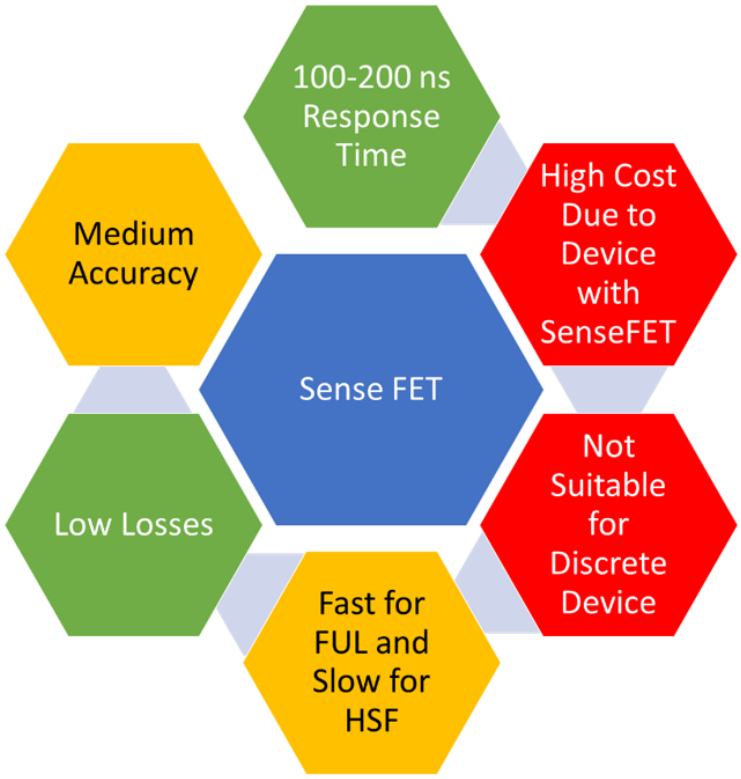

Figure 5.6 : Summary of senseFET method.

5.4 Inductive (di/dt) Sensing Method

The inductive (di/dt) sense method uses the voltage drop on the parasitic source inductance to measure the current. This method requires a Kelvin connection apart

from the source pin of the switch for sense current flowing on the semiconductor parasitic inductance, as shown in Figure 5.7.

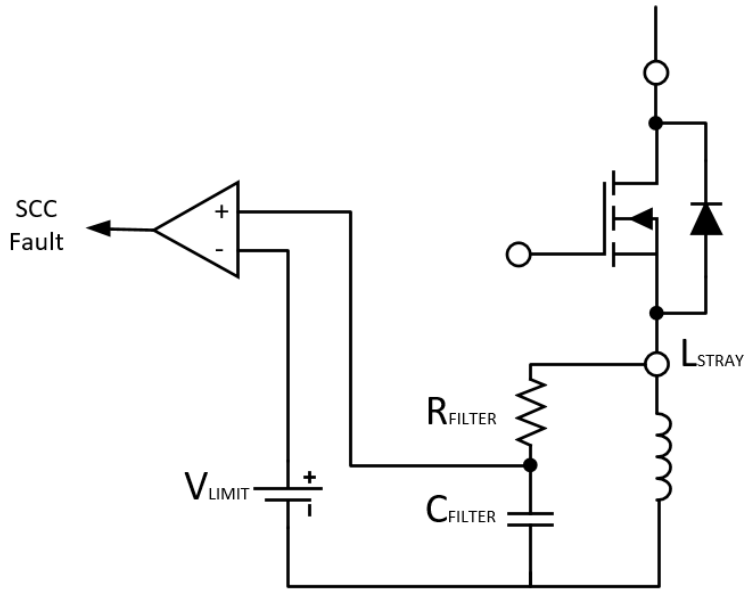

Figure 5.7 : Inductive (di/dt) sensing circuit.

In Figure 5.7 an RC circuit parallel to parasitic inductance is used to measure the voltage on stray inductance. At the output of this circuit, this signal is made ready for processing with a comparator or integrator to have the current required for short circuit protection. This method can be used in modules with separate terminals of kelvin source and main source. With this method, the blanking time in de-saturation is eliminated and a faster response to SC event is achieved. IGBTs have a higher short-circuit sense signal due to larger stray inductance [56, 57].

Moreover, there are also examples in SiC FETs [39, 54, 55, 58]. However, this method can be problematic, especially in FETs. This is because lower di/dt on overcurrent condition and the stability of the system depends on the tolerance of the stray inductance. Generally, with this method, if a different fast di/dt method can be provided, a more accurate result can be obtained. In [39], with the kelvin source-based di/dt method, protection was provided for a duration of approximately 190ns in FUL and approximately 220ns HSF short circuit. A summary of highlighted specifications of the Inductive (di/dt) method is given in Figure 5.8.

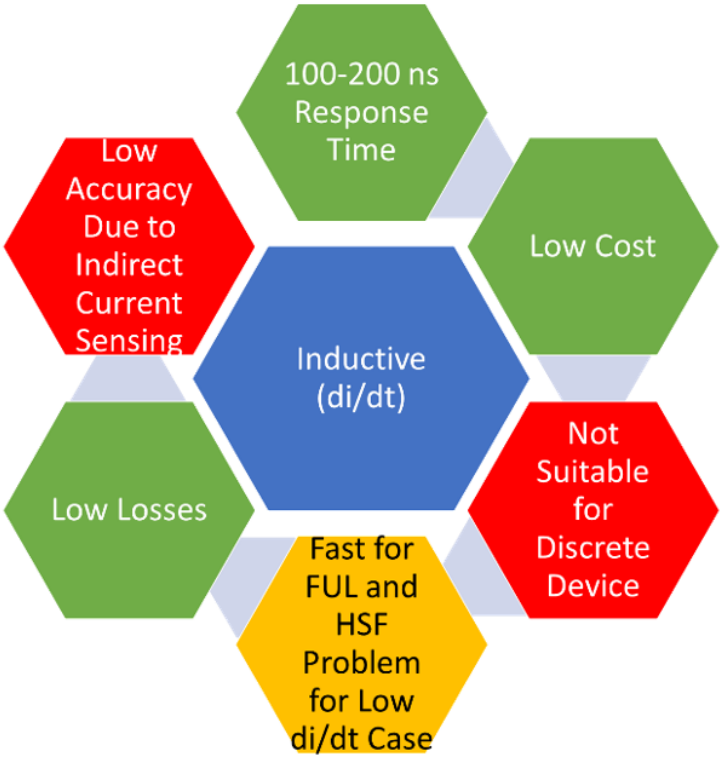

Figure 5.8 : Summary of inductive (di/dt) method.

5.5 Gate-Charge Method

This method works based on a response from gate-source voltage. How the gate-source voltage changes during short circuit versus normal operation define the overcurrent failure as can be seen in Figure 4.7 For this method, gate-source voltage, drain-source voltage, and drain-source current in normal operation and short circuit failure should be examined and compared transiently.

This method is widely used in the short circuit protection circuit for IGBTs [127–133]. As seen in Figure 5.9, the lack of high voltage connection is an advantage for selecting this method. Moreover, able to integrated into the driver circuit, and not having a blanking time are the other main benefits to use this method. Studies have been done on SiC MOSFETs for this method [60,61]. However, in SiC MOSFETs, there are a few drawbacks that need to be considered. First, it is difficult to measure the gate charge and voltage due to the low gate charge capacity. Second, since the gate-source voltage and gate charge capacity varies from device to device, the necessity of high accuracy to prevent false triggering, makes the design difficult. Third, SiC MOSFETs are much

faster than IGBTs and voltage ringing can be a drawback on design. Considering those drawbacks, this method is more suitable for HSF errors.

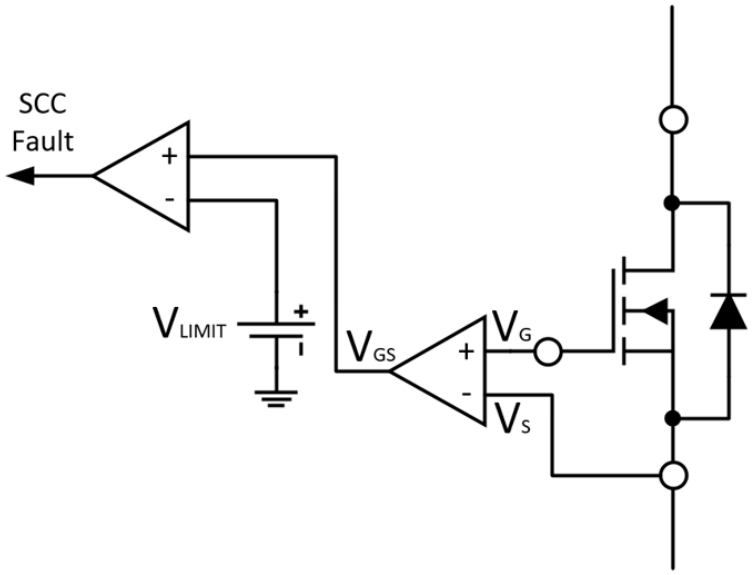

Figure 5.9 : Gate-charge sensing circuit.

Moreover, in the study performed for SiC MOSFET, a significant difference was detected on the gate-charge characteristics between normal turn-on conditions and HSF conditions [61]. In this study, an HSF can be detected within 1 µs. A summary of highlighted specifications of the gate-charge method is given in Figure 5.10.

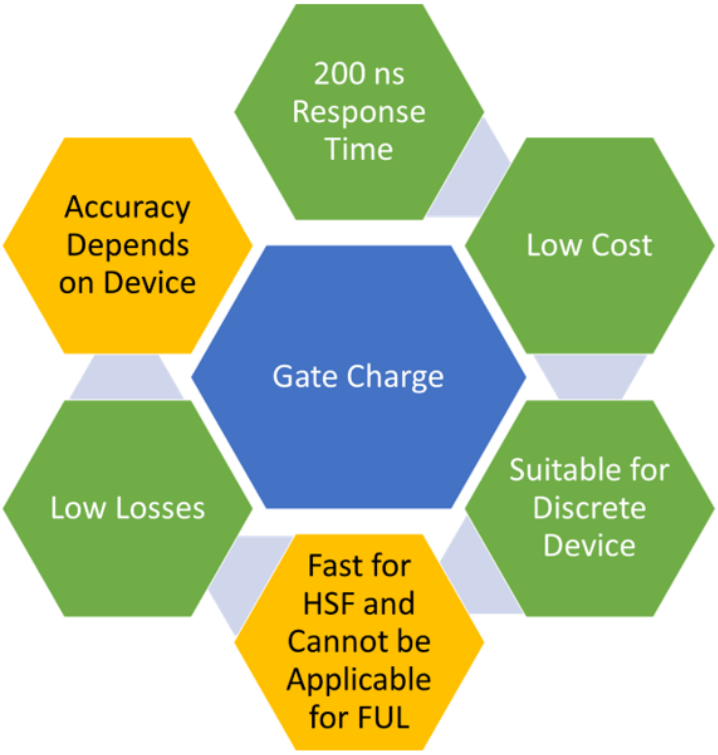

Figure 5.10 : Summary of gate-charge method.

5.6 Rogowski Coil Method and Current Transformer Method

The basic working principle of the Rogowski coil can be explained using Ampère's circuital law and Faraday electromagnetic induction law. A simple Rogowski coil sensing scheme can be seen in Figure 5.11. The Rogowski coil method may be preferred for the sake of its response times at nano-second levels, galvanic isolation, and the absence of losses [62,63]. However, this system is not applicable in automotive battery systems due to its operation only in AC systems and high cost. However, in order to use the Rogowski coil method as a short circuit and overcurrent protection system, it is necessary to improve especially on PCB mass production, EMC, and sensitivity subjects.

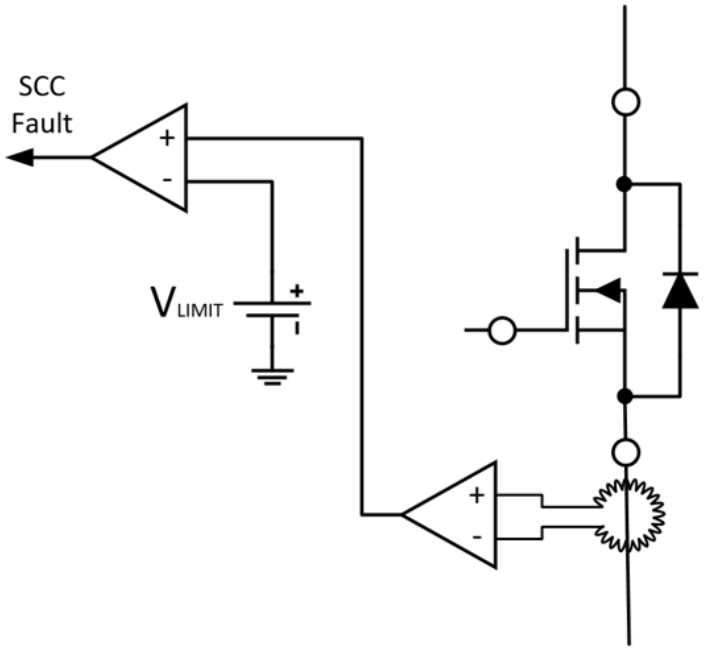

Figure 5.11 : Rogowski coil sensing circuit.

Another method providing galvanic isolation is based on measuring the short circuit current with the help of an air gap transformer connected to the source line [64]. Apart from providing isolation, this method also offers high bandwidth, but the signal processing circuitry is complex and the ICs required for this task are very expensive. In [64], the delay between the crossing of the overcurrent threshold and the reaction of the gate voltage is only 22ns. It was measured in this study that both FUL and HSF short circuit protection was realized in a 7kV system at 200ns. A summary of highlighted specifications of the Rogowski Coil and Current Transformer method is given in Figure 5.12.

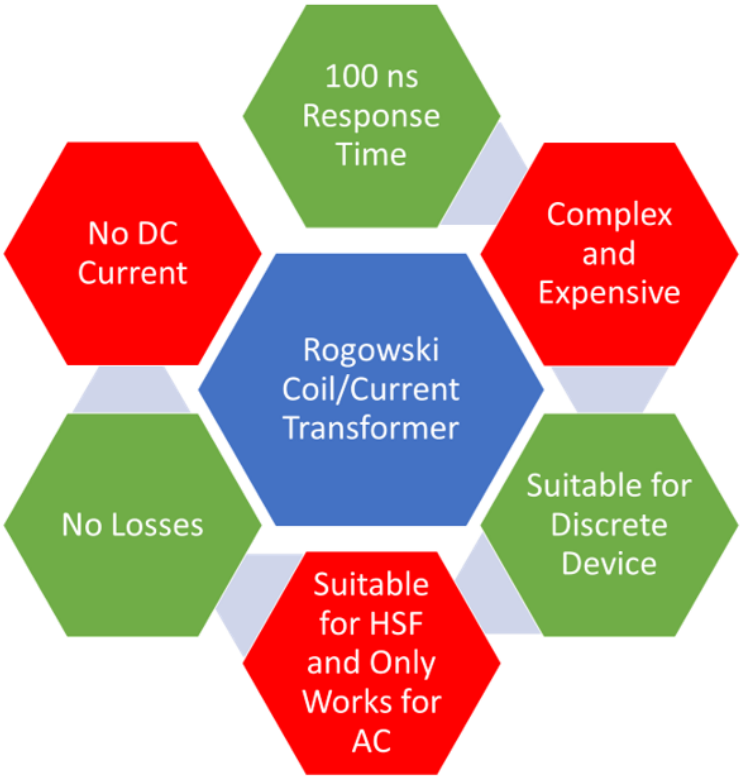

Figure 5.12 : Summary of rogowski coil and current transformer method.

5.7 Temperature Dependent Protection Method

The temperature of the semiconductor is very important in short circuit faults. This is because semiconductors fail due to thermal runaway caused by high current. In the study [65], the case temperature and drain current are continuously measured, and short circuit protection is provided through a real-time adjusted model. The temperature sensor based protection scheme can be seen in Figure 5.13. The biggest advantage of this method is that it eliminates false triggering errors since it is temperature-dependent. However, response to short circuit faults is slow due to the presence of sensors, signal processing circuits, and microprocessors. Therefore, the method is more suitable for general overcurrent protection circuits other than automotive battery systems.

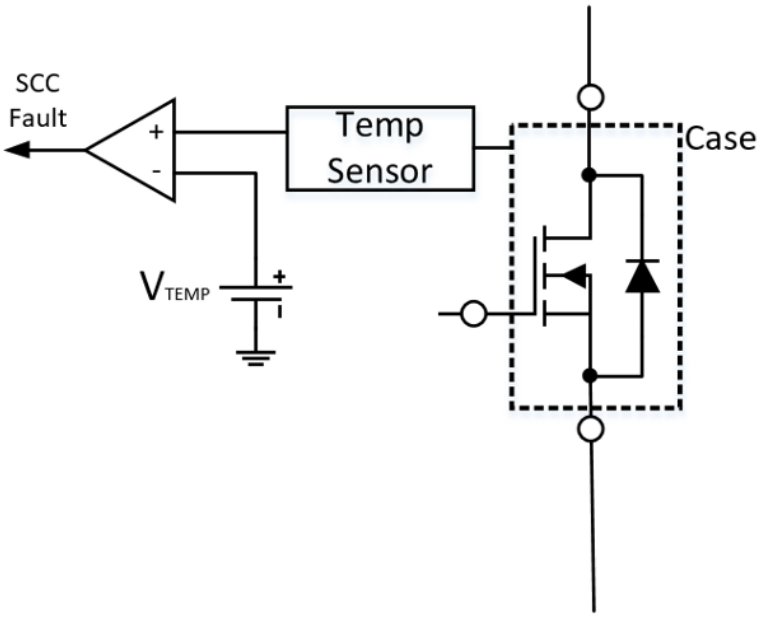

Figure 5.13 : Temperature-dependent sensing circuit.

In the study [65], tests were performed on 1200V MOSFETs at 250V DC. Depending on the temperature, the short circuit protection system was triggered for 35A at 27°C, 28A at 77°C, 17A at 122°C, and 7A at 142°C, respectively. This system shows protection speed between 1 and 10 µs depending on the temperature. A summary of highlighted specifications of the temperature-dependent method is given in Figure 5.14.

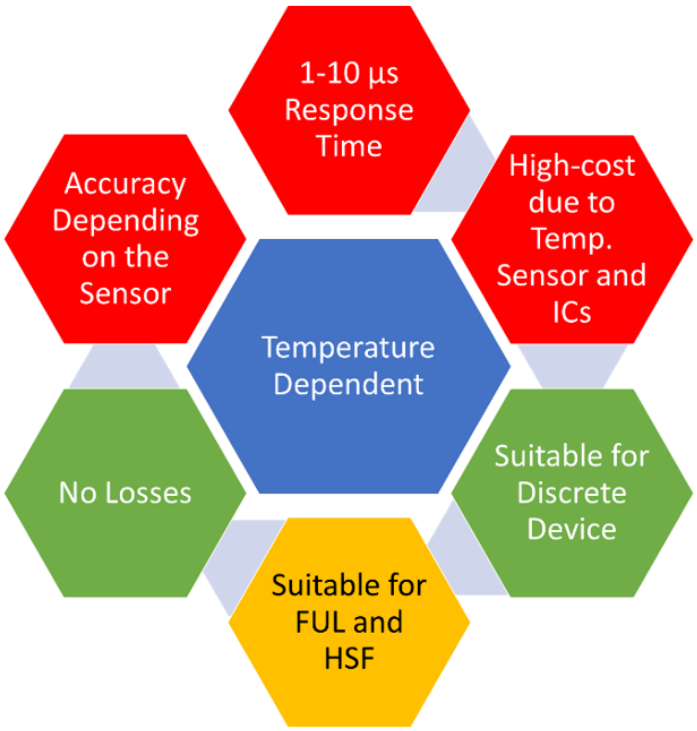

Figure 5.14 : Summary of temperature-dependent method.

5.8 Discussion

Table 5.1 shows the comparison of performance and costs of different short circuit protection methods for semiconductor switches. When short circuit robustness is taken into consideration, fast and reliable short circuit protection is crucial for SiC FETs to be competitive against Si IGBTs. Although SiC MOSFETs are behind SiC JFETs in terms of short circuit withstand, they are still preferred due to their domination of the market and their maturity in automotive products. Therefore, SiC MOSFET is promising to achieve a compact and efficient system.

Although there are many methods to protect the short circuit, the most prominent ones have been examined within the scope of this thesis. Shunt, SenseFet, Rogowski coil, and temperature-based methods are expensive solutions due to additional component necessity. In addition, Sense FET and Inductive (di/dt) methods can only be implemented with special modules, but it is not possible to design according to special requirements with discrete devices.

Moreover, de-saturation and gate-charge methods step forward in this comparison. Although they both have advantages and disadvantages against each other, the most

common point they encounter is error types. De-saturation is successful in FUL (Type2) errors, while gate-charge can be applied in HSF (Type1) errors. Since the accuracy of both is highly dependent on the selected semiconductor, it is possible that they also perform well in terms of accuracy. Consequently, short circuit protection utilizing the advantages of both methods has been proposed in [134]. In this study, 800V shoot through short circuit error was detected in a duration of 200ns, and protection was provided for SiC MOSFETs.

Table 5.1 : Comparison of overcurrent detection techniques.

	Accuracy	**Response Time**	**Cost**	**Losses**	**Fault Types**	**Suitable for Discrete Device**
De-sat	Accuracy Depends on RDS	>200 ns	Low Cost	No Losses	Fast for FUL and Slow for HSF	Yes
Shunt	High Accuracy	10-100 ns	High Cost Due to Fast ADC ICs	High Losses	Fast for Both FUL and HSF	Yes
Sense FET	Medium Accuracy	100-200 ns	High Cost Due to SenseFET Device	No Losses	Fast for FUL and Slow for HSF	Requires Sense Pin
Inductive (di/dt)	Low Accuracy	100-200 ns	Low C ost	No Losses	Fast for FUL and HSF	Requires Kelvin Source Pin
Gate Charge	Accuracy Depends on Device	200 ns	Low Cost	No Losses	Fast for HSF and Not Suitable for FUL	Yes
Rogowski Coil	No DC Current	100 ns	Complex and Expensive	No Losses	Only for HSF and AC Systems	Yes
Temp Sensor	Accuracy Depens on the Sensor	1-10 µs	High-cost due to Sensor and ICs	No Losses	Suitable for FUL and HSF	Yes

In order to meet the requirements of automotive battery systems, discrete semiconductor devices available in the market shall be paralleled and bi-directional connected to provide current flow and control in both charge and discharge directions. In addition to the semiconductor array, a combined de-saturation and gate charge based protection system is proposed in Figure 5.15.

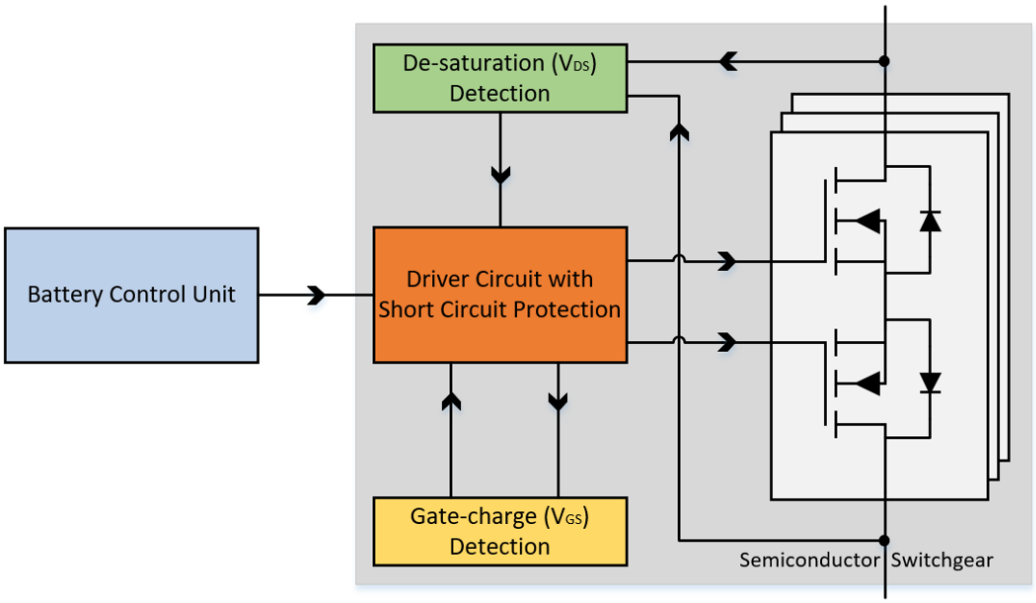

Figure 5.15 : Block diagram of the SSR with protection circuit.

6. DESIGN OF A SEMICONDUCTOR BASED HV BATTERY SWITCH WITH SHORT-CIRCUIT PROTECTION

6.1 Short-Circuit Protection Strategy with Semiconductor Switchgear

In this chapter, the shut-off strategy based on the semiconductor protection circuit is proposed. As opposed to the shut-off strategy (as given in Figure 3.2) achieved by conventional components, current zones in the shut-off strategy with semiconductor switchgear is proposed in Figure 6.1. In this strategy, thanks to the advantage of the fast response time of the semiconductor switch, the short circuit current, and the over-current current protection are achieved faster than the conventional system. As given in Figure 5.15, de-saturation and gate-charge based system are used in semiconductor switchgear. In the system, the protection of the short circuit zone (red area) in Figure 6.1 is made by the proposed protection circuit. Moreover, protection for the over-current zone (yellow area) is handled by the BMS over-current algorithm. Since there is enough time for over-current protection, conventional BMS over-current protection is sufficient regarding time. However, short-circuit protection shall be conducted faster to protect the semiconductor switch and the whole system. Since very high fault currents will never be encountered in the battery pack, cells, connection points, busbars, sensors, and connectors will also never be exposed to a no-go zone (blue area).

This study is intended to be in line with future automotive battery trends, as indicated in Figure 2.5. Accordingly, to widen the result of the study, the battery pack with a voltage range of 600V to 1000V is considered. At the same time, it is thought that this system is capable of providing 200A continuous current and 300A peak current for periods shorter than 10 seconds. Although this study varies for specific load profiles, since it will not affect its purpose and working principle, current values may vary in different studies.

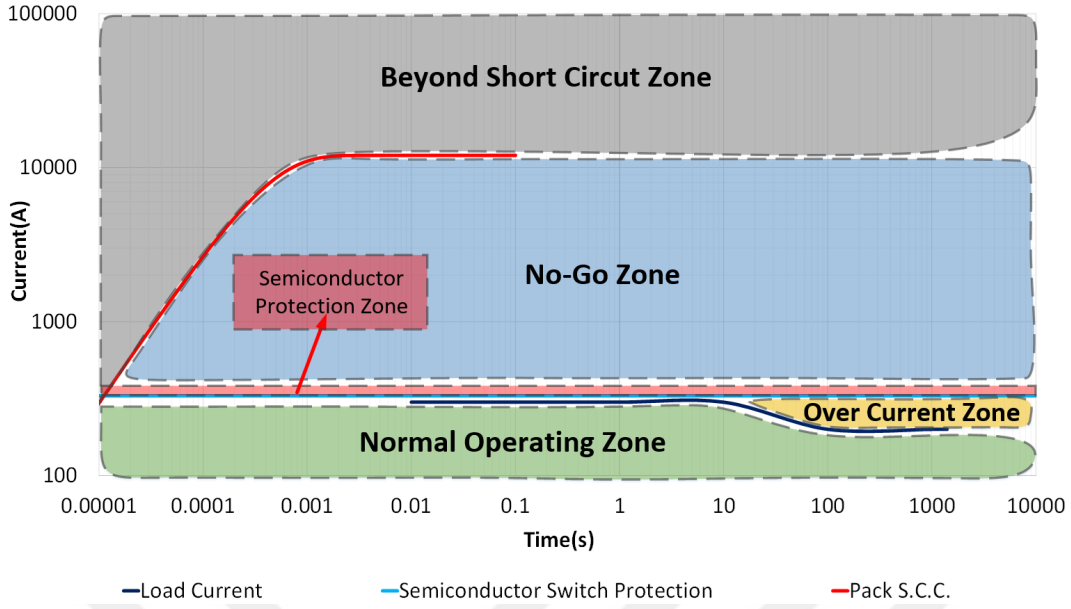

Figure 6.1 : Shut-off strategy with semiconductor switchgear.

6.2 Simulations of Semiconductor Switchgear and Protection Method

In this chapter, the HV battery switchgear is designed with the methods selected in the previous chapter which are de-saturation and gate-charge. In this simulation study, the short circuit scenario is performed for the batter system which is operating under 300A load. The simulation is repeated for the battery pack voltage of 600V, 800V, and 1000V to obtain the effect of the pack voltage on short circuit protection performance. In addition, the effect of the inductance on the short circuit protection system is also observed by changing the pack stray inductance between 10 and 40 µH. The semiconductor used in this circuit is also examined in terms of power losses. In the simulated circuit, apart from the semiconductor structure, de-saturation protection circuit and snubber circuits are also designed.

Two of the most important factors that play a role in determining the short circuit characteristics of battery packs are equivalent pack resistance and pack stray inductance as stated in detail in chapter 3.1. The internal resistance of a li-ion battery cell changes instantaneously according to the state of charge (SoC), temperature, current drawn, and the duration of the current. In the study conducted in [135], 0.39 mΩ DCIR is measured while 300A is drawn at 15C in a 20Ah cell which is selected for further calculations. To achieve 1000V maximum battery pack voltage with this cell, 235 cells need to be configured in series. At the same time, 3 cells are configured as

parallel to provide a current of 200A continuous and 300A for 10 seconds. Moreover, using equation 3.1 and considering the approximate internal resistance for the rest of the battery components, equivalent battery resistance is calculated as 50 mΩ in transient short circuit conditions. Besides, to also simulate the short circuit current increase as fast as possible, stray inductance is simulated between 10-40 µH. The simulation circuit containing the equivalent battery circuit, semiconductor switch array, protection circuit, and variable load realized in LTspice is given in Figure 6.2.

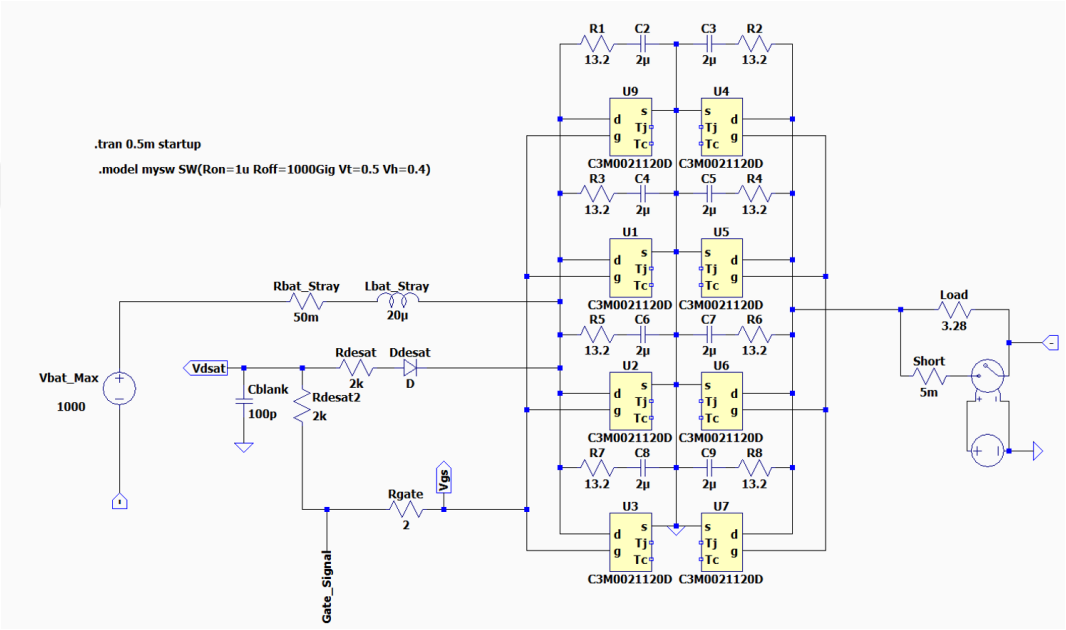

Figure 6.2 : Simulation circuit for short circuit protection.

SiC Power MOSFET with part number C3M0021120D from CREE is chosen for the semiconductor circuit [136]. This component plays the leading role in the short circuit simulation. The electrical characteristic from the datasheet of this MOSFET is given in Table 6.1. There are several reasonable motivations for selecting this semiconductor for the semiconductor array. First, CREE has a library that supports SPICE simulations. Thus, there is no need to model the semiconductor in the first place. Second, considering the switching overshoot, it is necessary to have at least 1200 V, especially for 1000V battery applications. Third, it has low on-state resistance compared to its competitors, and therefore current carrying capacity is high and losses are low. Finally, CREE defines this product as automotive qualified and compliant with AEC Q101.

Table 6.1 : Electrical characteristics of utilized MOSFET @ T_C=25C [136].

Symbol	Parameter	Value	Unit
V_{DSmax}	Drain - Source Voltage	1200	V
V_{GS}	Gate - Source Voltage	-4 / +15	V
I_D	Continuous Drain Current	74 @T_C= 100°C	A
$I_{D(pulse)}$	Pulsed Drain Current	200 (limited by T_{Jmax})	A
P_D	Power Dissipation	469 @T_C=25°C , @T_J= 175 °C	W
$R_{DS(on)}$	Drain-Source On-State Resistance	21	mΩ

Since this MOSFET is rated 1200V drain-source voltage, it will be suitable for battery systems with a maximum value of 1000V. However, a good snubber design is also important to prevent overshooting at fault switching. In this simulation, 4 parallel MOSFETs are used to provide the defined peak current value of 300A. Thus, 75A per MOSFET is sufficient at the peak current carry. For battery packs with a higher current requirement, either the number of the parallel device should be increased or a discrete device with a higher current carrying capacity should be selected. Besides parallel structure, to carry the load current and operate in both charge and discharge operations a bi-directional MOSFET array has been configured as reverse series-connected. Moreover, the output characteristics at T_J=25°C are given in Figure 6.3 according to different gate-source voltages. These graphs are used to determine the reference of the saturation voltage which is crucial for the protection circuit. However, for the fast response circuit, the reference value becoming very sensitive. Therefore, it has to be decided by trial and error in the simulation circuit.

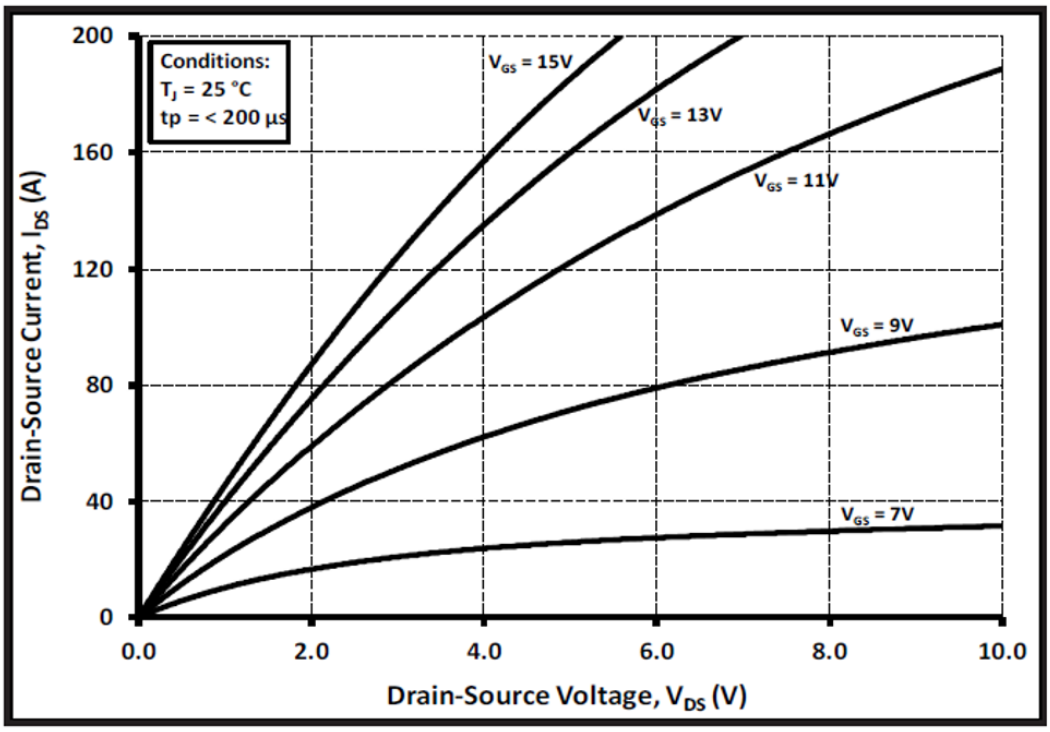

Figure 6.3 : Output characteristics of MOSFET for T_J = 25°C [136].

The proposed protection circuit is given in Figure 6.4 from the SPICE simulation. V_{DSAT} and V_{GS} are obtained within this circuit and used as the input of the logic circuit for reference comparison. V_{DSAT} voltage is the de-saturation voltage and its deviation from the reference voltage indicates the short circuit fault. V_{GS} is the gate-source voltage of the MOSFET and its deviation from the nominal gate voltage value indicates also the short circuit fault. Due to these principles, defining reference voltages is to be essential to the accuracy of the system. In the protection circuit, R_{DESAT} and C_{BLANK} are de-saturation resistance and blanking capacitance respectively. They are defining the blanking time. D_{DESAT} diode is used for blocking the system current to charge capacitance. In normal operation, the blanking capacitor is charged from gate voltage over R_{DESAT2} to forward voltage of the MOSFET plus forward voltage of the diode.

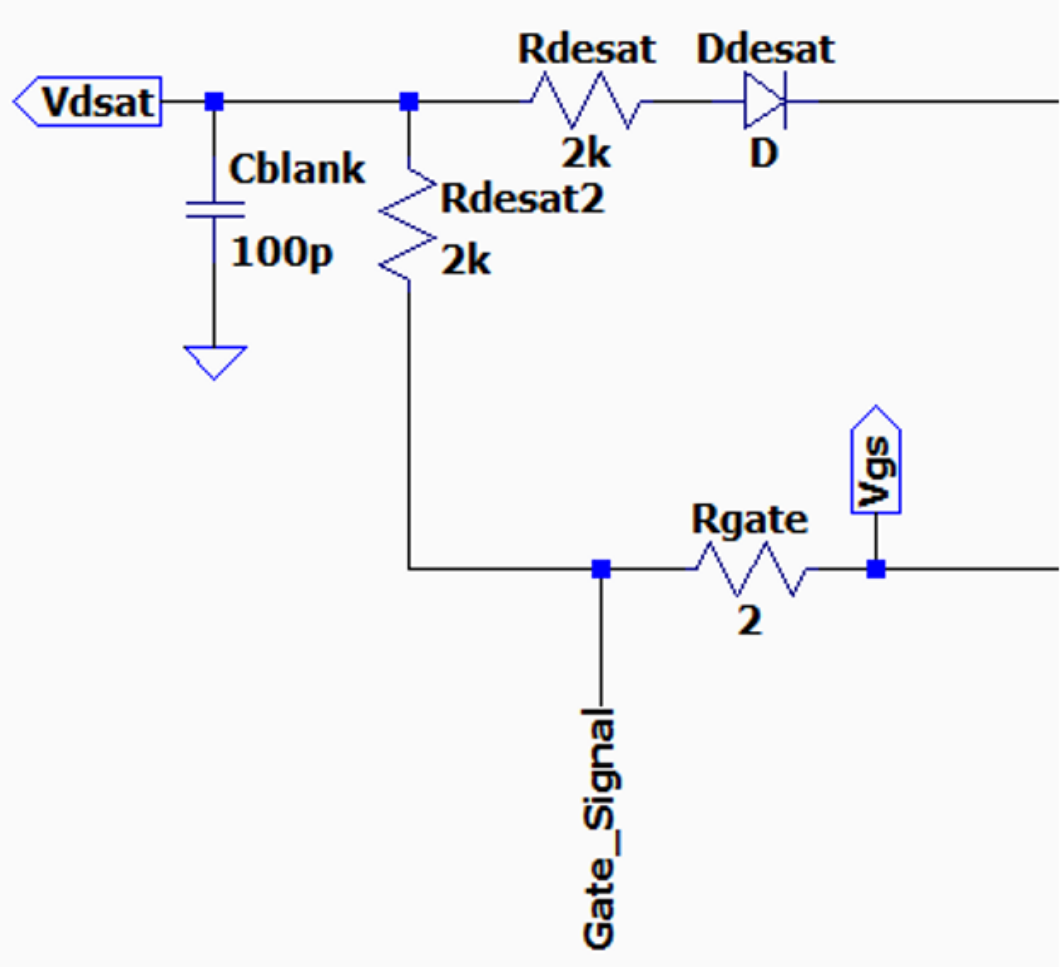

Figure 6.4 : De-saturation protection circuit.

The V_{DESAT} voltage is found approximately as 8.727 V by using Equation 6.1, and the reference voltage (V_{REF1}) was set to 8.75 V with the safety margin after manual adjustments on simulation for the desired accuracy. Here, V_{DF} is 0.685 V which is the diode forward voltage and V_{TH} is 1.77 V which is the minimum threshold voltage of MOSFET from Figure 6.3 at 15V gate-source voltage (V_{GS}) for 75A with trace amount margin. Moreover, R_{DESAT} and R_{DESAT2} are selected as 2 kΩ. However, unlike the simulation environment, in real-world applications, such a well-set precision becomes a challenge when considering component tolerances and temperature. Consequently, the fault signal is obtained by comparing the reference voltage with the de-saturation voltage.

$$V_{\mathrm{DESAT}} = (V_{\mathrm{GS}} - V_{\mathrm{DF}} - V_{\mathrm{TH}}) * \frac{R_{\mathrm{DESAT}}}{(R_{\mathrm{DESAT}} + R_{\mathrm{DESAT2}})} + V_{\mathrm{DF}} + V_{\mathrm{TH}} \tag{6.1}$$

Selection of R_{DESAT} and C_{BLANK} determines t_{BLANK} time. The blanking time was calculated with 2 kΩ R_{DESAT} and 100 pF kΩ C_{BLANK} as given in Equation 6.2, and as a result, a value of approximately 175 ns was found.

$$t_{\mathrm{BLANK}} = (C_{\mathrm{BLANK}} * R_{\mathrm{DESAT}}) * ln(\frac{V_{\mathrm{GS}}}{V_{\mathrm{GS}} - V_{\mathrm{REF1}}}) \tag{6.2}$$

Where V_{GS} is the 15 V and V_{REF1} is the 8.75 V as the reference voltage for the de-saturation. The blanking time should be short enough to protect the MOSFET and long enough to prevent undesired triggering. Besides, the blanking time alone is not enough to define the protection time, the turn-off delay time and fall time of the MOSFET, and delay times in other components used must be taken into account.

HSFs are prevented in battery packs thanks to battery diagnostic. For this reason, the gate-charge method working in only HSF does not have a significant effect. However, it is used alongside the de-saturation method in this simulation and it is seen in the simulation results that the gate-charge method can also be used to support de-saturation for FUL and adds plausibility to the protection circuit. The gate-charge protection method detects the V_{GS} and Q_G. Since the amount of gate charge under fault is smaller than that under normal turn-on conditions. Q_{REF} is selected according to Figure 6.5 preliminary and adjusted for 1000V drain-source voltage and 75A drain-source current as 127nC. For gate-source voltage comparison, V_{REF2} is set to 15.05V. This value is over sensitive for real-world applications. However, it is required to use the gate-charge method under FUL short circuit.

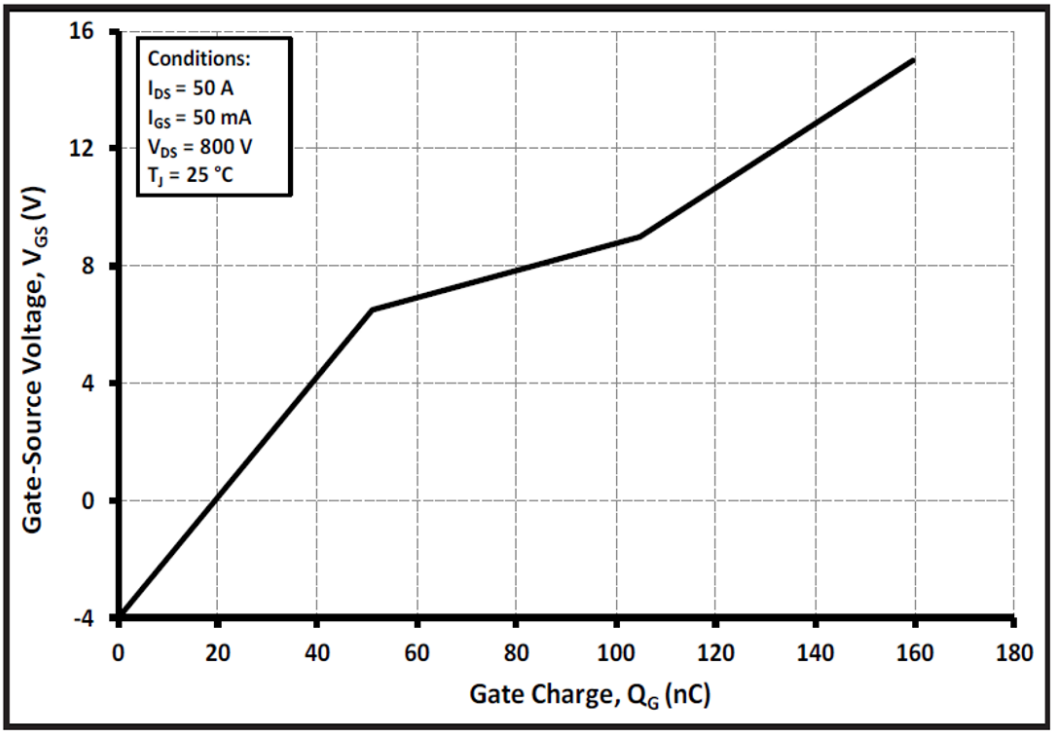

Figure 6.5 : Gate-charge characteristics of MOSFET [136].

Under the fault condition, Q_G is smaller than QRef when a V_{GS} is lower than V_{REF2}. Under normal conditions, Q_G is larger than Q_{REF} when a V_{GS} reaches V_{REF2}. Hence, a fault can be detected as soon as V_{GS} exceeds V_{REF2} . For this reason, they have been compared with the AND gate. Thus, a gate-charge fault signal is generated.

In a SPICE environment, the fault signal process circuit is simulated as given in Figure 6.6. In the circuit, V_{REF1} is used for de-saturation reference and it is compared with de-saturation voltage with a comparative statement in "B Voltage Source" named "B1". Likewise, gate-source voltage is referenced with V_{REF2} and a fault signal is generated from the B2 source. Along with this, Q_G is generated by integrating the gate current over gate resistance with the B4 source, and this is compared with V_{REF3} in the B5 source thus, the gate-source error signal is generated.

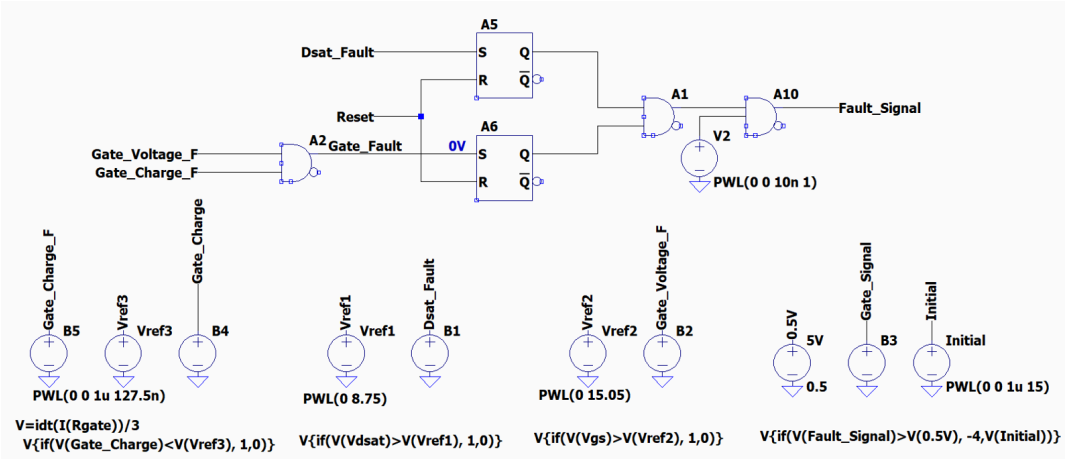

Figure 6.6 : Schematic of the fault signal processing circuit.

Finally, Desat Fault and Gate Fault signals are generated at the output of these comparators. Those signals should be held after occurring because both de-saturation and gate-charge methods are can be triggered in line with delay. Also after the gate signal is interrupted with a fault signal, the circuit shall be held off to prevent failure. This is achieved by two SR Flip Flop. Moreover, the truth table of the protection circuit is given in Table 6.2. The reset pin is controlled by the BMS and it is used to reset the protection circuit with the command it receives from the battery diagnostic system.

Table 6.2 : Truth table of the protection circuit.

Gate Fault	Desat Fault	Fault Signal
0	0	0
0	1	0
1	0	0
1	1	1

Consequently, after selecting the circuit components, making the necessary calculations, and determining the parameters, the protection circuit in Figure 6.7 was finally created. While this circuit provides over-current and short circuit current protection with its analog control system, it will also act as a full-capacity battery switch by applying the commands from the battery control unit in normal operation.

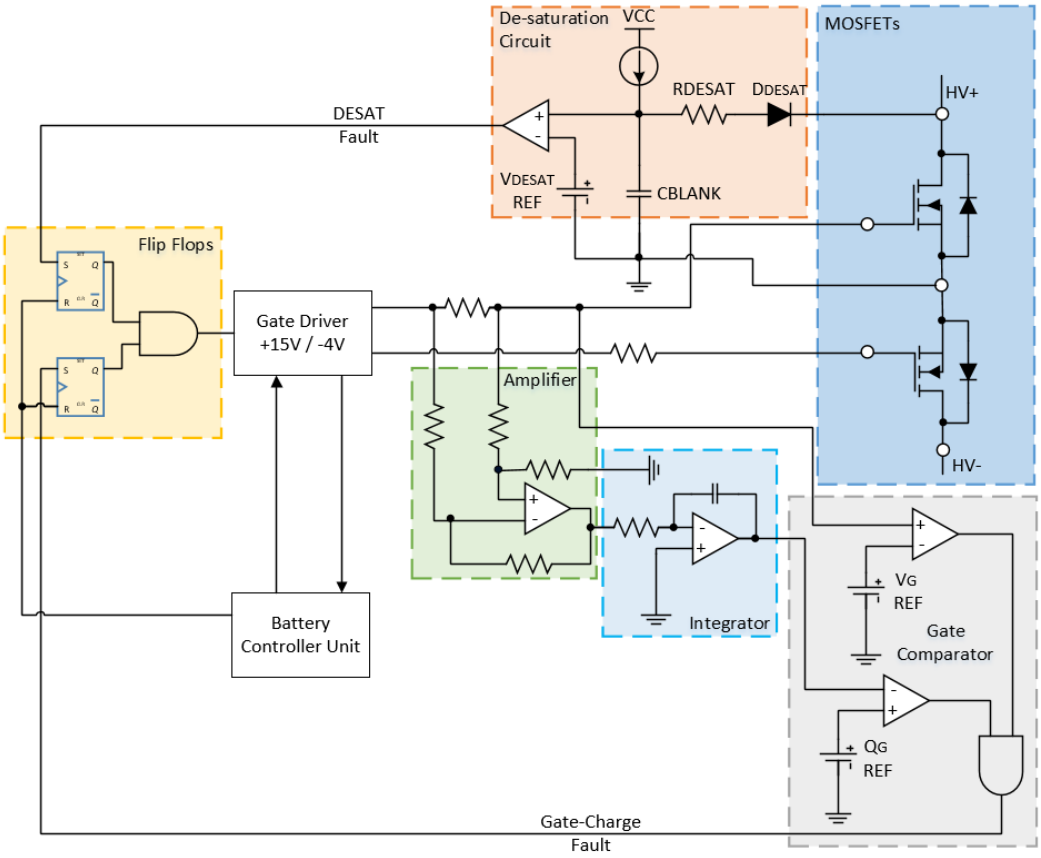

Figure 6.7 : Proposed Protection Circuit.

In the simulation scenario where 300A is drawn at 1000V battery voltage, there is a short circuit on the 5mΩ resistor at 250.89842μs exactly. After 184.63ns, the short circuit current stopped increasing. This result shows that the system provides short circuit protection under 200ns. Moreover, as seen in Figure 6.8 the simulation is repeated at 600V and 800V battery voltage values with the same constant current. However, except that the 1000V system reacts a 5ns faster than 800V and 30ns faster than the 600V system, there are no noticeable changes in the short circuit current between the simulations. As a result, short circuit protection with a semiconductor-based system provides much faster protection performance compared to the conventional system with a contactor and fuse.

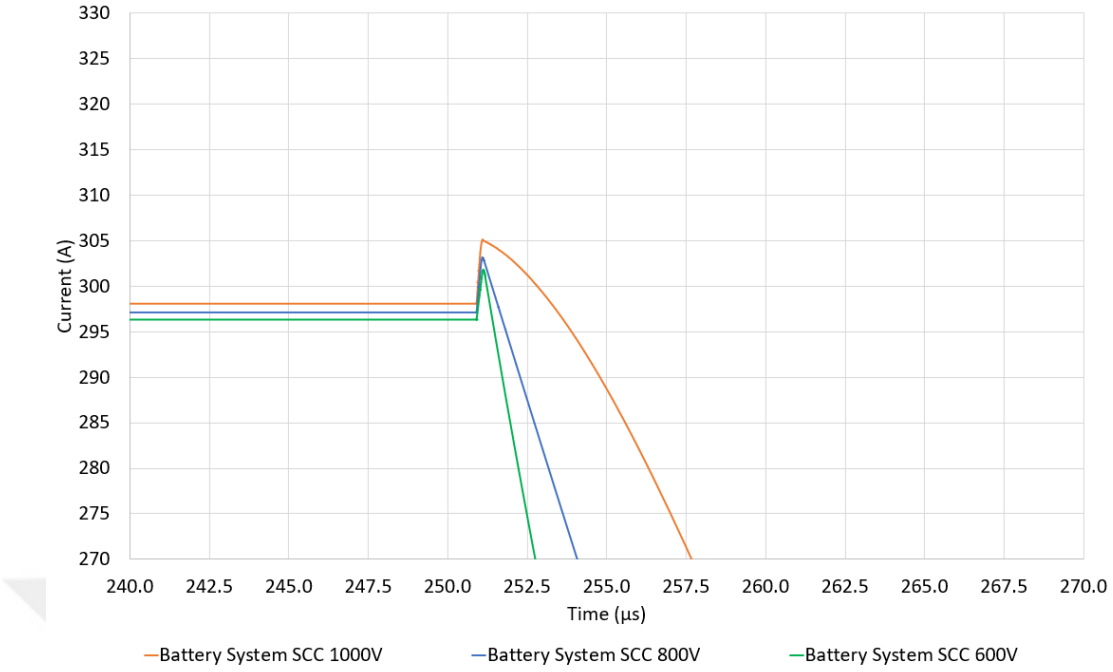

Figure 6.8 : SCC for different voltage levels.

Besides the effect of the pack voltage on the short circuit protection, the pack voltage is kept constant at 1000V to observe the effect of the pack stray inductance on the short circuit current and the protection time. Therefore, simulations are repeated for the stray inductance between 10-40 µH. The short-circuit currents observed from the simulations are shown in Figure 6.9. It is seen here that the current increases much faster at low inductance, but on the other hand, the protection system is activated faster also. Thus, the protection system is worked successfully at different inductances.

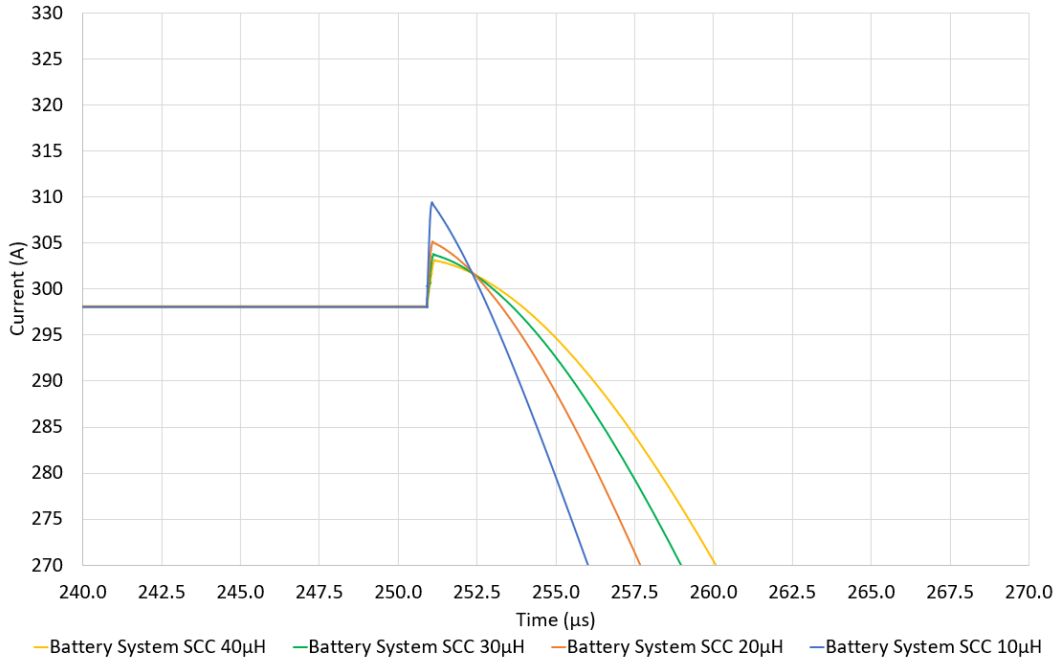

Figure 6.9 : SCC for different stray inductance.

All simulation results are given in Table 6.3. Consequently, short circuit protection with a semiconductor-based system provides much faster protection performance compared to the conventional system with a contactor and fuse. Moreover, since inductance is important for the switching losses, the snubber circuit should be re-designed for each inductance value.

Table 6.3 : Simulation results.

Short Circuit Scenario	Protection Time [ns]	Max. Fault Current [A]
1000V - 20µH	185	305.0
800V - 20µH	190	303.1
600V - 20µH	215	301.8
1000V - 10µH	160	309.4
1000V - 30µH	215	303.7
1000V - 40µH	250	303.1

Both de-saturation and gate-charge method fault signals are given in Figure 6.10. The gate-charge fault is triggered at 250.922 µs and the de-saturation fault is triggered at 250.979 µs. This delay comes from the blanking time of the blanking capacitor. Later, after the first gate-charge, de-saturation signals were latched, and a fault signal occurred at 250.981 µs.

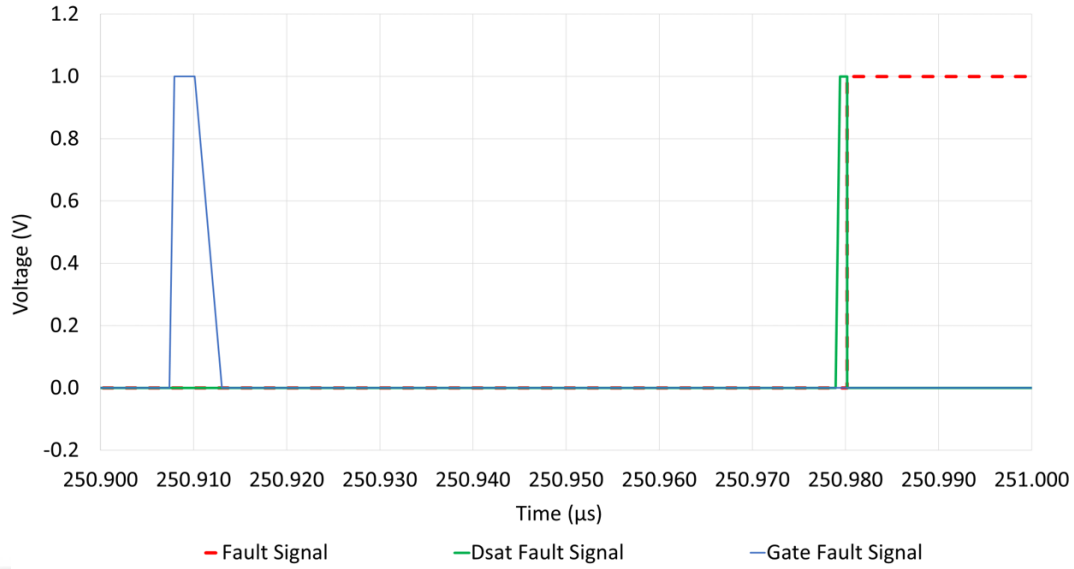

Figure 6.10 : Fault signals for 1000V-20µH case.

A timing demonstration of the short circuit protection circuit is given in Figure 6.11. Delay times vary from method to method. In this simulation, the de-saturation signal showed a slower response than the gate-source signal. However, this difference comes from the sensitivity of the reference voltages, the delay times of the logic components, the blanking time, and tolerances of the passive components. In real-world applications, contrary to simulation, all components and hardware layout boundaries should be considered in the development of such protection circuits. Finally, the delay time between the fault signal triggering and the current stop increasing comes from MOSFETs fall-time and turn-off delay time, for the selected MOSFET, these values are 72ns and 25ns, respectively. Those delays are affecting the MOSFET to switch to turn-off mode completely.

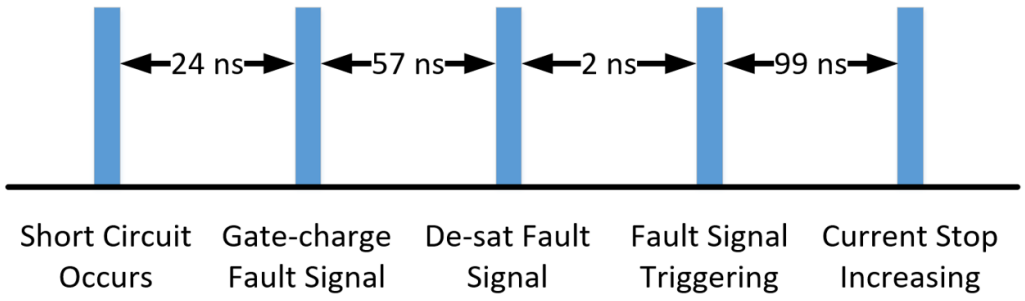

Figure 6.11 : Timing of protection circuit.

In addition to the semiconductor array, the snubber circuit has been established in the simulation. The purpose of this circuit is to protect the circuit when switching inductive loads such as batteries. Using equations 6.3 with L as the initial stray inductance of battery pack which is 20µH, E is calculated 1.8 J with 300A load current. In addition, in equation 6.4, $C_{SNUBBER}$ is calculated as 8µF for 1000V system voltage, and 2µF is taken for each MOSFET in parallel. Moreover, snubber resistance was calculated as 13.2Ω at 1000V and 75A based on Ohm's law.

$$E = \frac{1}{2}LI^2 \tag{6.3}$$

$$E = \frac{1}{2}CV^2 \tag{6.4}$$

The waveforms from the short circuit simulation of the V_{DS} voltage and IDS current at the switching are shown in Figure 6.12 for 1000V and 20µH case. As seen in the graph, thanks to the snubber circuit, V_{DS} does not exceed 1200V. However, in this case, while the MOSFET is protected, according to the simulation results, the snubber capacity instantly shows an 80A inrush current and the snubber resistance series with it shows power loss instantly reaching 90kW. Therefore, it is especially necessary to pay attention to the size of the snubber components in the hardware implementation.

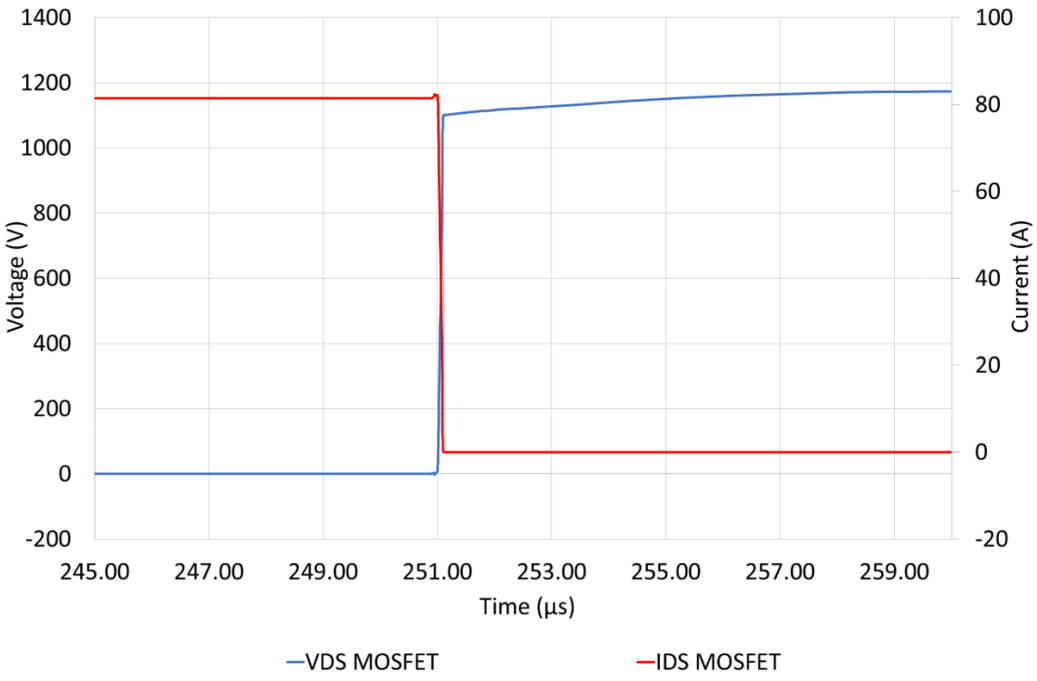

Figure 6.12 : V_{DS} and I_{DS} of the MOSFET during switching transient.

The power dissipated on the MOSFET at this transient switching is given in Figure 6.13. In this power peak state, which lasts for approximately 90ns, 22kW power is reached instantaneously. On the other hand, selected devices are rated for 74A at 1200V. This indicates the component can withstand 22kW peak power under transient conditions. Moreover, efficient cooler design is an advantage to improve withstand performance even further.

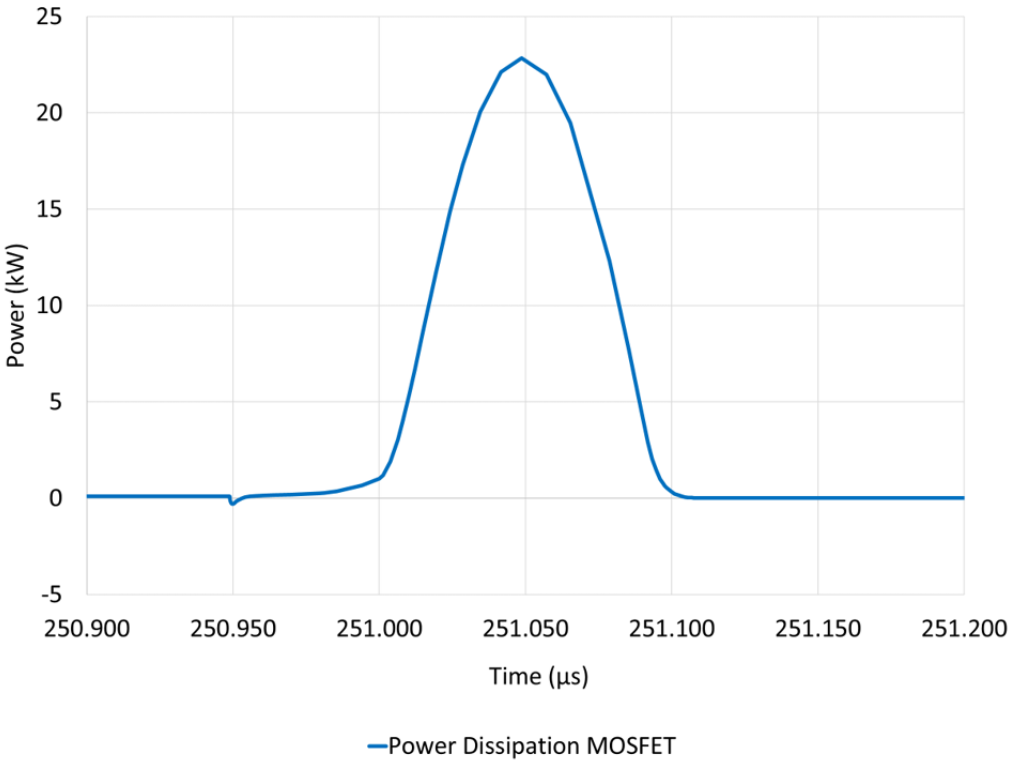

Figure 6.13 : Power loss of the MOSFET during switching transient.

7. CONCLUSIONS AND RECOMMENDATIONS

In this study, over-current and short circuit protection for automotive battery systems have been proposed with a semiconductor-based switch. In the first chapter, an in-depth literature survey was conducted for the automotive battery pack and its components as well as semiconductor technology and short circuit protection. In the second chapter, the architecture of the automotive battery system and its components from cell to pack was examined. It was emphasized that automotive battery systems are steering to 800V+ packs for efficiency and performance. In the third chapter, short circuit fault and protection measures for battery systems and conventional protection components were examined. The short circuit current that may occur in automotive battery packs was characterized and the conventional shut-off strategy was shown with components such as contactors and fuse. In addition to the conventional system, the pyro and smart fuses-based applications were also mentioned. It is shown that these components in the market are lagging to meet the requirements of battery packs, especially, for over-current protection. Therefore, semiconductor-based solutions were proposed. However, semiconductor-based components in the market can only be found for LV batteries. Thus, it is seen that developing semiconductor technology will bring such solutions to HV battery systems. In the fourth chapter, to find the optimal semiconductor device for semiconductor-based battery switch, experimental studies were examined, and semiconductors were compared from material level to system level, especially for short circuit robustness. Based on these studies, it is seen that SiC is the most preferred material in high power applications due to its high temperature withstand and low switching losses, especially in short circuit protection applications. As a result, considering availability on the market SiC MOSFETs were found to be suitable for HV battery switches with a proper short circuit protection scheme. The protection method is crucial for battery pack safety and improvement of the life cycle of components. In the fifth chapter, 7 different short circuit protection methods for semiconductors were examined by experimental and theoretical studies. In addition to the protection speed which is the most important factor in semiconductor-based short

circuit protection, the comparison is also made for cost, accuracy, and compatibility with the selected semiconductor. As a result, de-saturation and gate charge methods were found to be the most suitable methods. Moreover, the studies in the literature where these two methods are used together were examined to obtain positive features in both methods in the protection circuit for semiconductor-based battery switch. Then, the battery switch and protection circuit were proposed with the system-level block diagram. In the sixth chapter, the shut-off strategy with the proposed switch and protection circuit was presented. Moreover, to pave the way for the realizability of this system, the switch is simulated in a SPICE environment with SiC MOSFET selected from CREE. In the simulation study, a 1000V system carrying 300A current was short-circuited over 5mΩ in FUL condition, and short circuit protection was provided in under 200ns. In addition, the simulation was repeated at 600V and 800V voltage levels as well as 1000V to observe the effect of the voltage on the short circuit protection system. As a result, except that the 1000V system reacts quite faster, there are no noticeable changes in the short circuit current than 600V and 800V. Moreover, to obtain the effect of the stray inductance of the battery pack on short circuit protection, simulations were repeated for the stray inductance between 10-40μH. As a result, it is seen that as the inductance value decreased, the protection circuit triggered faster, and the short circuit current is rise faster also. Consequently, considering the obtained short-circuit protection speeds and the switching losses observed in the simulation, the use of a semiconductor-based battery switch is promising for short-circuit protection. However, it is necessary to realize real-world hardware tests to have a better understanding of the system.

7.1 Recommendations and Future Work

In addition to the proposed shut-off concept and simulated protection methods for battery switches in this study, hardware realization shall be done to broaden the scope of the study and demonstrate its applicability in automotive battery systems. This circuit shall be realized based on automotive standards. Tolerances in hardware design and components should also be taken into account for the protection circuit. In addition, it is important to follow the functional safety requirements according to ISO26262 standard and electrical safety requirements in IEC 60664, ISO 6469.

Moreover, for the system to be used in automotive battery packs, compliance with electrical, mechanical, environmental, and chemical tests according to ISO 16750 is also necessary.

REFERENCES

[1] **Pelegov, D.V. and Pontes, J.** (2018). Main drivers of battery industry changes: electric vehicles—a market overview, *Batteries*, *4*(4), 65.

[2] **Scrosati, B. and Garche, J.** (2010). Lithium batteries: Status, prospects and future, *Journal of power sources*, *195*(9), 2419–2430.

[3] **Gandoman, F.H.**, **Jaguemont, J.**, **Goutam, S.**, **Gopalakrishnan, R.**, **Firouz, Y.**, **Kalogiannis, T.**, **Omar, N. and Van Mierlo, J.** (2019). Concept of reliability and safety assessment of lithium-ion batteries in electric vehicles: Basics, progress, and challenges, *Applied Energy*, *251*, 113343.

[4] **Doughty, D.H. and Roth, E.P.** (2012). A general discussion of Li ion battery safety, *Electrochemical Society Interface*, *21*(2), 37.

[5] **Jung, C.** (2017). Power Up with 800-V Systems: The benefits of upgrading voltage power for battery-electric passenger vehicles, *IEEE Electrification Magazine*, *5*(1), 53–58.

[6] **Goodenough, J.B.** (2018). How we made the Li-ion rechargeable battery, *Nature Electronics*, *1*(3), 204–204.

[7] **HORIE, H.** (1997). Application study of li-ion battery for EVs and HEVs, *Journal of The Surface Finishing Society of Japan*, *48*(12), 1148–1152.

[8] **Miao, Y.**, **Hynan, P.**, **von Jouanne, A. and Yokochi, A.** (2019). Current Li-ion battery technologies in electric vehicles and opportunities for advancements, *Energies*, *12*(6), 1074.

[9] ISO6469-3:2018 Electrically propelled road vehicles - Safety specifications – Part 3: Protection of persons against electric shock, **Standard**, Geneva, CH.

[10] ISO6469-1:2019 Electrically propelled road vehicles — Safety specifications — Part 1: Rechargeable energy storage system (RESS), **Standard**, Geneva, CH.

[11] **Song, R.H. and Cho, H.M.** (2015). A study on the Interlock Circuit Abnormality of High Voltage System in HEV, *Journal of Energy Engineering*, *24*(3), 27–33.

[12] **Rajasekhar, M. and Gorre, P.** (2015). High voltage battery pack design for hybrid electric vehicles, *2015 IEEE International Transportation Electrification Conference (ITEC)*, IEEE, pp.1–7.

[13] **Gera, C. and Sharma, S.** (2019). A Method to Diagnose Failures in High Voltage Contactors and Fuse for Safe Operation of Battery Pack, *2019 IEEE Transportation Electrification Conference (ITEC-India)*, IEEE, pp.1–4.

[14] **Sakuraba, T.**, **Ouaida, R.**, **Chen, S. and Chailloux, T.** (2018). Evaluation of Novel Hybrid Protection Based on Pyroswitch and Fuse Technologies, *2018 International Power Electronics Conference (IPEC-Niigata 2018-ECCE Asia)*, IEEE, pp.2153–2157.

[15] **Sturk, D.**, **Gustafsson, P.**, **Holgers, A.**, **Sundmark, H.**, **Cavell, C.**, **Gaudinat, F. and Dugast, E.** (2015). E-Vehicle Safety–Pyro Switch as High Voltage Circuit Breaker & Bypass, *24th International Technical Conference on the Enhanced Safety of Vehicles (ESV) National Highway Traffic Safety Administration*, 15-0163.

[16] **Lell, P. and Volm, D.** (2018). Innovative Safety Concept to Shutdown Short Circuit Currents in Battery Systems up to 1000V Based on Ultrafast Pyrofuse Technology, *2018 IEEE Holm Conference on Electrical Contacts*, IEEE, pp.317–322.

[17] **Letor, R. and Crisafulli, R.** (2019). Smart Power devices and new electronic fuses compliant with new E/E architecture for autonomous driving, *2019 AEIT International Conference of Electrical and Electronic Technologies for Automotive (AEIT AUTOMOTIVE)*, IEEE, pp.1–6.

[18] **Koepf, H.**, **Wilkening, E.D.**, **Klosinski, C. and Kurrat, M.** (2014). Breaking performance of protection devices for automotive dc powertrains with a voltage of 450 V, *ICEC 2014; The 27th International Conference on Electrical Contacts*, VDE, pp.1–6.

[19] **Shi, Y.**, **Xie, R.**, **Wang, L.**, **Shi, Y. and Li, H.** (2016). Short-circuit protection of 1200V SiC MOSFET T-type module in PV inverter application, *2016 IEEE Energy Conversion Congress and Exposition (ECCE)*, IEEE, pp.1–5.

[20] **Bingjian, Y.**, **Yang, G.**, **Xiaoguang, W.**, **Zhiyuan, H.**, **Longlong, C. and Yunhai, S.** (2015). A hybrid circuit breaker for DC-application, *2015 IEEE First International Conference on DC Microgrids (ICDCM)*, IEEE, pp.187–192.

[21] **Shukla, A. and Demetriades, G.D.** (2014). A survey on hybrid circuit-breaker topologies, *IEEE Transactions on Power Delivery*, *30*(2), 627–641.

[22] **Usseglio, V. and Mourrier, A.** (2019). Smart 24 V Battery Switch for a Reliable Redundant Power Supply in Commercial, Construction, and Agriculture Vehicles (CAV), **Technical Report**, SAE Technical Paper.

[23] Infineon SBS Next Gen Demonstrator Board, **User manual**, Munich, Germany.

[24] Infineon Battery Switch 24V - System Demonstrator, **User manual**, Munich, Germany.

[25] **Rostaing, G.**, **Berkani, M.**, **Mechouche, D.**, **Labrousse, D.**, **Lefebvre, S.**, **Khatir, Z. and Dupuy, P.** (2013). Reliability of power MOSFET-based smart switches under normal and extreme conditions for 24 V battery system applications, *Microelectronics Reliability*, *53*(9-11), 1703–1706.

[26] VisIC Tech D³GaN based high voltage solid-state battery disconnect switch for electric drive systems, Available:https://visic-tech.com/news-and-updates, Access date: Dec 2020.

[27] **DiMarino, C.M.**, **Burgos, R. and Dushan, B.** (2015). High-temperature silicon carbide: characterization of state-of-the-art silicon carbide power transistors, *IEEE Industrial Electronics Magazine*, *9*(3), 19–30.

[28] **Millán, J.**, **Godignon, P.**, **Perpiñà, X.**, **Pérez-Tomás, A. and Rebollo, J.** (2013). A survey of wide bandgap power semiconductor devices, *IEEE transactions on Power Electronics*, *29*(5), 2155–2163.

[29] **Rabkowski, J.**, **Peftitsis, D. and Nee, H.P.** (2012). Silicon carbide power transistors: A new era in power electronics is initiated, *IEEE Industrial Electronics Magazine*, *6*(2), 17–26.

[30] **Mohapatra, S.**, **Nguyen, T.A. and Nguyen-Tri, P.** (2018). *Noble metal-metal oxide hybrid nanoparticles: Fundamentals and applications*, Elsevier.

[31] **Manias, S.** (2017). Power Electronics and Motor Drive Systems/Stefanos N. Manias.

[32] **She, X.**, **Huang, A.Q.**, **Lucía, Ó. and Ozpineci, B.** (2017). Review of silicon carbide power devices and their applications, *IEEE Transactions on Industrial Electronics*, *64*(10), 8193–8205.

[33] **Othman, D.**, **Berkani, M.**, **Lefebvre, S.**, **Ibrahim, A.**, **Khatir, Z. and Bouzourene, A.** (2012). Comparison study on performances and robustness between SiC MOSFET & JFET devices–Abilities for aeronautics application, *Microelectronics Reliability*, *52*(9-10), 1859–1864.

[34] **Huang, X.**, **Wang, G.**, **Li, Y.**, **Huang, A.Q. and Baliga, B.J.** (2013). Short-circuit capability of 1200V SiC MOSFET and JFET for fault protection, *2013 Twenty-Eighth Annual IEEE Applied Power Electronics Conference and Exposition (APEC)*, IEEE, pp.197–200.

[35] **Wang, Z.**, **Shi, X.**, **Tolbert, L.M.**, **Wang, F.**, **Liang, Z.**, **Costinett, D. and Blalock, B.J.** (2015). Temperature-dependent short-circuit capability of silicon carbide power MOSFETs, *IEEE Transactions on Power Electronics*, *31*(2), 1555–1566.

[36] **Berthou, M.**, **Planson, D. and Tournier, D.** (2015). Short-circuit capability exploration of silicon carbide devices, *Materials Science Forum*, volume821, Trans Tech Publ, pp.810–813.

[37] **Chen, C.**, **Labrousse, D.**, **Lefebvre, S.**, **Petit, M.**, **Buttay, C. and Morel, H.** (2015). Study of short-circuit robustness of SiC MOSFETs, analysis of the failure modes and comparison with BJTs, *Microelectronics Reliability*, *55*(9-10), 1708–1713.

[38] **Bertelshofer, T.**, **Maerz, A. and Bakran, M.M.** (2017). Design rules to adapt the desaturation detection for SiC MOSFET modules, *PCIM Europe 2017; International Exhibition and Conference for Power Electronics, Intelligent Motion, Renewable Energy and Energy Management*, VDE, pp.1–8.

[39] **Wang, Z.**, **Shi, X.**, **Xue, Y.**, **Tolbert, L.M.**, **Wang, F. and Blalock, B.J.** (2014). Design and performance evaluation of overcurrent protection schemes for silicon carbide (SiC) power MOSFETs, *IEEE Transactions on Industrial Electronics*, *61*(10), 5570–5581.

[40] **Sadik, D.P.**, **Colmenares, J.**, **Tolstoy, G.**, **Peftitsis, D.**, **Bakowski, M.**, **Rabkowski, J. and Nee, H.P.** (2015). Short-circuit protection circuits for silicon-carbide power transistors, *IEEE transactions on industrial electronics*, *63*(4), 1995–2004.

[41] **Kar, A.**, **Ahmad, S.S.**, **Narayanan, G. and Sengupta, M.** (2017). Design, performance evaluation, fabrication and testing of a SiC MOSFET gate driver, *2017 IEEE International Conference on Signal Processing, Informatics, Communication and Energy Systems (SPICES)*, IEEE, pp.1–6.

[42] **Wang, H.**, **Zhao, J.**, **Zheng, Z. and Sun, H.** (2018). Driving a silicon carbide power MOSFET with a fast short circuit protection, *2018 1st Workshop on Wide Bandgap Power Devices and Applications in Asia (WiPDA Asia)*, IEEE, pp.260–265.

[43] **Zhang, X.**, **Sheh, G.**, **Gant, L. and Banerjee, S.** (2018). In-Depth Study of Short-Circuit Robustness and Protection of 1200 V SiC MOSFETs, *PCIM Europe 2018; International Exhibition and Conference for Power Electronics, Intelligent Motion, Renewable Energy and Energy Management*, VDE, pp.1–7.

[44] **Liu, J.**, **Wang, Y.**, **Zheng, Z.**, **Peng, Z. and Li, Y.** (2017). Comparison of two gate drivers for SiC MOSFETs on switching performance and over current protection, *2017 20th International Conference on Electrical Machines and Systems (ICEMS)*, IEEE, pp.1–5.

[45] **Kumar, A.**, **Ravichandran, A.**, **Singh, S.**, **Shah, S. and Bhattacharya, S.** (2017). An intelligent medium voltage gate driver with enhanced short circuit protection scheme for 10kV 4H-SiC MOSFETs, *2017 IEEE Energy Conversion Congress and Exposition (ECCE)*, IEEE, pp.2560–2566.

[46] **Rice, J. and Mookken, J.** (2015). SiC MOSFET gate drive design considerations, *2015 IEEE International Workshop on Integrated Power Packaging (IWIPP)*, IEEE, pp.24–27.

[47] **Spang, M. and Hofstoetter, N.** (2017). Evaluation of current measurement accuracy for a power module with integrated shunt resistors, *PCIM Europe 2017; International Exhibition and Conference for Power Electronics, Intelligent Motion, Renewable Energy and Energy Management*, VDE, pp.1–8.

[48] IXYSIC Application Note AN-401, **Application note**, USA.

[49] **Zhang, W.**, **Wang, F.**, **Zhang, Z. and Holzinger, B.** (2019). Fast Wide-bandgap Device Overcurrent Protection with Direct Current Measurement, *2019 10th International Conference on Power Electronics and ECCE Asia (ICPE 2019-ECCE Asia)*, IEEE, pp.1–6.

[50] **Fink, K.**, **Volke, A.**, **Wei, W.**, **Wiesner, E. and Thal, E.** (2016). Gate-driver with full protection for SiC-MOSFET modules, *PCIM Asia 2016; International Exhibition and Conference for Power Electronics, Intelligent Motion, Renewable Energy and Energy Management*, VDE, pp.1–7.

[51] **Wiesner, E.**, **Thal, E.**, **Volke, A. and Fink, K.** (2016). Advanced protection for large current full SiC-modules, *PCIM Europe 2016; International Exhibition and Conference for Power Electronics, Intelligent Motion, Renewable Energy and Energy Management*, VDE, pp.1–5.

[52] **Cui, Y.**, **Zhang, Z.**, **Yi, P. and Wei, L.** Investigation of Current Mirror Based Overcurrent Protection for 1200V 800A High Power SiC MOSFET Modules, *2019 IEEE Energy Conversion Congress and Exposition (ECCE)*, IEEE, pp.6161–6165.

[53] **Kudoh, M.**, **Hoshi, Y.**, **Momota, S.**, **Fujihira, T. and Sakurai, K.** (1996). Current sensing IGBT for future intelligent power module, *8th International Symposium on Power Semiconductor Devices and ICs. ISPSD'96. Proceedings*, IEEE, pp.303–306.

[54] **Sukhatme, Y.**, **Krishna, M.V.**, **Ganesan, P. and Hatua, K.** (2018). A drain current based short circuit protection technique for SiC MOSFET, *2018 International Symposium on Devices, Circuits and Systems (ISDCS)*, IEEE, pp.1–6.

[55] **Sun, K.**, **Wang, J.**, **Burgos, R.**, **Boroyevich, D.**, **Kang, Y. and Choi, E.** (2018). Analysis and design of an overcurrent protection scheme based on parasitic inductance of SiC MOSFET power module, *2018 IEEE Applied Power Electronics Conference and Exposition (APEC)*, IEEE, pp.2806–2812.

[56] **Wang, Z.**, **Shi, X.**, **Tolbert, L.M.**, **Wang, F. and Blalock, B.J.** (2013). A di/dt feedback-based active gate driver for smart switching and fast overcurrent protection of IGBT modules, *IEEE Transactions on Power Electronics*, *29*(7), 3720–3732.

[57] **Oinonen, M.**, **Laitinen, M. and Kyyrä, J.** (2014). Current measurement and short-circuit protection of an IGBT based on module parasitics, *2014 16th European Conference on Power Electronics and Applications*, IEEE, pp.1–9.

[58] **Awwad, A.E. and Dieckerhoff, S.** (2015). Short-circuit evaluation and overcurrent protection for SiC power MOSFETs, *2015 17th European Conference on Power Electronics and Applications (EPE'15 ECCE-Europe)*, IEEE, pp.1–9.

[59] **Wickramasinghe, T.**, **Allard, B.**, **Buttay, C.**, **Joubert, C.**, **Martin, C.**, **Mogniotte, J.F.**, **Morel, H.**, **Bevilacqua, P.**, **Le, T.L. and Azzopardi, S.** (2019). A Study on Shunt Resistor-based Current Measurements for Fast Switching GaN Devices, *IECON 2019-45th Annual Conference of the IEEE Industrial Electronics Society*, volume 1, IEEE, pp.1573–1578.

[60] **Climaco-Arvizu, O.**, **Hernández-González, L. and Rodríguez-Blanco, M.** (2015). Fault detection for SiC-Mosfet based on the behavior of gate signal, *2015 IEEE 10th International Symposium on Diagnostics for Electrical Machines, Power Electronics and Drives (SDEMPED)*, IEEE, pp.71–76.

[61] **Horiguchi, T.**, **Kinouchi, S.i.**, **Nakayama, Y. and Akagi, H.** (2015). A fast short-circuit protection method using gate charge characteristics of SiC MOSFETs, *2015 IEEE Energy Conversion Congress and Exposition (ECCE)*, IEEE, pp.4759–4764.

[62] **Wang, J.**, **Shen, Z.**, **DiMarino, C.**, **Burgos, R. and Boroyevich, D.** (2016). Gate driver design for 1.7 kV SiC MOSFET module with Rogowski current sensor for shortcircuit protection, *2016 IEEE Applied Power Electronics Conference and Exposition (APEC)*, IEEE, pp.516–523.

[63] **Yoon, H. and Cho, Y.** (2019). Application of the Rogowski Coil Current Sensor for Overcurrent Detection and Blocking in Power Conversion Systems, *2019 10th International Conference on Power Electronics and ECCE Asia (ICPE 2019-ECCE Asia)*, IEEE, pp.1–7.

[64] **Rothmund, D.**, **Bortis, D. and Kolar, J.W.** (2018). Highly compact isolated gate driver with ultrafast overcurrent protection for 10 kV SiC MOSFETs, *CPSS Transactions on Power Electronics and Applications*, *3*(4), 278–291.

[65] **Wang, Z.**, **Tong, C. and Zhang, Y.** (2018). Research on Temperature-Dependent Overcurrent Protection Schemes for SiC MOSFETs, *2018 21st International Conference on Electrical Machines and Systems (ICEMS)*, IEEE, pp.822–826.

[66] **Chen, H.**, **Cong, T.N.**, **Yang, W.**, **Tan, C.**, **Li, Y. and Ding, Y.** (2009). Progress in electrical energy storage system: A critical review, *Progress in natural science*, *19*(3), 291–312.

[67] **May, G.J.**, **Davidson, A. and Monahov, B.** (2018). Lead batteries for utility energy storage: A review, *Journal of Energy Storage*, *15*, 145–157.

[68] **Fetcenko, M.**, **Koch, J. and Zelinsky, M.**, (2015). Nickel–metal hydride and nickel–zinc batteries for hybrid electric vehicles and battery electric vehicles, Advances in Battery Technologies for Electric Vehicles, Elsevier, pp.103–126.

[69] **Johnson, N.**, (2014). Battery technology for CO2 reduction, Alternative Fuels and Advanced Vehicle Technologies for Improved Environmental Performance, Elsevier, pp.582–631.

[70] **Yoshino, A.** (2012). The birth of the lithium-ion battery, *Angewandte Chemie International Edition*, *51*(24), 5798–5800.

[71] **Warner, J.T.** (2015). *The handbook of lithium-ion battery pack design: chemistry, components, types and terminology*, Elsevier.

[72] **Kim, H.J.**, **Krishna, T.**, **Zeb, K.**, **Rajangam, V.**, **Gopi, C.V.**, **Sambasivam, S.**, **Raghavendra, K.V.G. and Obaidat, I.M.** (2020). A comprehensive review of Li-ion battery materials and their recycling techniques, *Electronics*, *9*(7), 1161.

[73] **Zschornak, M.**, **Meutzner, F.**, **Lück, J.**, **Latz, A.**, **Leisegang, T.**, **Hanzig, J.**, **Nentwich, M.**, **Zosel, J. and Balbuena, P.B.** (2018). Fundamental principles of battery design, *Physical Sciences Reviews*, *3*(11).

[74] **Chawla, N.**, **Bharti, N. and Singh, S.** (2019). Recent advances in non-flammable electrolytes for safer lithium-ion batteries, *Batteries*, *5*(1), 19.

[75] **Zubi, G.**, **Dufo-López, R.**, **Carvalho, M. and Pasaoglu, G.** (2018). The lithium-ion battery: State of the art and future perspectives, *Renewable and Sustainable Energy Reviews*, *89*, 292–308.

[76] **Schmuch, R.**, **Wagner, R.**, **Hörpel, G.**, **Placke, T. and Winter, M.** (2018). Performance and cost of materials for lithium-based rechargeable automotive batteries, *Nature Energy*, *3*(4), 267–278.

[77] **Ulvestad, A.** (2018). A brief review of current lithium ion battery technology and potential solid state battery technologies, *arXiv preprint arXiv:1803.04317*.

[78] **Siczek, K.** (2020). The Toxicity of Secondary Lithium-Sulfur Batteries Components, *Batteries*, *6*(3), 45.

[79] **Débart, A.**, **Paterson, A.J.**, **Bao, J. and Bruce, P.G.** (2008). α-MnO2 nanowires: A catalyst for the O2 electrode in rechargeable lithium batteries, *Angewandte Chemie International Edition*, *47*(24), 4521–4524.

[80] EN50110-1 Operation of electrical installations - Part 1: General requirements, **Standard**.

[81] Lucid Website, www.lucid.com, access date: Dec 2020.

[82] Tesla Website, www.tesla.com, access date: Dec 2020.

[83] Chevrolet Website, www.chevrolet.com, access date: Dec 2020.

[84] Volkswagen Website, www.vw.com, access date: Dec 2020.

[85] Audi Website, www.audi.com, access date: Dec 2020.

[86] Porsche AG Website, www.porsche.com, access date: Dec 2020.

[87] Hyundai Motor Company, www.hyundai.com, access date: Dec 2020.

[88] Nissan Motor Corp. Website, /www.nissan-global.com, access date: Dec 2020.

[89] BMW Website, www.bmw.com, access date: Dec 2020.

[90] Mercedes-Benz Webiste, www.mercedes-benz.com, access date: Dec 2020.

[91] Jaguar Website, www.jaguar.com, access date: Dec 2020.

[92] **Eren, M.K.**, **Eymen, İ.**, **Kadir, A.**, **Gücükoğlu, T. and Erhan, K.** (2018). Effects of cell and module configuration on battery system in electric vehicles, *International Journal of Engineering Technologies*, *4*(4), 143–152.

[93] IEC60664-1:2016 Insulation coordination for equipment within low-voltage systems - Part 3: Use of coating, potting or moulding for protection against pollution, **Standard**.

[94] ISO6469-2:2018 Electrically propelled road vehicles — Safety specifications — Part 2: Vehicle operational safety, **Standard**.

[95] ISO26262-3:2018 Road vehicles — Functional safety — Part 3: Concept phase, **Standard**.

[96] ISO16750-l:2018 Road vehicles — Environmental conditions and testing for electrical and electronic equipment — Part 1: General, **Standard**.

[97] AEC-Q101 Failure Mechanism Based Stress Test Qualification For Discrete Semiconductors, **Standard**.

[98] **Abaza, A.**, **Ferrari, S.**, **Wong, H.K.**, **Lyness, C.**, **Moore, A.**, **Weaving, J.**, **Blanco-Martin, M.**, **Dashwood, R. and Bhagat, R.** (2018). Experimental study of internal and external short circuits of commercial automotive pouch lithium-ion cells, *Journal of Energy Storage*, *16*, 211–217.

[99] **Maleki, H. and Howard, J.N.** (2009). Internal short circuit in Li-ion cells, *Journal of Power Sources*, *191*(2), 568–574.

[100] **Yoshio, M.**, **Brodd, R.J. and Kozawa, A.** (2009). *Lithium-ion batteries*, volume 1, Springer.

[101] **Biensan, P.**, **Simon, B.**, **Peres, J.**, **De Guibert, A.**, **Broussely, M.**, **Bodet, J. and Perton, F.** (1999). On safety of lithium-ion cells, *Journal of Power Sources*, *81*, 906–912.

[102] **Zavalis, T.G.**, **Behm, M. and Lindbergh, G.** (2012). Investigation of short-circuit scenarios in a lithium-ion battery cell, *Journal of The Electrochemical Society*, *159*(6), A848.

[103] **Tobishima, S.i. and Yamaki, J.i.** (1999). A consideration of lithium cell safety, *Journal of Power Sources*, *81*, 882–886.

[104] **Ozguc, M.K. and Aras, K.** (2021). Selective Shut-off Strategy in Distributed Battery System, *International Journal of Automotive Science And Technology*, *5*, 27 – 33.

[105] **Ozguc, M.K.**, **Ipek, E.**, **Aras, K. and Erhan, K.** (2019). Comprehensive Analysis of Pre-Charge Sequence in Automotive Battery Systems, *Transactions on Environment and Electrical Engineering*, *4*(1), 1–6.

[106] **Cline, C. and Stultz, J.** (1995). Fuse protection of DC systems, *Proceedings of the American Power Conference*, volume 57, ILLINOIS INSTITUTE OF TECHNOLOGY, pp.20–20.

[107] **Jebramcik, J. and Berger, F.** (2014). Observations on switching characteristics of arc chutes in DC contactors, *ICEC 2014; The 27th International Conference on Electrical Contacts*, VDE, pp.1–6.

[108] **Fernández, M.**, **Perpiñá, X.**, **Vellvehi, M.**, **Jordà, X.**, **Cabeza, T. and Llorente, S.** (2017). Analysis of solid state relay solutions based on different semiconductor technologies, *2017 19th European Conference on Power Electronics and Applications (EPE'17 ECCE Europe)*, IEEE, pp.P–1.

[109] **Singh, R. and Pecht, M.** (2008). Commercial impact of silicon carbide, *IEEE Industrial Electronics Magazine*, *2*(3), 19–31.

[110] **Baliga, B.** (2008). Fundamentals of power semiconductor devices: Springer Science+ Business Media LLC.

[111] **Liu, W.** (2004). Electro-thermal simulations and measurements of silicon carbide power transistors, *Ph.D. thesis*, Mikroelektronik och informationsteknik.

[112] **Jain, H.**, **Rajawat, S. and Agrawal, P.** (2008). Comparision of wide band gap semiconductors for power electronics applications, *2008 International Conference on Recent Advances in Microwave Theory and Applications*, IEEE, pp.878–881.

[113] **Raj, J.S.S.**, **Sivaraman, P.**, **Prem, P. and Matheswaran, A.** (2020). Wide Band Gap semiconductor material for electric vehicle charger, *Materials Today: Proceedings*.

[114] **Lidow, A.**, **De Rooij, M.**, **Strydom, J.**, **Reusch, D. and Glaser, J.** (2019). *GaN transistors for efficient power conversion*, John Wiley & Sons.

[115] **Ivanov, P.**, **Potapov, A.**, **Samsonova, T. and Grekhov, I.** (2016). Electric-field dependence of electron drift velocity in 4H–SiC, *Solid-State Electronics*, *123*, 15–18.

[116] **Buttay, C.**, **Planson, D.**, **Allard, B.**, **Bergogne, D.**, **Bevilacqua, P.**, **Joubert, C.**, **Lazar, M.**, **Martin, C.**, **Morel, H.**, **Tournier, D.** *et al.* (2011). State of the art of high temperature power electronics, *Materials Science and Engineering: B*, *176*(4), 283–288.

[117] Infineon SiC Power Devices
Available:https://www.infineon.com/cms/en/product/power/mosfet/
Accessed:December 2020, **Database**.

[118] CREE SiC Power Devices
Available:https://www.wolfspeed.com/power/products/sic-mosfets/
Accessed:December 2020, **Database**.

[119] ROHM SiC Power Devices
Available:https://www.rohm.com/products/sic-power-devices/
Accessed:December 2020, **Database**.

[120] **Cooper, J.A.**, **Melloch, M.R.**, **Singh, R.**, **Agarwal, A. and Palmour, J.W.** (2002). Status and prospects for SiC power MOSFETs, *IEEE Transactions on Electron Devices*, *49*(4), 658–664.

[121] ROHM 1200 V/180 A Full SiC PowerModule with Integrated SiC Trench-MOSFET, Available: https://www.rohm.com, Access date: DEC 2020, **Application note**.

[122] **Sun, J.**, **Wei, J.**, **Zheng, Z.**, **Wang, Y. and Chen, K.J.** (2019). Repetitive Short Circuit Energy Dependent Instability of 1.2 kV SiC Power MOSFETs, *2019 31st International Symposium on Power Semiconductor Devices and ICs (ISPSD)*, IEEE, pp.263–266.

[123] **Li, Y.**, **Zhao, Y.**, **Huang, A.Q. and Zhang, L.** (2020). Degradation Assessment of SiC MOSFETs under the Repetitive Short Circuit Ageing with Different Gate-Source Voltage Bias, *2020 IEEE 21st Workshop on Control and Modeling for Power Electronics (COMPEL)*, IEEE, pp.1–6.

[124] **Du, H.**, **Reigosa, P.D.**, **Iannuzzo, F. and Ceccarelli, L.** (2019). Impact of the Case Temperature on the Reliability of SiC MOSFETs Under Repetitive Short Circuit Tests, *2019 IEEE Applied Power Electronics Conference and Exposition (APEC)*, IEEE, pp.332–337.

[125] **Chen, M.**, **Xu, D.**, **Zhang, X.**, **Zhu, N.**, **Wu, J. and Rajashekara, K.** (2017). An improved IGBT short-circuit protection method with self-adaptive blanking circuit based on V CE measurement, *IEEE Transactions on Power Electronics*, *33*(7), 6126–6136.

[126] **Wada, K. and Yamashita, A.** (2014). Wide bandwidth and low propagation time delay current sensor applied to a laminated bus bar, *2014 IEEE Energy Conversion Congress and Exposition (ECCE)*, IEEE, pp.3083–3088.

[127] **Oberdieck, K.**, **Schuch, S. and DeDoncker, R.W.** (2016). Short circuit detection using the gate charge characteristic for trench/fieldstop-IGBTs, *2016 18th European Conference on Power Electronics and Applications (EPE'16 ECCE Europe)*, IEEE, pp.1–10.

[128] **Miyazaki, K.**, **Omura, I.**, **Takamiya, M. and Sakurai, T.** (2016). 20-ns Short-circuit detection scheme with high variation-tolerance based on analog delay multiplier circuit for advanced IGBTs, *2016 IEEE 2nd Annual Southern Power Electronics Conference (SPEC)*, IEEE, pp.1–4.

[129] **Horiguchi, T.**, **Kinouchi, S.i.**, **Nakayama, Y.**, **Oi, T.**, **Urushibata, H.**, **Okamoto, S.**, **Tominaga, S. and Akagi, H.** (2014). A high-speed protection circuit for IGBTs subjected to hard-switching faults, *IEEE Transactions on Industry Applications*, *51*(2), 1774–1781.

[130] **Horiguchi, T.**, **Kinouchi, S.i.**, **Nakayama, Y.**, **Oi, T.**, **Urushibata, H.**, **Okamoto, S.**, **Tominaga, S. and Akagi, H.** (2015). Short-circuit protection method based on a gate charge characteristic, *IEEJ Journal of Industry Applications*, *4*(4), 360–369.

[131] **Tanimura, T.**, **Yuasa, K. and Omura, I.** (2011). Full digital short circuit protection for advanced IGBTs, *2011 IEEE 23rd International Symposium on Power Semiconductor Devices and ICs*, IEEE, pp.60–63.

[132] **Kim, M.S.**, **Park, B.G.**, **Kim, R.Y. and Hyun, D.S.** (2011). A novel fault detection circuit for short-circuit faults of IGBT, *2011 Twenty-Sixth Annual IEEE Applied Power Electronics Conference and Exposition (APEC)*, IEEE, pp.359–363.

[133] **Rodriguez-Blanco, M.A.**, **Claudio-Sanchez, A.**, **Theilliol, D.**, **Vela-Valdés, L.G.**, **Sibaja-Terán, P.**, **Hernandez-Gonzalez, L. and Aguayo-Alquicira, J.** (2010). A failure-detection strategy for IGBT based on gate-voltage behavior applied to a motor drive system, *IEEE Transactions on Industrial Electronics*, *58*(5), 1625–1633.

[134] **Wang, Z.**, **Tong, C. and Huang, W.** (2020). Short-circuit protection method for medium-voltage SiC MOSFET based on gate-source voltage detection, *Journal of Power Electronics*, *20*(4), 1066–1075.

[135] **Barai, A.**, **Uddin, K.**, **Widanage, W.**, **McGordon, A. and Jennings, P.** (2018). A study of the influence of measurement timescale on internal resistance characterisation methodologies for lithium-ion cells, *Scientific reports*, *8*(1), 1–13.

[136] CREE C3M0021120D Silicon Carbide Power MOSFET, **Datasheet**.

CURRICULUM VITAE

Name Surname: Murat Kubilay Özgüç

EDUCATION:

- **B.Sc.:** 2018, Yıldız Technical University, Electrical-Electronics Faculty, Electrical Engineering

PROFESSIONAL EXPERIENCE AND REWARDS:

- 2018-Present Battery Development Engineer-AVL Research and Engineering Turkey

PUBLICATIONS, PRESENTATIONS AND PATENTS ON THE THESIS:

- Ozguc MK, Ipek E, Aras K, Erhan K. Comprehensive Analysis of Pre-Charge Sequence in Automotive Battery Systems. Transactions on Environment and Electrical Engineering. 2019 Dec 25;4(1):1-6.
- Ozguc M , Aras K . Selective Shut-off Strategy in Distributed Battery System. International Journal of Automotive Science And Technology. 2021; 5(1): 27-33.